

# FEASIBILITY STUDY OF A HYBRID PASSIVE/ACTIVE NOISE ABSORPTION SYSTEM

by

Samson Beyene

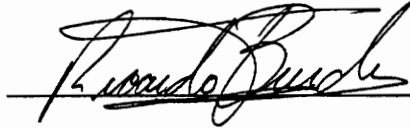
Thesis submitted to the Faculty of the  
Virginia Polytechnic Institute and State University  
in partial fulfillment of the requirements for the degree of

MASTERS OF SCIENCE

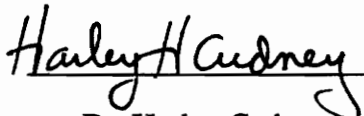
IN

MECHANICAL ENGINEERING

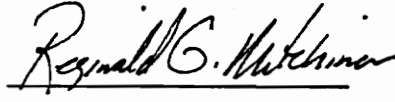
APPROVED:

A handwritten signature in black ink, appearing to read "Ricardo Burdisso", written over a horizontal line.

Dr. Ricardo A. Burdisso, chair

A handwritten signature in black ink, appearing to read "Harley Cudney", written over a horizontal line.

Dr. Harley Cudney

A handwritten signature in black ink, appearing to read "Reginald G. Mitchiner", written over a horizontal line.

Dr. Reginald Mitchiner

April , 1995

Blacksburg, Virginia

C.2

LD  
5055  
V855  
1995  
B394  
C.2

# **FEASIBILITY STUDY OF A HYBRID PASSIVE/ACTIVE NOISE ABSORPTION SYSTEM**

by

Samson Beyene

Committee Chairman: Ricardo A. Burdisso  
Mechanical Engineering

## **(ABSTRACT)**

The work described in this thesis was directed towards the development of a compact hybrid Passive/Active noise absorption system that would be effective over a wide frequency range. The Passive/Active system efficiently integrates both passive and active noise control methods. Both theoretical and experimental investigations were carried out in this work.

A simple numerical model was developed to simulate the Passive/Active system. The passive sound absorbing material used in the system was the partially-reticulated polyurethane foam. This material was characterized using its sound propagation constant and its characteristic impedance which were empirically determined.

Three different control strategies were investigated for the Passive/Active system. These control strategies were: (i) directly minimizing the reflected wave, (ii) inducing a pressure-release boundary condition on the back surface of the absorbing layer and (iii) a new approach consisting of minimizing the reflected wave in the airspace. The latter results in a match between the impedance in the air cavity and the impedance of a plane wave in air. This impedance-matching control approach was selected for the Passive/Active system because it meets the goal of optimum absorption over a wide frequency range and offers practical advantages. In this system, the error sensing process

takes place inside of the airspace which results in a compact design with all the necessary sensors and actuators built into the system.

Parametric analysis were performed on the impedance-matching control approach to investigate the sensitivity of the performance of the system to variation in absorbing layer thickness and airspace depth. The performance of the system was determined to be independent of the airspace depth and marginally sensitive to absorbing layer thickness. In addition, in order to study the feasibility of using the Passive/Active system for other sound absorbing materials, an experimental investigation was performed with the polyurethane foam replaced by a porous metal sheet, commercial name FELTMETAL®. The result of this investigation showed an improvement in the absorption property of the FELTMETAL, opening a number of potential applications for the Passive/Active system by using different absorbing materials.

## ACKNOWLEDGMENTS

I would like to express my sincere appreciation to my advisor, Dr. Ricardo Burdisso, for his guidance, support and the opportunity to work on this exciting project. Without his constructive criticism and his superb editorial insight, the preparation of this thesis would have been very difficult.

I am very grateful to Dr. Reginald Mitchiner for serving in my advisory committee and for always being easy to talk to. I am also indebted to Dr. Harley Cudney for his service in my advisory committee and also for persuading me to pursue a Master's degree. Without his guidance in the last two years of my undergraduate years, I would not have made the decision to pursue a graduate degree.

I wish to thank Dr. Criag Rogers for giving me a chance to work on an undergraduate research. I also would like to thank my fellow graduate students and research associates in the Acoustics and Vibration Laboratories. I am indebted for all their assistance and helpful suggestions. I also thank Dr. Chris Fuller and Dawn Williams.

# TABLE OF CONTENTS

	Page
Abstract.....	ii
Acknowledgments.....	iv
Table of contents.....	v
List of Figures.....	vii

## Chapter 1

<b>Introduction.....</b>	<b>1</b>
1.1 Passive Sound Control - A brief Review.....	3
1.2 Active Sound Control - A brief Review.....	4
1.3 Hybrid Sound Control System - Literature Review.....	7
1.4 Proposed Passive/Active noise control system.....	10
1.5 Overview of Thesis.....	12

## Chapter 2

<b>Analytical Model.....</b>	<b>14</b>
2.1 Derivation of the Analytical Model.....	14
2.2 Boundary Conditions.....	18
2.3 Control strategies.....	21
2.3.1 Direct minimization of reflected wave - Ideal Performance.....	21
2.3.2 Pressure-release boundary condition.....	22
2.3.3 Impedance-matching condition.....	23
2.4 Calculation of acoustical properties.....	23
2.5 Determination of propagation parameters $\Gamma$ and $Z_a$ .....	25
2.6 Summary.....	30

## Chapter 3

<b>Numerical Results.....</b>	<b>35</b>
3.1 Passive system.....	35

3.2 Numerical analysis of Active/Passive system.....	39
3.2.1 Direct minimization of reflected wave.....	40
3.2.2 Pressure-release boundary condition.....	41
3.2.3 Impedance-matching condition.....	43
3.3 Parametric Analysis.....	47
3.3.1 Effect of foam thickness on system performance.....	47
3.3.2 Effect of variation of airspace depth on system performance.....	48
3.4 Summary.....	49
 <b>Chapter 4</b>	
<b>Experimental Results.....</b>	<b>79</b>
4.1 Experimental setup .....	79
4.2 Direct minimization of reflected wave - Experimental study.....	82
4.3 Pressure-release boundary-condition - Experimental study.....	84
4.4 Impedance-matching condition - Experimental study.....	85
4.5 Effect of foam thickness on system performance - Experimental study.....	85
4.6 Feasibility of using other absorbing material - Experimental study.....	87
4.7 Summary.....	87
 <b>Chapter 5</b>	
<b>Conclusions and Recommendations.....</b>	<b>102</b>
Conclusions.....	102
Recommendations.....	104
 <b>List of References.....</b>	 <b>106</b>
 <b>Appendices.....</b>	 <b>108</b>
Appendix A: Determination of $\Gamma$ and $Z_a$ .....	109
Appendix B: Wave deconvolution.....	112
Appendix C: Adaptive controller .....	116
 Vita.....	 120

## LIST OF FIGURES

Figure	Page
2.1 Waves in the hybrid system two-layered media.....	17
2.2 Polynomial curve fit for propagation constant $\Gamma$ .....	31
2.3 Complex propagation constant for partially reticulated polyurethane foam.....	32
2.4 Complex characteristic impedance for partially reticulated polyurethane foam.....	33
2.5 Absorption coefficient of four different thickness samples rigidly backed samples...	34
3.1 Absorption coefficient of three different size samples rigidly backed.....	50
3.2 Absorption coefficient of three different size samples backed by airspace.....	51
3.3 Specific input impedance of passive system w/2.5cm foam layer & 10cm airspace..	52
3.4 Specific input impedance of passive system w/5.0cm foam layer & 10cm airspace..	53
3.5 Specific input impedance of passive system w/7.5cm foam layer & 10cm airspace..	54
3.6 Profile of specific impedance across two-layer passive system (freq. = 450Hz).....	55
3.7 Profile of specific impedance across two-layer passive system (freq. = 900Hz).....	56
3.8 Profile of specific impedance across two-layer passive system (freq. = 1380Hz).....	57
3.9 Profile of specific impedance across two-layer passive system (freq. = 1700Hz).....	58
3.10 Control wall velocity required for direct minimization of reflected wave.....	59
3.11 Control wall displacement required for direct minimization of reflected wave.....	60
3.12 Absorption coefficient due to pressure-release boundary condition.....	61
3.13 Control wall velocity required for pressure-release boundary condition.....	62
3.14 Control wall displacement required for pressure-release boundary condition .....	63
3.15 Specific input impedance of system due to pressure-release boundary condition....	64
3.16 Acoustic pressure reduction due to pressure-release boundary condition.....	65
3.17 Absorption coefficient due to impedance-matching condition.....	66
3.18 Control wall velocity required for active impedance-matching condition.....	67
3.19 Control wall displacement required for impedance-matching condition.....	68
3.20 Specific input impedance of system due to impedance-matching condition.....	69
3.21 Acoustic pressure reduction due to impedance-matching condition.....	70



3.22	Profile of specific impedance across system due to impedance-matching condition for frequency=450Hz.....	71
3.23	Profile of specific impedance across system due to impedance-matching condition for frequency=900Hz.....	72
3.24	Profile of specific impedance across system due to impedance-matching condition for frequency=1350Hz.....	73
3.25	Profile of specific impedance across system due to impedance-matching condition for frequency=1700Hz.....	74
3.26	Effect of change in foam sample thickness on absorption coefficient.....	75
3.27	Variation of control velocity requirement with foam sample thickness.....	76
3.28	Effect of airspace depth variation on absorption coefficient of system.....	77
3.29	Variation of control velocity requirement with airspace depth.....	78
4.1	Experiment setup.....	89
4.2	Laboratory experimental setup.....	90
4.3	Absorption coefficient of system due to direct minimization of reflected wave.....	91
4.4	Experimental setup for pressure-release boundary condition study.....	92
4.5	Absorption coefficient due to pressure-release boundary condition.....	93
4.6	Experimental setup for impedance-matching condition study.....	94
4.7	Detail of dual-microphone setup for wave separation.....	95
4.8	Absorption coefficient of system due to impedance-matching condition.....	96
4.9	Absorption coefficient of system with 2.5cm foam sample.....	97
4.10	Absorption coefficient of system with 5.0cm foam sample.....	98
4.11	Absorption coefficient of system with 7.5cm foam sample.....	99
4.12	Absorption coefficient of system using FELTMETAL and 7.5cm airspace.....	100
4.13	Absorption coefficient of system using FELTMETAL and 10.0cm airspace.....	101

## Chapter 1

### INTRODUCTION

The detrimental effects of noise on the health of human beings have been a concern of many researchers for the last few decades. More recently, psychological effects of noise on the performance of human beings have been more apparent. To this end, the Environmental Protection Agency (EPA) and the Occupation Safety and Health Administration (OSHA) publish numerous exposure limit indexes in order to protect the general population from hearing damage. As we learn more about the consequences of noise, the need for more effective noise abatement methods becomes evident.

In general, noise can be controlled in three different ways. These are: (i) reduction of noise at the source, (ii) control of noise transmission paths, and (iii) protection of the receiver [1]. Noise reduction at the source include surrounding the plant with an enclosure in order to prevent sound pressure from propagating. This process requires the *insulation* of sound. In addition to enclosures, the noise at the source can also be controlled by modifying the plant, which in general requires the redesign or replacement of parts. Controlling noise by altering its transmission path can be achieved using barriers. Barriers work by *reflecting* or *refracting* sound waves away from the transmission path between the noise source and the receiver. If controlling either the radiation or transmission of sound waves is not possible, the receiver could be protected using ear plugs, over-ear protectors or other devices. If the sound radiation is taking place within an enclosed room, the noise perceived by the receiver is usually higher than the noise generated by the source. This is because in addition to the direct transmission of noise from the source to the receiver, the reflection of sound waves from the walls results in a

reverberant or diffuse sound field. This sound field can be reduced through the use of sound absorbers. In this process, the interior reflecting surfaces of the room are fully or partially covered with sound absorbing materials. Generally, sound absorbing methods are classified either as dissipative absorbers such as glass fiber and foam, or reactive types such as panel and Helmholtz resonators.

These noise abatement approaches are generally referred to as 'passive noise control' methods. The focus of the work reported in this thesis is the absorption of sound. In particular, among the two types of absorbers, only the dissipative type are considered. Therefore, the phrases 'passive absorbers' or 'passive absorption' in this work will infer to the use of dissipative absorbers. Passive absorbers in general are more efficient in absorbing sound waves at the middle to higher frequency ranges. At low frequencies, these materials are not efficient absorbers and lead to bulky designs. More recently, the development of active noise control showed that noise could be effectively reduced at the lower frequencies. However, active control in general is not efficient in reducing noise at the higher frequencies.

With the complementary strengths and weaknesses of active and passive noise control methods, the rational direction of noise control research leads to a noise control system that can be used to suppress noise over a broad frequency range. Therefore, a hybrid noise control method that combines the features of both active and passive noise control methods would be valuable in the absorption of noise over a broad frequency range. The goal of this thesis is to present numerical and experimental studies done on such a system that efficiently integrates the features of both passive and active noise absorption methods. This system features a new control approach and has a potential to be implemented in a number of applications that include reverberation control in architectural acoustics and low frequency noise absorption in airplane fuselage.

## 1.1 Passive Noise Control - A brief review

Currently, passive noise control is the conventional way of dealing with noise problems. Passive control involves the use of sound absorption materials. Some of the popular absorbing materials include glassfiber and fully and partially reticulated polyurethane foams. Passive noise control is well understood and its wide applications in reverberation control include architecture, airplane trim panels, machine enclosures, and so forth.

Sound absorbing materials absorb sound in two different ways depending whether the acting sound wave has a low or high frequency. At high frequency, acoustic waves are absorbed in two different ways. First, the impinging sound pressure oscillates the air molecules within the material. These oscillations result in frictional loss of the sound pressure amplitude [17]. Tortuosity is the second way by which sound is absorbed in passive materials. Tortuosity is defined as the deflection from a straight line and the pores in an absorptive material are highly tortuous. This effect results in changes in the flow direction of the acting sound wave. In addition, the irregular shape and size of the pores result in rapid compression and expansion of the acting wave. These two phenomena, tortuosity and irregularity of the pores, result in the loss of momentum of the wave leading to further absorption of the acting wave [17]. At low frequency, the periodic compression and expansion of the acting wave is accompanied by temperature change. During the temperature fluctuation, some of the acoustic energy of the wave is converted into heat energy leading to partial absorption of the acting wave [2].

Sound absorbing materials are efficient ways of reducing noise at the middle to higher frequencies. However, at low frequencies thick and bulky materials are required. In general the thickness of an absorptive material should be at least one fourth of the wave length of the acting wave. For example, in order to absorb a sound wave of 1000 Hz

frequency, 8.6 cm thick material is required. However, in order to absorb a 100 Hz sound wave moderately, more than 86 cm thick material is required. It is obvious that the use of bulky materials is not acceptable for applications such as airplane trim panels where compact and light weight materials are desired. Therefore, using passive control methods in order to reduce low frequency noise is not only inefficient but also not practical.

## **1.2 Active Noise Control (ANC) - A brief review**

Numerous papers have been published on the subject of active noise control. In particular, Guicking presents a complete historical background [3] and Nelson and Elliott have published several papers on this field covering every aspect of active control system design [4, 5]. For completeness, a brief explanation of the fundamental concept of ANC and its limiting weakness will be presented.

The principle of ANC dates back to the 1930's. Dr. Paul Lueg, a German physicist filed the first patent on active sound control in 1934 [6]. Not only did Lueg describe the principle of ANC in his patent application, but he also included recommendations for non-sinusoidal sound and for three-dimensional sound fields. This patent gives Lueg the recognition that he was the first person who clearly understood and described the principle of active noise control. Guicking, in his historical report on the invention of active noise control, presents a brief history of Lueg and his patent [3]. The study of active noise control has gone through different phases of an evolutionary process since Lueg's work. For almost two decades after Lueg's patent, no improvement was made on the basic concept of ANC and no applications were reported. In 1950's several applications of active noise control were reported. One of the landmark papers on this subject was published in 1953 by Harry Olson and Everet May. Olson and May published a paper on the application of an active control system to suppress noise in cars and aircraft

[7]. Their system employed a simple feedback control. Three years later in 1956, William Conover published a paper on the control of sound radiated by large transformers using feed-forward control based active system [8]. In the 1980's the introduction of faster signal processing systems resulted numerous developments in this field. Warnaka presents a concise review of work done on active control over the first fifty years after its conception [9].

The principle of active noise cancellation is simple. In order to cancel an unwanted acoustic signal, another signal 180 degrees-out-of phase to the original signal but of equal magnitude is created and superimposed with the original signal. The result is a destructive interference of the two waves. The requirement that the secondary or control signal should be an exact mirror replica of the primary signal is referred by Nelson and Elliot as *temporal constraint* [4]. In addition to the temporal constraint, a *spatial constraint* is required for a global control of sound field to take place. Spatial constraint is more complicated than the temporal requirement. This constraint requires that the secondary wave should match the primary wave both in time and in space. Therefore, despite the simplicity of the principle of superposition, both temporal and spatial constraints should be met for a global destructive interference of two signals to take place [4].

Spatial constraint can be met by having the separation between the primary and secondary sources to be smaller than, or at most of the same order as a quarter of the acoustic wavelength  $\lambda$ . This physical restriction imposes an upper frequency limitation on the effective operation of active sound control. For example, to cancel a 100 Hz acoustic signal, the separation between the primary and secondary waves should be about 0.86 meters. However, to cancel a 10000 Hz acoustic signal, the separation should be in the order of 0.85 millimeters, which is not easy to accomplish nor practical to implement. Therefore, active control of sound is efficient only for relatively low frequencies. As the

frequency is increased, the efficiency of active sound control progressively diminishes due to the spatial constraint described above. In addition to the high frequency limitation, ANC suffers from constructive interference of the sound field at points other than the “zone of quiet” where the error sensor is located. Olson and May [7] suggested close positioning of the primary and secondary sound sources to remedy this problem. Their arrangement introduced some design implications but showed better coupling of the two sources and the pressure at points further away from the secondary source was not significantly affected. Therefore, even with Olson and May’s arrangement, the pressure at points further away from the vicinity of the “zone of quiet” was only left unaffected and “global” sound reduction was not possible.

One of the physical configurations in which the spatial matching is easier to meet is the one-dimensional case of plane sound waves propagating in a duct. Note this was the first case to be investigated for active sound control by Lueg. Guicking used this concept to show the effectiveness of ANC in absorbing sound at the low frequencies [10]. His setup included a control loudspeaker attached to the open end of a standard impedance tube. The signal detected by a set of microphones located within the impedance tube was compensated for a time delay between the two signals. This enabled Guicking to separate the incident and reflected waves within the tube. The incident wave signal was then sent to the control speaker after passing through a filtering amplifier with adjustable gain and phase shift. Using appropriate control settings, the reflected wave in the tube was controlled. The result of this experiment showed complete absorption of tonal plane waves over the frequency range 100Hz to 800Hz.

### 1.3 Hybrid Sound Control System - a literature review

As stated above, active and passive noise control methods have complementary strengths and weaknesses. In the last few years, many attempts have been made to integrate both methods in order to come up with a system that is effective in absorbing noise over a broad frequency range. Perhaps the first published work on a noise control system that comprises both active and passive control methods is that of Guicking and Lorenz [11]. Guicking and Lorenz described their experimental work as “an active equivalent of the quarter wavelength resonance absorber”. The passive component of this work comprised of a porous plate. The porous plate was located in an impedance tube a small distance from the open end of the tube. The open end of the tube was then terminated by a control speaker. Two microphones were located in the tube to detect the pressure field. The first microphone was located in front of the porous plate and the second was placed just behind it. The signal picked up by the first microphone in front of the porous plate is sent to the control speaker after it was passed through a combination of open-loop and closed-loop analog control schemes. The second microphone controls the complex amplification factor such that the sound pressure at that location is minimized. A total of four different commercially available porous plates were investigated. Almost total absorption of the acoustic energy was reported over the frequency range 100Hz to 700Hz. The performance of this system was not reported for high frequencies. The trend in the sound pressure reduction showed the absorption of the system declines with increase in frequency. Nevertheless, this work has inspired many into using the same technique for other applications and opened the way for a hybrid noise control research.

Howarth, *et al.*, [12] implemented Guicking’s concept into an active composite coating for reflection control for underwater applications. Their “active acoustic coating” is composed of a piezocomposite actuator, a layer of elastomer, and two layers of PVDF



films. The dual sensor arrangement is used to separate the incident and reflected components of an acoustic field. The piezocomposite is then actuated to minimize the reflected wave. An echo reduction of up to 58dB was reported for a frequency range of 3.75kHz to 11kHz. A similar commercial version of the active acoustic coating designated as “piezorubber” is described by Lafleur, *et al.*, [13].

Bolton and Green [14] presented a theory that showed the possibility of the improvement of low frequency performance of a finite-depth layer of elastic porous material by applying an appropriate force to the solid phase at the front surface of the layer. Their work showed that the solid phase of the foam can be forced so as to create a perfect impedance match with the incident plane wave, thus causing the incident wave to be completely absorbed. They presented the force, displacement, and control power required for a specific “smart foam” configuration. Again, Bolton and Green’s work is only theoretical and no experimental results were reported.

Thenail, *et al.*, [15] presented a work that includes a fiberglass layer and an active control scheme. Their work was intended to show that a zero pressure condition on the back surface of the fiberglass leads to improvement in absorption. They investigated two different control approaches. In the first control approach, an error microphone was located on the back surface of the fiberglass layer and the pressure at that location minimized using a standard ‘bi-quad’ analog filter with two poles and two zeros. The result of this study showed an improvement of absorption that declines with increase in frequency. The result reported was for the frequency range of 200Hz to 800Hz. The second control approach included was similar to Guicking’s work with only two exceptions. Guicking’s porous plate was replaced with the fiberglass layer and instead of the open/closed control scheme, a ‘bi-quad’ analog filter was employed. The two microphones were arranged in front and behind the fiberglass layer. Their results show

almost total absorption for the frequency range of 500Hz to 1400Hz. Therefore, the two control methods they investigated in improving the absorption of the fiberglass layer work either at the low frequency range of 200Hz - 800Hz, or the middle-high frequency range of 500Hz - 1400Hz. The authors also have calculated an optimum layer fiberglass thickness of only 2cm for absorption at the low frequencies.

Fuller, *et al.*, [16] presented an experimental study done on the potential of an "adaptive foam" for radiation and reflection control. Their adaptive foam included a PVDF (Polyvinylidene fluoride) film imbedded in polyurethane foam in a sine wave shape. In the radiation control study, the noise source was a mechanical shaker located underneath a metal piston enclosed in a casing 0.76m tall with a diameter of 0.3m. The piston was exposed by a circular cavity on top of the casing. The activation of the shaker creates a radiation pattern that is similar to a monopole radiation in half space. The adaptive foam was placed in the exposed cavity. The error detector for their experiment was a circular piece of PVDF film mounted on top of the adaptive foam. A control signal generated by a Filtered-x LMS controller was then sent to the adaptive foam where the embedded PVDF film was used as a control sound source in order to cancel the radiated field. Although a frequency range of 70Hz to 400Hz was mentioned, the result provided was only for a frequency of 340Hz.

In the reflection control experiment, the adaptive foam was positioned at the open end of an impedance tube. Two identical microphones were located close to the adaptive foam and the signals detected by these microphones were sent to a wave deconvolution circuit. The incident and reflected waves in the tube were separated using the wave deconvolution circuit and the reflected wave signal was minimized. The experiment performed was for a frequency range of 100Hz to 1000Hz. At frequencies above 600Hz, an attenuation of upto 40 dB was reported. At frequencies between 150Hz and 300Hz, a

10 db attenuation was achieved with the adaptive foam. Without active control, the authors mentioned that the passive attenuation of the adaptive foam is low. From the author's experience, imbedding PVDF film in polyurethane foam reduces the passive absorption property of the foam. This is because incident waves are reflected back by the film due to its impermeable nature. Therefore, embedding a PVDF film in a foam sample may not be worthwhile because it severely compromises its passive absorption.

#### **1.4 Proposed Passive/Active noise control system**

In the above mentioned hybrid systems, the noise absorption achieved was either at the low frequency range, as in the systems described by Guicking or the middle-high frequency range as the system described by Thenail. The proposed hybrid noise absorption system in this work will be effective in achieving optimum absorption of noise over a wide frequency range that includes both low and high frequencies. This system will be based on an efficient integration of both passive and active noise control methods.

The Passive/Active system proposed here is based on the simple concept of mounting a layer of sound absorbing material at a distance from a rigid wall, creating an airspace between the absorber and the rigid wall. This concept is well understood and widely used in practice. The presence of the airspace results in high absorption peaks at some frequencies and low absorption at others. The location of the high and low absorption bands is a function of the depth of the airspace. The high absorption occurs in general when the depth of the airspace is a quarter wavelength of the operating frequency. Subsequent absorption peaks occur at odd multiples of the frequency. The low absorption occur when the depth is one half wavelength of the operating frequency and succeeding absorption lows occur at even multiples of the frequency. Therefore, the depth of the airspace has to be adjusted with change in frequency in order to take advantage of the

absorption peaks. In addition, at the lower frequencies the required airspace depth for maximum absorption tends to be large.

In the proposed Passive/Active system, the rigid wall is replaced with an active wall. Three different control approaches were investigated to determine the velocity of the active wall required for maximum absorption over a broad frequency range. A simple useful numerical model was developed to simulate the performance of the Passive/Active system for the three control strategies. The control approach selected for the system include the minimization of the reflected wave in the airspace. This condition leads to the matching of the impedance in the airspace to that of a plane wave propagating in air. This impedance-matching condition resulted in a consistent maximum absorption of 0.89 - 1.0 over the frequency range 100Hz - 2000Hz. Experimental studies performed validated the developed model. In the experimental study, the sound absorber, a layer of polyurethane foam was placed within an impedance tube and the open end of the tube fitted with a control speaker. Two microphones and a wave deconvolution circuit were employed to isolate the reflected wave signal that needed to be minimized. The two microphones were both placed in the airspace instead of being positioned in front and behind the passive absorber as in Guicking's and Thenail's work, or both microphones in front of the absorber as the system described by Fuller. This system has many advantages over the hybrid systems mentioned above. First, the Passive/Active system is effective in absorbing sound over an extended frequency range that include both low and high frequencies. Second, the necessary actuator and sensors are all contained within the airspace and the system could be designed in a compact and packaged form.

Parametric analysis of the proposed Passive/Active system showed, the system is not sensitive to changes in airspace depth and is only marginally sensitive to changes in sound absorber thickness. Further, the robustness of the system was demonstrated by

replacing the polyurethane absorber by a porous metal sheet, commercial name FELTMETAL, in the experimental study. The result showed a consistent absorption coefficient of 0.8 - 0.9 throughout the frequency range of 100Hz to 2000Hz. In summary, the proposed Passive/Active system features a new control approach. The system showed optimum absorption of noise over a wide frequency range and parametric analysis showed that the system could be designed in a compact, self-contained unit even for low frequency absorption.

## **1.5 Overview of Thesis**

This thesis is organized in five chapters. In Chapter 2, the derivation of the numerical model of the Passive/Active noise control system is presented. The three Passive/Active control strategies investigated are also described. The characterization of the sound absorber layer was based on its propagation parameters. These parameters along with the method employed in obtaining them are also presented in Chapter 2. In chapter 3, the validation of the developed model is presented in detail. The performance of the model for the three different control strategies is investigated. The impedance-matching control approach is selected for the Passive/Active system and the performance of this control strategy is then investigated for different absorbing material and airspace sizes. In order to validate the model, different experiments were carried out and the results can be found in Chapter 4. The robustness of the developed Passive/Active system was demonstrated experimentally for a different passive absorber and the result of this experiment can also be found in chapter 4. Comparison between theoretical and experimental results showed good agreement. Finally, the conclusion and some recommendations for future work are outlined in Chapter 5. Appendix A contains description of the method employed to determine the propagation parameters of the sound

absorbing layer. In Appendix B, a description of a wave separation method employed during this work is presented. The adaptive controller used in the experimental study is briefly discussed in Appendix C.

## Chapter 2

### ANALYTICAL MODEL

As it has been shown by Zwicker and Kosten and many others in the field of acoustics, sound-absorbing materials can be fully characterized using only two of their acoustic properties, mainly the complex characteristic impedance  $Z_a$  and the complex propagation constant  $\Gamma$  [17]. The simulation of the Passive/Active noise control system is based on a simple useful model centered around these two propagation parameters. The goal of developing the model is to numerically analyze the performance of the Passive/Active system, to investigate different control approaches and select the most appropriate control strategy and to perform parametric analysis of the system for sensitivity studies. In this chapter, the model will first be presented and three different control strategies proposed. The method employed in obtaining the two propagation parameters will then be described and the accuracy of the determined parameters validated. Only normally incident plane waves will be considered in all formulation.

#### 2.1 Derivation of Analytical Model

The Passive/Active system is modeled as a two-layer media where the first medium is a layer of a sound absorbing material and the second medium is a cavity of air backed by an active wall as shown in Fig. 2.1. The fluid in front of the foam sample is also assumed to be air. All of the fundamental equations of acoustics for wave transmission through the two-layer media and all the boundary conditions that apply to such a system will be defined. The control approach in the Passive/Active system is to determine the active wall velocity required for maximum absorption over a broad frequency range.

When a plane wave is incident on a boundary between two media, some of the incident wave is reflected and some is transmitted through the boundary. The incident wave  $p_i$  and reflected wave  $p_r$  at the front surface of the foam may be represented in their exponential form as:

$$p_i(x,t) = A_1 e^{i(\omega t - k_o x)} = A_1 e^{-ik_o x} e^{i\omega t} \quad (2.1.a)$$

$$p_r(x,t) = B_1 e^{i(\omega t + k_o x)} = B_1 e^{ik_o x} e^{i\omega t} \quad (2.1.b)$$

The coefficients  $A_1$  and  $B_1$  are wave amplitudes of the incident and reflected waves. The angular frequency  $\omega = 2\pi f$ , where  $f$  is the frequency of the acoustic wave. The wave number for air is given by  $k_o = \omega/c_o$ ,  $c_o$  being the speed of sound in air.

The particle velocity for planar harmonic waves can be derived as  $v = \pm p/Z$  by integrating Euler's equation given below for  $v$ .

$$\left( \frac{\partial p}{\partial x} = -\rho \frac{\partial v}{\partial t} \right) \quad (2.2)$$

Here, the + and - signs represent right and left traveling waves,  $p$  stands for sound pressure and  $Z$  is the characteristic impedance of the medium. The characteristic impedance of air for plane waves is  $\rho c_o$  where  $\rho$  is the density of air. Therefore, using equation 2.2 the particle velocity of the pressure waves given above are:

$$v_{+1}(x,t) = \frac{A_1 e^{-ik_o x} e^{i\omega t}}{\rho c_o} \quad (2.3.a)$$

$$v_{-1}(x,t) = -\frac{B_1 e^{ik_o x} e^{i\omega t}}{\rho c_o} \quad (2.3.b)$$

In the absorbing material layer, again both positive and negative traveling waves exist. These waves have the same form as the waves expressed above for air except the



the wave constant  $k_o$  is replaced by a propagation constant  $\Gamma$  and the impedance of air  $\rho c_o$  is replaced by the characteristic impedance of the absorbing layer  $Z_a$ . Due to the dissipative nature of the polyurethane foam, the propagation constant  $\Gamma$  is complex and can be expressed as  $\Gamma = \alpha + ik_a$ . The real part,  $\alpha$  is called the attenuation constant and defines the dissipative nature of the material. The imaginary part,  $k_a$  is called the phase constant and represents the wave number within the material. The pressure waves in the absorbing layer along with their corresponding particle velocities can be expressed as [17]:

$$p_{+2}(x,t) = A_2 e^{-\Gamma x} e^{i\omega t} \quad (2.4.a)$$

$$p_{-2}(x,t) = B_2 e^{\Gamma x} e^{i\omega t} \quad (2.4.b)$$

$$v_{+2}(x,t) = \frac{A_2 e^{-\Gamma x} e^{i\omega t}}{Z_a} \quad (2.5.a)$$

$$v_{-2}(x,t) = -\frac{B_2 e^{\Gamma x} e^{i\omega t}}{Z_a} \quad (2.5.b)$$

The second medium in the two-layer model is an air cavity, the pressure and velocity equations for this case will be similar to equations (2.1.a, b) and can be expressed as:

$$p_{+3}(x,t) = A_3 e^{-ik_o x} e^{i\omega t} \quad (2.6.a)$$

$$p_{-3}(x,t) = B_3 e^{ik_o x} e^{i\omega t} \quad (2.6.b)$$

$$v_{+3}(x,t) = \frac{A_3 e^{-ik_o x} e^{i\omega t}}{\rho c_o} \quad (2.7.a)$$

$$v_{-3}(x,t) = -\frac{B_3 e^{ik_o x} e^{i\omega t}}{\rho c_o} \quad (2.7.b)$$

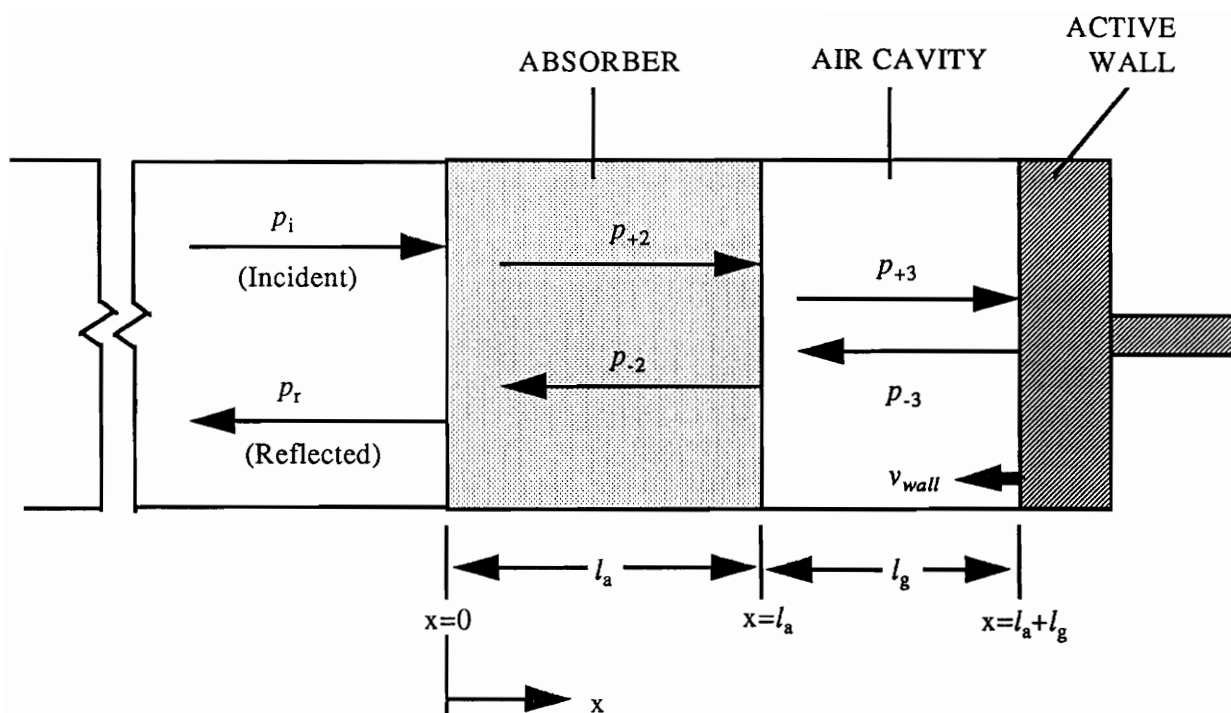


Fig. 2.1 Waves in the hybrid system two-layered model

## 2.2 Boundary Conditions

At the boundary between two different materials, the velocity and pressure must change continuously from one medium to the other. This leads to the conditions of continuity of pressure and particle velocity at the boundaries of the two-layer model. Since the time dependent term  $e^{i\omega t}$  is present in all equations, it will be omitted for simplicity in the following equations. There are five boundary conditions in the two-layer model and these boundary conditions are as follows.

- i. Continuity of pressure at the front surface of the absorber layer ( $x=0$ ) leads to:

$$p_i(0,t) + p_r(0,t) = p_{+2}(0,t) + p_{-2}(0,t) \quad (2.8)$$

$$A_1 + B_1 = A_2 + B_2 \quad (2.9)$$

- ii. Continuity of velocity at front surface of the absorber layer ( $x=0$ ) leads to:

$$v_i(0,t) + v_r(0,t) = v_{+2}(0,t) + v_{-2}(0,t) \quad (2.10)$$

$$\frac{A_1 - B_1}{\rho c} = \frac{A_2 - B_2}{Z_a} \quad (2.11)$$

- iii. Continuity of pressure at interface between absorber and airspace ( $x=l_a$ ) results in;

$$p_{+2}(l_a,t) + p_{-2}(l_a,t) = p_{+3}(l_a,t) + p_{-3}(l_a,t) \quad (2.12)$$

$$A_2 e^{-\Gamma l_a} + B_2 e^{\Gamma l_a} = A_3 e^{-ik_a l_a} + B_3 e^{ik_a l_a} \quad (2.13)$$

- iv. Continuity of velocity at interface between absorber and airspace ( $x=l_a$ );

$$v_{+2}(l_a,t) + v_{-2}(l_a,t) = v_{+3}(l_a,t) + v_{-3}(l_a,t) \quad (2.14)$$

$$\frac{A_2 e^{-\Gamma l_a} - B_2 e^{\Gamma l_a}}{Z_a} = \frac{A_3 e^{-ik_a l_a} - B_3 e^{ik_a l_a}}{\rho c} \quad (2.15)$$

v. Continuity of velocity at interface between airspace and active wall ( $x = l_a + l_g$ ):

$$v_{+3}(l_a + l_g, t) + v_{-3}(l_a + l_g, t) = v_{wall} \quad (2.16)$$

$$\frac{A_3 e^{-ik_o(l_a + l_g)}}{\rho c} - \frac{B_3 e^{ik_o(l_a + l_g)}}{\rho c} = v_{wall} \quad (2.17)$$

where  $v_{wall}$ , the velocity of the active wall is the control input to be determined for optimum absorption. The boundary conditions represented by equations 2.8 to 2.17 can be expressed in matrix form as:

$$[H]\{W\} = \{P_d\}A_1 + \{P_c\}v_{wall} \quad (2.18)$$

where,  $A_1$  represents the disturbance input

$v_{wall}$  is the control input

$$\{W\} = \{B_1, A_2, B_2, A_3, B_3\}^T$$

is a vector of waves wave amplitudes

$$\{P_d\} = \left\{ -1, \frac{-1}{\rho c_o}, 0, 0, 0 \right\}^T$$

is a vector of waves due to disturbance

$$\{P_c\} = \{0, 0, 0, 0, 1\}^T$$

is a vector of waves due to control input

and  $[H]$  is a matrix given as:

$$[H] = \begin{bmatrix} 1 & -1 & -1 & 0 & 0 \\ \frac{-1}{\rho c} & \frac{-1}{Z_a} & \frac{1}{Z_a} & 0 & 0 \\ 0 & e^{-\Gamma l_s} & e^{\Gamma l_s} & -e^{-ikl_s} & -e^{ikl_s} \\ 0 & \frac{e^{-\Gamma l_s}}{Z_a} & -\frac{e^{\Gamma l_s}}{Z_a} & \frac{-e^{-ikl_s}}{\rho c_o} & \frac{e^{ikl_s}}{\rho c_o} \\ 0 & 0 & 0 & \frac{e^{-ik(l_s+l_s)}}{\rho c_o} & \frac{-e^{ik(l_s+l_s)}}{\rho c_o} \end{bmatrix}$$

Inverting matrix  $\{H\}$ , the wave amplitudes due to the disturbance input  $A_1$  and control input  $v_{wall}$  could be determined as shown below:

$$\{W_d\} = [H]^{-1} \{P_d\} A_1 \quad (2.19)$$

$$\{W_c\} = [H]^{-1} \{P_c\} v_{wall} \quad (2.20)$$

The vector  $\{W\}$  expressed in equation 2.18 could now be re-written as:

$$\{W\} = \{W_d\} + \{W_c\} \quad (2.21)$$

Now the acoustic pressure and velocity at any location within the two-layer model can be expressed as a function of the disturbance input, incident wave amplitude  $A_1$ , and the control input  $v_{wall}$ . The disturbance input, incident wave amplitude  $A_1$ , was assumed to have a magnitude of unity. An acoustic wave with amplitude of unity corresponds to a sound pressure level of 90.97 dB.

## 2.3 Control strategies

Three different control strategies were considered for determining the wall velocity  $v_{wall}$  required for maximum absorption over a broad frequency range. In the first control strategy, the control wall velocity  $v_{wall}$  necessary for directly cancelling the total reflected wave  $p_r$ , was determined. This control approach represents the ideal performance of the Passive/Active system. In the second control strategy, a pressure-release boundary condition was induced on the back surface of the foam at  $x=l_a$  and the wall velocity  $v_{wall}$  required to maintain such boundary condition over a wide frequency range determined. In the third control approach, the reflected wave within the airspace,  $p_3$  as shown in Fig. 2.1 was minimized. This condition leads to a match between the airspace impedance and the impedance of a plane wave in air,  $\rho c_o$ , and will be appropriately referred to as “impedance-matching condition”. In experimental studies, these control approaches correspond to different error signal sensing strategies.

### 2.3.1 Direct minimization of reflected wave - Ideal performance

The first control strategy to be studied is the direct minimization of the total reflected wave,  $p_r$  in front of the sound absorbing layer. This case simulates the ideal performance of the Passive/Active system at any given frequency. This arrangement is similar to the many ANC applications where the error sensor is located in or near the desired “zone of quiet”. Since there are two sets of incident and reflected waves at any location within the two-layer media due to the disturbance and the control input, the total reflected wave  $p_r(x,t)$  to be minimized can be expressed as:

$$p_r(x,t) = B_{1d} + B_{1c} * v_{wall} \quad (2.22)$$

where  $B_{1d}$  and  $B_{1c}$  represent the reflected waves due to the disturbance and the control input, respectively. Since the total reflected wave  $p_r$  is to be minimized, setting Equation 2.22 to zero, the wall velocity  $v_{wall}$  for this case is determined as follows:

$$v_{wall} = -\frac{B_{1d}}{B_{1c}} \quad (2.23)$$

### 2.3.2 Pressure-release boundary condition

The second control strategy to be studied is the presence of a pressure-release boundary condition on the back surface of the material sample at  $x=l_a$ . A pressure-release boundary condition is created when an acoustic wave propagating from one medium to another is reflected back with  $180^\circ$  phase shift at the interface. Since, the amplitude of the incident and reflected waves are the same, the interaction of the two waves results in zero acoustic pressure at the interface. Therefore, this boundary condition can be created by minimizing the total pressure  $p_t$  at the interface between the absorbing material and the airspace,  $x=l_a$ . Due to the continuity of pressure at this interface, the total pressure  $p_t$  could be determined as the summation of the incident and reflected waves on either side of the boundary. The airspace side of the boundary is considered in calculating the total pressure  $p_t$  which is given below.

$$p_t(x=l_a, t) = (A_{3d} + B_{3d}) + (A_{3c} + B_{3c})v_{wall} \quad (2.24)$$

where  $A_{3d}$  and  $B_{3d}$  are the positive and negative traveling wave amplitudes due to the disturbance, and  $A_{3c}$  and  $B_{3c}$  are those due to the control input. Setting equation 2.24 to zero, the wall velocity  $v_{wall}$  for this case is determined as follows,

$$v_{wall} = - \frac{(A_{3d} + B_{3d})}{(A_{3c} + B_{3c})} \quad (2.25)$$

### 2.3.3 Impedance-matching condition

The third case to be modeled is the minimization of the reflected wave in the airspace. This condition leads to a matching of the airspace impedance to the impedance of a plane wave in air,  $\rho c_o$ . The reason that a one-directional plane wave propagating in air has a constant impedance  $\rho c_o$  is due to the absence of a reflected wave. Therefore, the impedance of any plane wave in a confined structure could be matched to  $\rho c_o$  if all reflected waves are minimized. The impedance-matching control strategy for the Passive/Active system will be achieved by minimizing the reflected wave in the airspace.

The total reflected wave in the airspace,  $p_{.3}$  is the summation of the reflected waves due to the disturbance and the control input as shown below:

$$P_{.3}(x,t) = B_{3d} + B_{3c} * v_{wall} \quad (2.26)$$

where,  $B_{3d}$  is the reflected wave due to disturbance and  $B_{3c}$  is due to the control input. Setting equation 2.26 to zero, the wall velocity  $v_{wall}$  for this case is determined as follows,

$$v_{wall} = - \frac{B_{3d}}{B_{3c}} \quad (2.27)$$



## 2.4 Calculation of acoustical properties

The primary acoustic property selected to study the performance of the Passive/Active system is the absorption coefficient  $\alpha$ . Absorption coefficient is the ratio of the absorbed energy to incident energy and can be calculated using the equation below.

$$\alpha = 1 - |R|^2 \quad (2.28)$$

where,  $R$  is the reflection coefficient and is defined for a plane sound field as the ratio of the reflected sound pressure to the incident sound pressure in front of a medium. The total reflected and incident pressure waves in front of the sound absorbing material,  $p_r$ , and  $p_i$ , can be expressed as:

$$p_i(x,t) = A_{ld}e^{-ik_o x}e^{i\omega t} + (A_{lc}e^{-ik_o x}e^{i\omega t}) * v_{wall} \quad (2.29)$$

$$p_r(x,t) = B_{ld}e^{ik_o x}e^{i\omega t} + (B_{lc}e^{ik_o x}e^{i\omega t}) * v_{wall} \quad (2.30)$$

where,  $A_{ld}$  and  $B_{ld}$  are incident and reflected waves due to the disturbance and  $A_{lc}$  and  $B_{lc}$  are incident and reflected waves due to the control input. Therefore, the reflection coefficient of the system can be expressed as:

$$R = \frac{p_r(x,t)}{p_i(x,t)} \quad (2.31)$$

In addition to the absorption coefficient,  $\alpha$ , other acoustic properties used in the analysis of the Passive/Active system include the wave impedance  $Z$  and the pressure

reduction in dB. The wave impedance at any location in the two-layer media can be determined from the pressure  $p$  and the particle velocity  $v$  of the wave as:

$$Z = \frac{p_{total}}{v_{total}} \quad (2.32)$$

The reduction in acoustic pressure,  $\gamma$ , achieved after active control is implemented could be calculated in terms of dB as,

$$\gamma = 10 \log_{10} \left( \frac{|B_{1d}|^2}{|B_1|^2} \right) \quad (2.33)$$

where,  $B_{1d}$  and  $B_1$  represent the amplitude of the reflected waves from the Passive/Active system before and after control was implemented. Simulation of the passive performance of the system before active control was implemented was achieved by setting the wall velocity  $v_{wall}$  in the model to zero to simulate a rigid backing.

## 2.5 Determination of $\Gamma$ and $Z_a$ - Pyett's method

The model for the Passive/Active system for the three different control strategies was developed in sections 2.1 and 2.2. The only unknown acoustic properties in the model are the propagation constant  $\Gamma$  and complex characteristic impedance  $Z_a$  of the absorber. The sound absorbing material chosen for the Passive/Active system was the partially reticulated polyurethane foam. The partially reticulated foam is a sound absorbing foam in which some of its cell membranes are removed in the manufacturing process. The partial removal of the members introduces a new phase in the attenuation process of the foam. The two phases of the partially reticulated foam are the solid or frame phase, and the fluid phase. One of the characteristics of this foam is its large

structure factor. Structure factor is a dimensionless number which takes into account the effect of the pores and cavities of a sound absorbing material that are perpendicular to the propagation direction of sound wave. This characteristic results in increases in the viscous and inertial effects which in turn result in a stronger coupling between the motions of frame and the fluid within the frame [17]. The presence of these two different motions makes the determination of some of the acoustic properties of partially reticulated foam complicated. Two manufacturers of these materials were requested to provide the propagation properties of their products. However, neither manufacture was able to supply the information requested and no published result was found in the literature that could provide the propagation properties of these materials. Thus, a number of different methods of determining the propagation parameters for the polyurethane foam were investigated. A simple and accurate method that can be implemented in a standard impedance tube was selected and is described below.

The method for determining  $\Gamma$  and  $Z_a$  adopted in this work was first derived by Pyett [18] and involves the deduction of  $\Gamma$  and  $Z_a$  from experimentally determined surface impedance of two samples of the same material but of different thickness. Pyett's method is derived in detail in Appendix A. However, some of the key equations will be repeated in this section.

The input impedance  $Z$  of a layer of absorbing material placed against a hard wall is given as [17]:

$$Z = Z_a \coth(\Gamma d) \quad (2.34)$$

where  $d$  is the thickness of the sample material. The input impedance  $Z$ , of a sample can be experimentally determined in an impedance tube using a standard acoustic property measuring technique such as the ASTM C384 or ASTM E1050. The two microphone

method (ASTM E1050) was selected for the determination of the input impedance of the two samples since it provides more accurate complex data. In this method, the sample is placed at one end of the impedance tube and at the other a speaker generates a random signal. The transfer function between the two identical microphones located close to the sample is then analyzed to decompose the incident and reflected wave components of the random signal. The complex reflection coefficient is then determined as follows [20]:

$$R = \frac{H - e^{-iks}}{e^{iks} - H} e^{i2k(l+s)} \quad (2.35)$$

where  $H$  = transfer function between the two microphones signals

$k_o$  = acoustic wave number,  $2\pi f / c_o$  ( $m^{-1}$ )

$c_o$  = speed of sound in air (345 m/s)

$f$  = frequency (Hz)

$l$  = distance from the test sample to the nearest microphone (m)

$s$  = spacing between microphones (m)

The input impedance is then calculated from the reflection coefficient as follows [19]:

$$Z = \frac{(1 + R)}{(1 - R)} \quad (2.36)$$

With the input impedance of the two samples,  $Z_1$  and  $Z_2$  measured, the ratio of these impedance was expressed using equation 2.34 as follows,

$$\frac{Z_1}{Z_2} = \frac{\coth(\Gamma d_1)}{\coth(\Gamma d_2)} \quad (2.37)$$

where,  $d_1$  and  $d_2$  are the thickness of the foam samples. Pyett have shown that the choice of the thickness ratio of the two samples should be two to one for simplification, i.e.  $d_2=2d_1$ . The two samples used were of thickness  $d_1=2.5\text{cm}$  and  $d_2=5.0\text{cm}$ . The only unknown variable in equation 2.37, the propagation constant  $\Gamma$ , can then be determined using some hyperbolic identities as shown in Appendix A from which the characteristic impedance  $Z_a$  be deduced from equation 2.34.

Although it was attempted to determine the values of  $\Gamma$  for the frequency range 100Hz - 2000Hz, accurate complex data could not be determined at the low frequency range of 100Hz - 450Hz. The reason accurate values were not determined at this frequency range was due to a phase mismatch between the particular microphones used in the measurement of the input impedance of the two samples. In order to determine the values of the complex propagation parameters at the lower frequencies, the magnitude and phase of the experimentally obtained propagation constant  $\Gamma$  were independently fitted with a two degree polynomial function using a linear regression analysis. The regression analysis used was based on least squares fit. The two polynomial functions were then combined to form the complex propagation constant  $\Gamma$  which was extrapolated to cover the lower frequencies. The characteristic impedance  $Z_a$  was then determined from the extrapolated data using Equation 2.34.

The values of  $\Gamma$  and  $Z_a$  for partially reticulated polyurethane foam can then be expressed as functions of frequency in polynomial form as:

$$\Gamma = a_2 f^2 + a_1 f + a_0 \quad (2.38)$$

$$Z_a = b_2 f^2 + b_1 f + b_0 \quad (2.39)$$

where  $f$  is frequency and the regression coefficients  $a_i$  and  $b_i$ ,  $i=0,1,2$  are:

$$\begin{aligned} a_2 &= -1.888*10^{-7} + 4.484*10^{-8}i & b_2 &= -1.266*10^{-8} + 8.560*10^{-8}i \\ a_1 &= 0.0084 + 0.0340i & b_1 &= 5.769*10^{-4} + 3.913*10^{-5}i \\ a_0 &= 1.0778 + 4.3688i & b_0 &= 1.0862 - 0.2814i \end{aligned}$$

Since both propagation parameters are complex, the determined coefficients of the polynomial equations are also complex. The experimentally determined magnitude and phase values of the propagation constant  $\Gamma$  along with the curve fit are presented in Fig. 2.2 as a function of frequency. Figure 2.3 shows the real and imaginary components of the propagation parameter  $\Gamma$  and the regression fit appears to be almost linear. The real and imaginary components of the characteristic impedance  $Z_a$  for the same material are presented in Fig. 2.4.

In order to show the accuracy of the determined propagation parameters, the model developed was used to simulate the absorption properties of four rigidly backed polyurethane foam samples of different thickness. To simulate the rigid backing, the airspace depth  $l_a$  and the wall velocity  $v_{wall}$  were set to zero in the developed model. The absorption coefficient of the same samples were then determined experimentally using the standing-wave measurement technique [22] and compared to the numerical results. These numerical and experimental absorption coefficient of the samples are shown in Fig. 2.5. The four samples studied include the primary samples from which  $\Gamma$  and  $Z_a$  were determined,  $d_1=2.5\text{cm}$  and  $d_2=5.0\text{cm}$ . Additional two samples, one smaller (1.25cm) and another larger (7.25cm) than the initial two samples were also studied. The results show strong agreement between the experimental and numerical results and verify the accuracy of the determined values of  $\Gamma$  and  $Z_a$ .

## 2.6 Summary

In this chapter, the model developed to simulate the Passive/Active noise control system was presented. Three different control strategies were considered for the system and a brief description of each one was presented. The passive component of the system, a layer of polyurethane foam was characterized using its propagation parameters. The two parameters, the propagation constant and the characteristic impedance of the foam, were determined and validated experimentally. The method employed in obtaining the propagation parameters was also discussed.

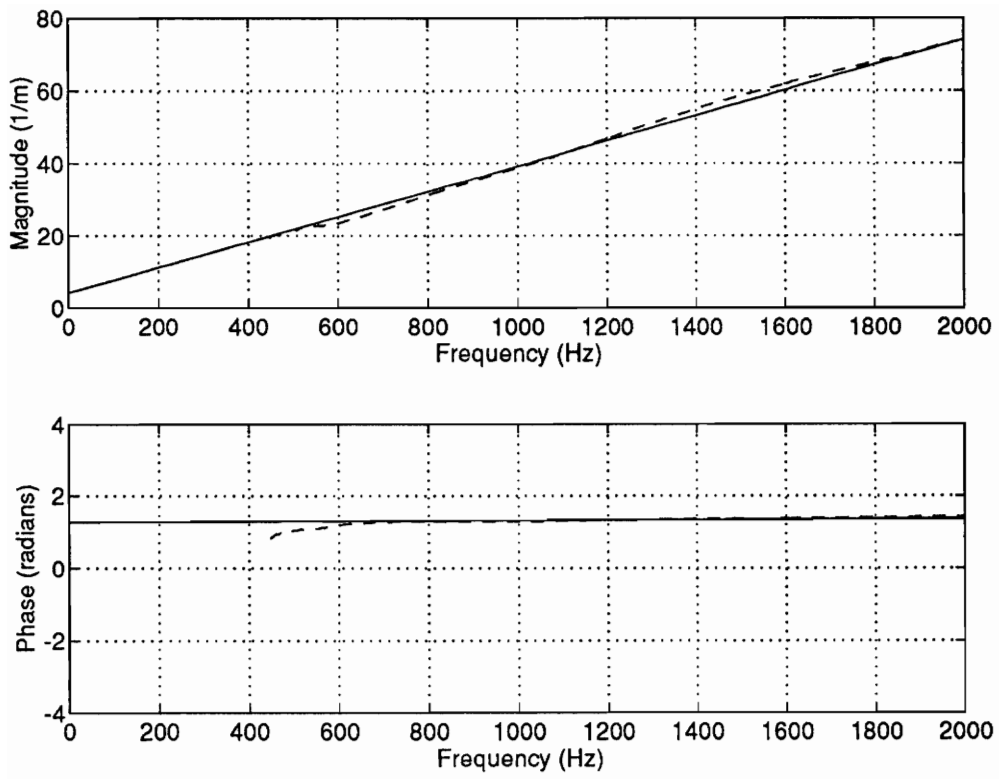


Fig. 2.2. Polynomial curve fit for propagation constant  $\Gamma$ .

--- experimental, \_\_ least squares fit



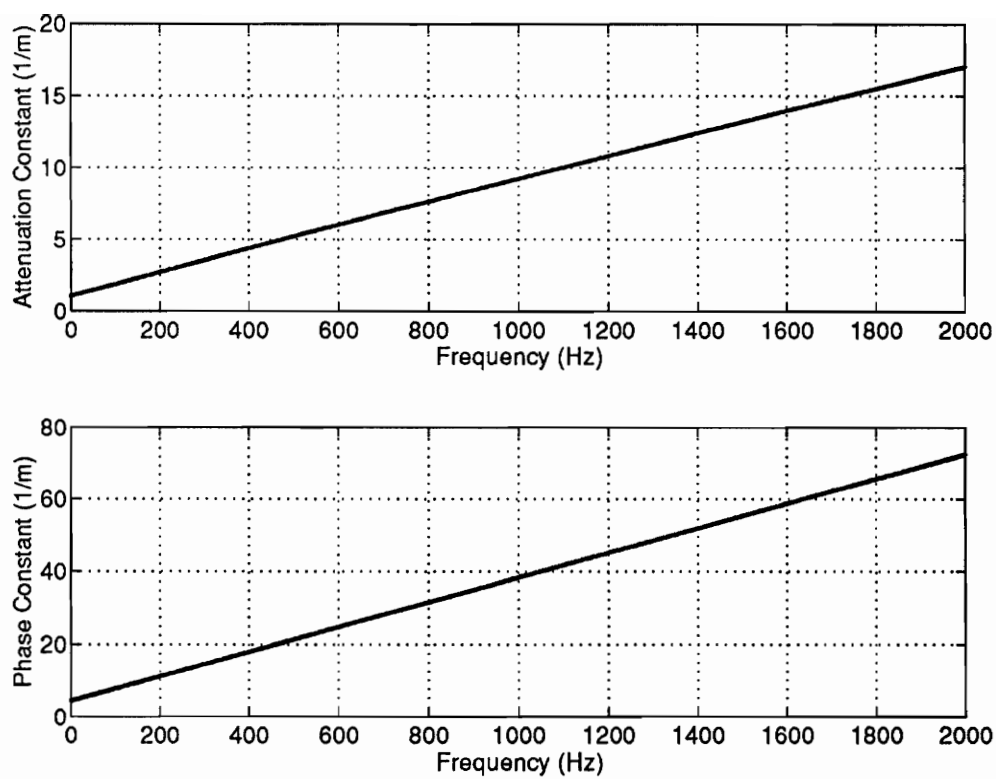


Fig. 2.3 Complex propagation constant  $\Gamma$  for partially reticulated polyurethane foam.

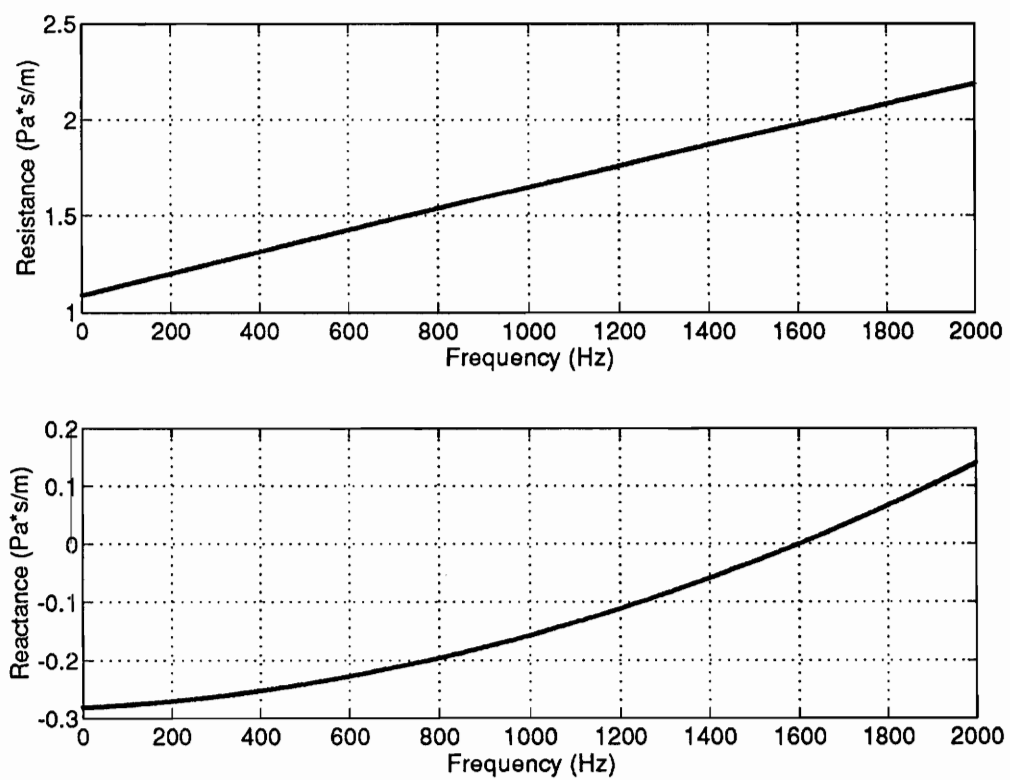


Fig 2.4 Complex characteristic impedance  $Z_a$  for partially reticulated polyurethane foam.

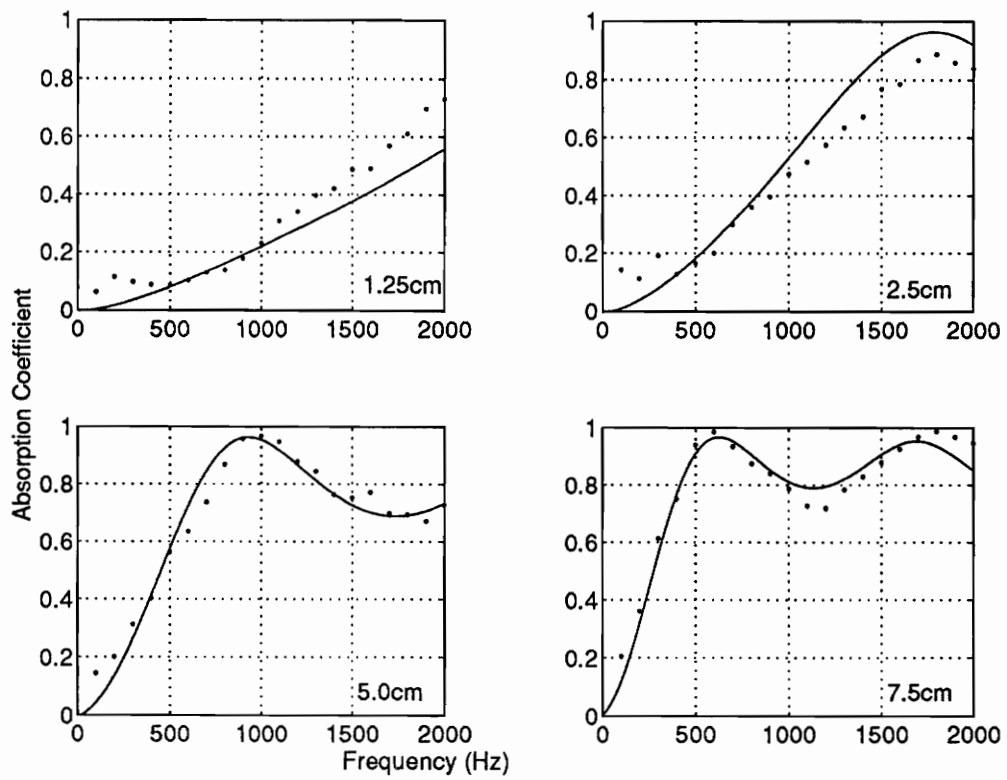


Fig. 2.5 Absorption coefficient of four different size samples backed by rigid wall.

... Experimental, — Numerical simulation

## CHAPTER 3

### NUMERICAL RESULTS

In chapter 2, the model developed for the Passive/Active system and the propagation parameters  $\Gamma$  and  $Z_a$  on which it is based were presented. Three potential control approaches for the Passive/Active system were also described. In this chapter, the model will first be used to investigate the absorption performance of a passive system. The absorption properties of foam samples rigidly backed will be studied followed by the same samples mounted at a distance from a wall. The Passive/Active system will then be studied for the three control strategies: (i) direct minimization of reflected wave, (ii) pressure-release boundary condition and (iii) impedance-matching condition. In studying the performance of the Passive/Active system, the primary parameter of interest was the absorption coefficient. Other properties investigated include the input impedance  $Z$ , control wall velocity  $v_{wall}$  and acoustic pressure reduction in dB.

#### 3.1 Passive System

In section 2.5, the numerical and experimental absorption coefficient  $\alpha$  of different samples was presented to show the accuracy of the determined propagation parameters. Some of the numerically determined absorption plots will be again presented in this section as part of the model validation. The absorption coefficients of three foam samples simply backed by a rigid wall is presented in Fig. 3.1. The three foam samples studied in this chapter were of thickness 2.5cm, 5.0cm and 7.5cm respectively. The general trend in absorption characteristic of all sound absorbing materials is that the absorption coefficient  $\alpha$  at the lower frequencies improves with increase in the sample thickness. This trend can

be observed in Fig. 3.1 where the absorption coefficient of the three samples is presented as a function of frequency. In getting these numerical results, the developed Passive/Active model was employed with the airspace depth and the velocity of the active wall set to zero to simulate rigid backing. Equations 2.16 - 2.19 were used by the model to calculate the absorption coefficient of the samples.

The absorption coefficient of the 2.5cm sample peaks to 0.95 at 1800Hz frequency. For the 5.0cm sample, the peak occurs at a lower frequency of 900Hz and significant improvement at the mid frequencies is observed over the absorption of the 2.5cm sample. Further improvement in absorption coefficient at the lower frequencies is observed with the 7.5cm sample, which peaks at 600Hz. The high absorption peaks follow the well known rule that maximum absorption occurs at frequencies when the thickness of the sound absorbing layer is in general a quarter of the wavelength of the operating frequency. Subsequent absorption peaks occur at odd multiples of the quarter wavelength. The general rule also states that low absorption occurs when the thickness of the sound absorbing layer is one half of the wavelength of the operating frequency. This rule also holds for the low absorption trends of the three samples shown in Fig. 3.1.

In Fig. 3.2, numerical absorption coefficient of the same foam samples backed by a 10cm airspace is presented. In determining the numerical absorption coefficient of the samples, the Passive/Active model was used with the velocity of the active wall set to zero. This arrangement is important since in practical applications, mounting sound absorbers at a distance from a rigid wall is sometimes favored than simply affixing them to the wall. The advantage of keeping the airspace behind the sound absorbing layer is characterized by improvement in absorption at low frequencies. Zwicker and Kosten theorize that the presence of the airspace decreases the stiffness of the air contents in the sound absorbing layer at these frequencies [17] which leads to improvement of absorption

coefficient at the lower frequencies. In addition to absorption improvement at the lower frequencies, narrow band absorption peaks occur with the presence of the airspace. These peaks in general occur when the depth of the airspace is a quarter wavelength of the operating frequency. However, narrow bands of low absorption are also introduced when the airspace is half of the wavelength of the operating frequency.

The absorption coefficient of the 2.5cm backed by the airspace peaks to 0.75 at 600Hz frequency. At this frequency, the absorption coefficient of the rigidly backed sample was observed to be only 0.25 in Fig. 3.1. However, the absorption coefficient at 1300Hz drops from 0.75 to 0.4 with the introduction of the airspace. The absorption coefficient of the 5.0cm sample backed by airspace shows the presence of a new absorption peak at 450Hz. However, at 900Hz the absorption coefficient drops from 0.95 to 0.63 with the introduction of the airspace. Again, for the 7.5cm sample, an improvement in absorption at the low frequencies with a peak at 350Hz is observed. The decline in absorption for this sample occurs at 650Hz.

The performance of the passive system could also be investigated by looking at the specific input impedance of the system at the front surface of the absorbing layer ( $x=0$ ). The definition of specific impedance is the wave impedance  $Z$  at a location normalized to that of air ( $Z / \rho c_0$ ). When the reflection of a wave impinging on a surface is desired to be minimum, the magnitude of the specific input impedance of the surface should closely match unity and the phase should be zero. This means that the surface should not resist the sound more than the unbounded air does [19]. The input impedance of a passive system with 5.0cm thick foam layer and 10cm airspace is presented in Fig. 3.4 as a function of frequency. Analogous to the absorption coefficient of the system, at 1350Hz where total absorption was observed, the magnitude of the specific impedance approaches unity and the phase is zero. Correspondingly, the magnitude of the specific impedance at

frequencies where low absorption occurred is maximum. The specific impedance of the passive systems with 2.5cm and 7.5cm thick foam samples as shown in Figs. 3.3 and 3.5 follow the same trend.

In order to fully understand the physics of the passive system, the wave specific impedance at every location across the two-layer system could be investigated at the frequencies where high and low absorption coefficient was observed. The profile of the specific impedance for these frequencies are presented in Figs. 3.6 - 3.9 for the passive system with the 5.0cm absorbing layer sample. In Fig. 3.6, a profile of the specific impedance across the two-layer media is presented for a frequency of 450Hz as a function of co-ordinate  $x$ . At this frequency, a high absorption coefficient was observed in Fig. 3.2 for the 5.0cm foam sample. The specific impedance in front of the system is shown between co-ordinates -0.1m and 0.0m. The location 0.0m to 0.5m shows the specific wave impedance across the 5cm thick sound absorbing layer and the 10cm airspace is represented between co-ordinates 0.5m and 1.5m. The specific input impedance of the system,  $x=0.0$ m, at this frequency is observed to be slightly lower than unity. The specific impedance on the back surface of the absorbing layer,  $x=0.05$ m, for the same frequency is observed to be almost one. At the rigid wall location,  $x=1.5$ m, the specific impedance is observed to be very large. This is because, at this location the particle velocity is zero due to the rigidity of the wall. Since impedance is defined as the ratio of pressure to particle velocity, the impedance at this location theoretically goes to infinity. In Fig. 3.7, the poor absorption of the passive system at 900Hz is shown by the high specific impedance at the front surface of the absorbing layer. The specific input impedance of the passive system at this frequency is about 3.5 times that of air. On the back surface of the absorbing layer, the specific input impedance of the system at this frequency was observed to be as low as 0.1. In Fig. 3.8, the specific impedance of the system is shown for a frequency of 1350Hz

as a function of co-ordinate  $x$ . At this frequency, total absorption was achieved due to passive control. This total absorption is indicated here by the specific impedance of unity at the front surface of the absorbing layer. The specific impedance on the back surface of the absorbing layer at this frequency is close to unity. The phase of the specific impedance at the same location is zero. Note the same condition was observed at 450Hz, another location of high absorption due to passive control. Figure 3.9 shows the profile of the specific impedance of the passive system for 1700Hz, a frequency associated with a low absorption coefficient. At this frequency, the input specific impedance of the system at  $x=0.0\text{m}$  is observed to be 3.2 times the optimum of unity. The specific impedance on the back surface of the absorbing layer at this frequency is observed to be very high indicating the presence of low particle velocity. Half way in the airspace, the phase of the specific impedance shifts by  $180^\circ$ .

In summary, mounting sound absorbing materials at a distance from a wall improves the absorption of the absorbers and could be an alternative to using bulky absorbers. However, this setup suffers from two weaknesses. First, the absorption peaks occur over relatively narrow frequency bands and bands of low absorption coefficient are also introduced. Therefore, wide frequency absorption cannot be achieved using this arrangement. Secondly, the depth of the airspace needs to be adjusted with change in frequency in order to take advantage of the absorption peaks. This is because the location of the peaks are related to the wavelength of the operating frequency.

### **3.2 Numerical analysis of Passive/Active system**

In the above section, the advantages and weaknesses of the passive system were presented. The Passive/Active model is based on the passive system described above, however instead of achieving absorption peaks over narrow frequency bands, the goal of



such a system is to achieve maximum absorption over a wide frequency range. To this end, three control approaches were investigated for the Passive/Active system. These control approaches were (i) direct minimization of the reflected wave, (ii) induction of pressure-release boundary condition on the back surface of the absorbing layer and (iii) impedance-matching condition. In the following sections, numerical results for each control strategy will be presented and analyzed. The control approach that gives wide frequency range absorption and is feasible from design point of view will then be selected for further investigation of the model. The system investigated in all three control cases was comprised of 5.0cm thick polyurethane foam and the airspace depth was set at 10cm. However, parametric studies involving different sound absorbing material thickness and airspace depth will be presented for the control strategy selected.

### **3.2.1 Direct minimization of reflected wave**

Direct minimization of the reflected wave simulates the optimum performance of the Active/Passive system since it signifies total absorption at any operating frequency. This control approach was accomplished by setting the total reflected wave in front of the sound absorbing layer,  $p_r$  to zero. The absorption coefficient  $\alpha$  of the model was then determined to be 1 over the whole frequency range of interest. The control wall velocity and displacement required for this case were investigated and are shown in Figs. 3.10 and 3.11 as functions of frequency. Figure 3.10 shows the magnitude and phase of the control wall velocity required to minimize the total reflected wave. For comparison, the required wall velocity for an active system is also plotted along with that for the Passive/Active system. In the latter case, the thickness of the passive absorber in the developed model was set to zero to simulate the absence of any passive absorption. For the Passive/Active system, the required wall velocity at 1350Hz is seen to be almost zero. This corresponds

with the total absorption already achieved at that frequency using passive control as shown in Fig. 3.2. Since, total absorption corresponds to zero reflection, at 1350Hz there is no reflected wave to be minimized and the control effort of the Passive/Active system at this frequency is zero. Similarly, the control velocity at the frequency of the second absorption peak, 450Hz is minimum. The control effort at frequencies 900Hz, 1700Hz and those under 400Hz was observed to be maximum. These frequencies coincide with the low absorption trend shown in Fig. 3.2 for the 5.0cm sample. Therefore, for optimum absorption, the active part of the Passive/Active system plays a bigger role at the frequencies where the absorption due to passive control is minimum. The phase of the control velocity shows a  $180^\circ$  shift at frequencies 450Hz and 1350Hz where the required wall velocity is minimum.

The control wall displacement required for directly minimizing the reflected wave is shown in Fig. 3.11 as a function of frequency. This figure shows that the required wall displacement increases with decreasing frequency. However, even at low frequencies the displacement is observed to be significantly small. For example to absorb a 100Hz wave, the wall would have to move a mere 0.22mm. Therefore, a practical application of the Passive/Active system would be successful even at the lower frequencies without the need for bulky and powerful control sound sources. Again direct minimization of the reflected wave represents the “ideal performance” of the Passive/Active system. The magnitude of the specific input impedance of this system is unity over the whole frequency range of interest and the phase is zero.

### 3.2.2 Pressure-release boundary condition

The second control approach to be investigated was the presence of a pressure-release boundary condition on the back surface of the sound absorbing layer,  $x = l_a$ . A

pressure-release boundary condition occurs when a wave incident at a boundary is reflected back with  $180^\circ$  phase shift at the boundary. The interaction of the two waves results in zero acoustic pressure *at the boundary*. This boundary condition has been successfully implemented in some active noise control applications in canceling noise at a given location. Here, it is investigated for sound absorption. This control approach was simulated by setting the total pressure  $p_t$  at  $x = l_a$  to zero. Due to the continuity of pressure at this location, the total pressure,  $p_t$  could be determined through the summation of the incident and reflected waves on either side of the boundary. The total pressure on the airspace side of the boundary was determined and minimized to simulate the pressure-release boundary condition. The total pressure  $p_t$  includes two sets of incident and reflected waves corresponding to the disturbance and the control input. The absorption coefficient of the pressure-release boundary simulation before and after control is presented in Fig. 3.12. As shown in the figure, the absorption coefficient below 200Hz was improved using the pressure-release boundary condition. However, a consistent of less than 0.8 absorption coefficient was observed throughout the rest of the frequency range of interest. Significant reduction in absorption was observed at 1300Hz and 2000Hz. Therefore, the pressure-release boundary condition as used in this work did not show any improvement in absorption of the system.

Figure 3.13 shows the wall velocity required to maintain the pressure-release boundary condition as a function of frequency. The observed high and low values of the control velocity do not coincide with the absorption coefficient of the passive system. The required wall displacement for this case is presented in Fig. 3.14 and at the low frequencies, it is greater than the displacement required for the “ideal performance” described in section 3.2.1. At 580Hz and 1700Hz frequencies, the control effort for this case was zero, and the system operates as a passive system. Therefore, the absorption

coefficient before and after control at this frequencies is the same as shown in Fig. 3.12. The specific input impedance of the system is presented in Fig. 3.15 and is observed to be high at the mid to high frequency range, an indication of poor absorption. The acoustic pressure reduction in dB in front of the sound absorbing layer is given in Fig. 3.16. A positive value in this figure indicates a reduction in the acoustic pressure. Therefore, the pressure-release boundary condition actually results in an increase in pressure outside of the system for most of the frequencies.

Pressure-release boundary condition is very practical for some active noise control technologies such as noise-canceling headsets [23]. In this application, the unwanted sound is filtered and minimized at the proximity of the ears. However, in the Passive/Active model, absorption of noise in front of the system is desired. Therefore, the pressure-release boundary condition as studied in this work is not a good control approach for the Passive/Active system.

### 3.2.3 Impedance-matching condition

The third control approach to be investigated is the matching of the incident wave impedance in the airspace, to the impedance of a plane wave in air,  $\rho c_0$ . As stated previously, the reason that a one-directional plane wave propagating in air has a constant impedance of  $\rho c_0$  is due to the absence of a reflected wave. Therefore, the impedance-matching control strategy for the Passive/Active system will be achieved by minimizing the reflected wave in the airspace.

Figure 3.17 shows before and after control absorption coefficient of the Passive/Active system due to the impedance-matching control approach. As the figure shows, the dynamic matching of the impedance in the airspace to the characteristic impedance of air  $\rho c_0$  successfully resulted in high absorption coefficient over the whole

frequency range of interest. Although, the absorption peaks at 1350Hz and 2000Hz due to passive control were slightly reduced with the introduction of the impedance-matching control approach, overall a consistent high absorption coefficient of 0.89 - 1.0 was achieved throughout the frequency range of interest. At frequencies below 200Hz, almost total absorption was observed.

The required control wall velocity and displacement for this case are shown in Figs. 3.18 and 3.19. Figure 3.18 shows the complex control wall velocity required to maintain the impedance-match as a function of frequency. At 450Hz, 1350Hz and 2000Hz where a high absorption was already achieved using passive control, the required control wall velocity is minimum. Interestingly enough, comparison of Figs. 3.10 and 3.18 shows that the control velocity requirement for the impedance-matching case is observed to be lower than the “ideal performance” at the mid to high frequency range, with the exception of 1350Hz.

Figure 3.19 shows the required control displacement of the active wall for the impedance-matching control strategy. Corresponding to the control wall velocity, the displacement requirement for this case was slightly lower than the ideal case at the mid to high frequency except at 1350Hz. At 100Hz, the control displacement required is observed to be 0.2mm, 0.02mm lower than the ideal case at that frequency.

In Fig. 3.20 the specific input impedance of the system is presented and is observed to be between the values of 1 and 2, an indication of strong absorption property of the system since the optimum specific impedance is unity. Note, the phase of the impedance is almost zero at any frequency. In Fig. 3.21, the positive acoustic pressure reduction in front of the sound absorbing layer is given for the impedance-matching control strategy. A maximum pressure reduction of 20dB is observed at 100Hz. At the frequency of 1350Hz, a sharp reduction of pressure is noted. This frequency corresponds to the total

absorption achieved using passive control. As Fig. 3.17 showed, the absorption coefficient at this frequency was reduced with the introduction of the active control. Overall, at frequency ranges 4Hz to 1250Hz and 1500Hz to 1900Hz, a positive reduction of acoustic pressure is observed. Therefore, this figure indicates that the minimization of the reflected wave in the airspace results in acoustic pressure reduction outside of the system.

In Fig. 3.22, a profile of the specific impedance across the two-layer media is presented for a frequency of 450Hz as a function of co-ordinate  $x$ . Both before and after control results are presented for comparison. The frequency of 450Hz is again a location of absorption peak due to passive control. The specific input impedance of the system,  $x=0.0\text{m}$ , was slightly lower than unity before active control. After control, the specific input impedance at this frequency is observed to be higher than unity by 0.6. Before control, the specific impedance on the back surface of the absorbing layer,  $x=0.05\text{m}$ , is observed to be almost one. After control, the specific impedance at any location within the airspace is unity. Note the phase after control is zero across the airspace. Therefore, the impedance-matching condition does not affect the impedance of the system at this location. In Fig. 3.23, a profile of the specific impedance across the two-layer media is presented for a frequency of 900Hz as a function of co-ordinate  $x$ . At this frequency, the absorption coefficient of the system before control was observed to be low. The high input specific impedance of 3.5 at the front surface of the absorbing layer,  $x=0.0\text{m}$ , before control is an indication of the poor absorption of the system before the impedance-matching condition was implemented. After control the specific input impedance was reduced to 1.9 at this location. On the back surface of the absorbing layer, the specific input impedance of the system at the same frequency was observed to be as low as 0.1. In Fig. 3.24, the profile of the specific impedance of the system is shown for a frequency of 1350Hz. At this frequency, total absorption was achieved due to passive control. This

total absorption is indicated by the specific impedance of unity at the front surface of the absorbing layer before control. After control, the specific impedance at the same location,  $x=0.0$ , was slightly increased to 1.75. This increase in input specific impedance at this frequency agrees with the small reduction of absorption noted in Fig. 3.17. Before control, the specific impedance on the back surface of the absorbing layer was observed to be close to unity. Note the same condition was observed at 450Hz, another location of high absorption due to passive control. Figure 3.25 shows the profile of the specific impedance across the system for 1700Hz, a frequency associated with a low absorption coefficient of the passive system. The input specific impedance of the system at this frequency before control was observed to be 3.2 times the optimum of unity. The specific impedance on the back surface of the absorbing layer at this frequency is observed to be very high indicating the presence of low particle velocity. Half way in the airspace, the phase of the specific impedance shifts by  $180^\circ$ . After control, the input specific impedance is reduced to 1.8. At frequencies where low absorption was observed, Figs. 3.23 and 3.25, the specific impedance on the back surface of the absorbing layer was either close to zero or infinity. At the frequencies of high absorption coefficient, Figs. 3.22 and 3.24, the specific impedance on the back surface of the absorbing layer was close to unity. Therefore, if total absorption is desired, the specific impedance at this location should be exactly one. A specific impedance of either greater or less than one results in poor absorption.

Since, the pressure-release boundary condition did not meet the goal of maximum absorption over wide frequency range, the control strategy for the Passive/Active system falls to either the direct minimization of the reflected wave or the impedance-matching control approach. The impedance-matching control strategy has the advantage of having the sensors necessary for detection of the error signal hidden in the airspace rather than in

front of the sound absorbing layer where the response is desired. The location of error sensors at the desired “zone of quiet” are not usually at one’s disposal. Therefore, from design point of view, the impedance-matching control strategy is more advantageous than the direct minimization of reflected wave and is selected for the Passive/Active system.

### **3.3 Parametric Analysis**

In section 3.2.3, the impedance-matching control approach was found to be the ideal control strategy for the Passive/Active system. All numerical results given in section 3.2 were for a 5.0cm absorbing layer and 10.0cm airspace. In this section, parametric analysis for the Passive/Active system will be presented in order to investigate the sensitivity of the system to absorbing layer thickness and airspace depth. The influence of variation of the absorbing layer thickness on system performance will first be presented in section. 3.3.1. The effect of change in airspace depth on system performance will then follow in section 3.3.2.

#### **3.3.1 Effect of foam thickness on system performance**

The absorption coefficient of the model for three different samples is presented with and without active control in Fig. 3.26. The three samples were of 2.5cm, 5cm and 7.5cm thickness. The depth of the air cavity was kept at 10cm in all cases. Before control, increase in the thickness of the foam sample resulted in a shift of the absorption coefficient to the lower frequencies with more peaks becoming apparent. After control, good absorption for all three foam samples was achieved. However, the absorption coefficient of the 2.5cm sample shows a progressively decreasing absorption pattern with increasing frequency. This declining effect is due to the fact that the absorption of the



system at the high frequencies is achieved by the passive component and passive absorption is a function of absorber thickness. The result for the 5cm and 7.5cm samples show a consistent absorption coefficient of 0.85 - 1.0 throughout the frequency range of interest. The control velocity required to maintain the impedance-matching condition for all three foam samples is presented in Fig. 3.27. With increase of foam thickness, a reduction in the required control velocity is observed. Therefore, there is a trade-off between reducing the thickness of the foam and reducing the control wall velocity and one will have to be compromised in practical application design. However, despite the fact that overall higher velocity is required for samples with smaller thickness, at the lower frequencies the difference is not significant. Therefore, the Passive/Active system shows minimal sensitivity to changes in the absorbing layer thickness.

### **3.3.2 Effect of variation of airspace depth on system performance**

The effect of variation of the airspace depth on the performance of the Passive/Active system was investigated for one foam sample. In this study, the thickness of the foam sample was 5cm and three different airspace depths were investigated. Figure 3.28 shows the absorption coefficient of the system for air gap depth of 5.0cm, 7.5cm, and 10cm. Before control, an increase in air gap depth results in a similar trend as an increase in the foam size. The absorption coefficient slightly shifts towards the lower frequencies revealing more peaks. However, after control, variation of the airspace depth had no effect on the performance of the system. This conclusion is theoretically expected since the impedance-match is maintained adaptively. As the airspace depth is changed, the control velocity simply adapts to maintain the condition required for maximum absorption. The required velocity is shown in Fig. 3.29. Therefore, the Passive/Active system is not

sensitive to changes in the airspace depth. For design purposes, the depth of the air gap is dictated only by physical constraints.

### **3.4 Summary**

In this chapter, the absorption of a passive system was first investigated for three different size absorbing layer samples. The performance of the Passive/Active system was then investigated numerically for three different control strategies. The impedance-matching control approach was found to be practical in effectively achieving maximum absorption over a wide frequency range and was selected for the Passive/Active system. This control approach has the benefit of having all the necessary error sensors hidden in the airspace. In practical design, this advantage results in a compact and self-contained unit. Parametric analysis were performed on the final model to investigate sensitivity of the Passive/Active system for variation in absorbing layer thickness and airspace depth. The performance of the system was determined to be independent of the airspace depth and marginally sensitive to absorbing layer thickness. This indicates that the airspace could be further reduced in size.

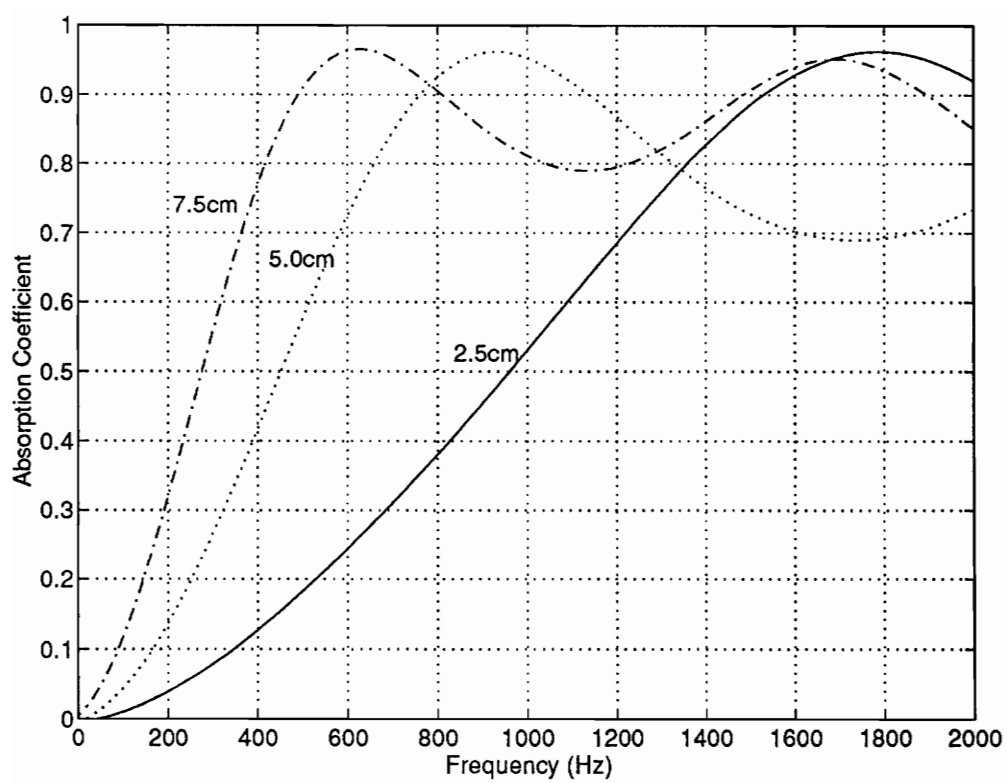


Fig. 3.1 Absorption coefficient  $\alpha$  of three different size foam samples backed by rigid wall.

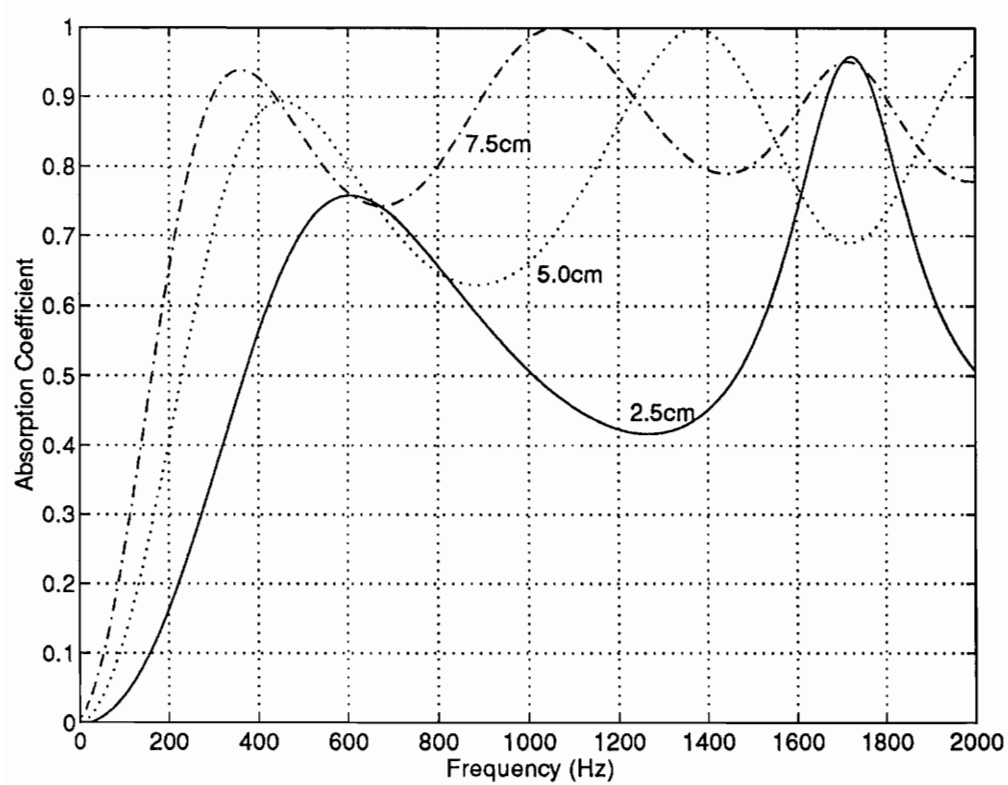


Fig. 3.2 Absorption coefficient  $\alpha$  of three different size foam samples backed by a 10cm air gap.

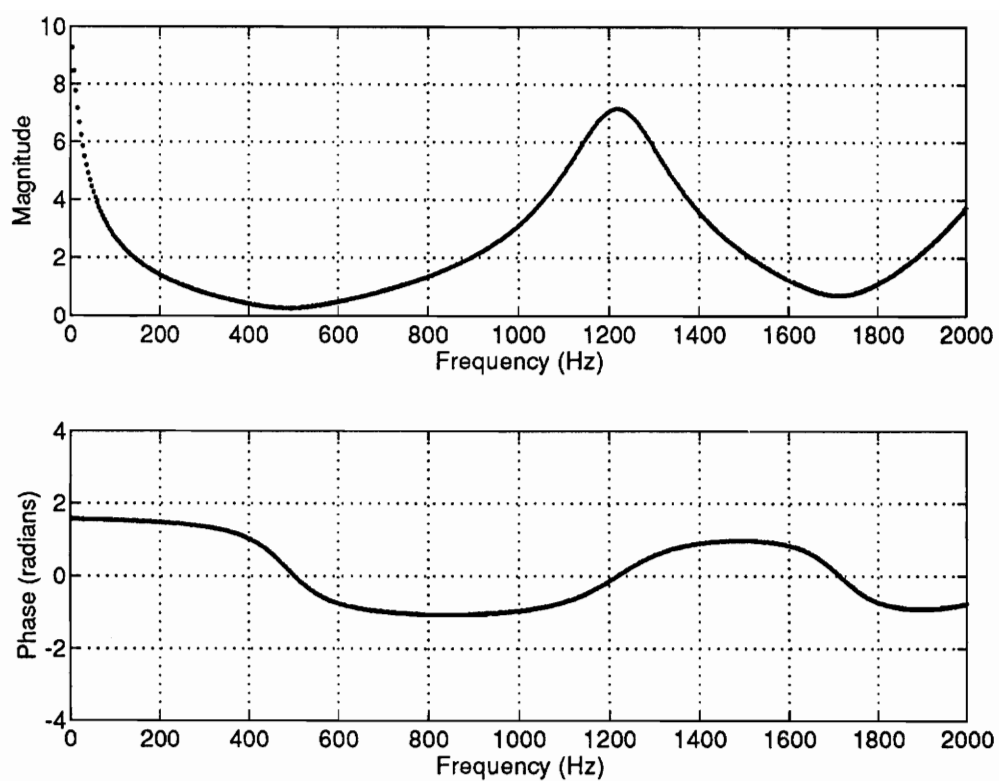


Fig 3.3 Specific input impedance of passive system with 2.5cm foam layer and 10cm airspace.

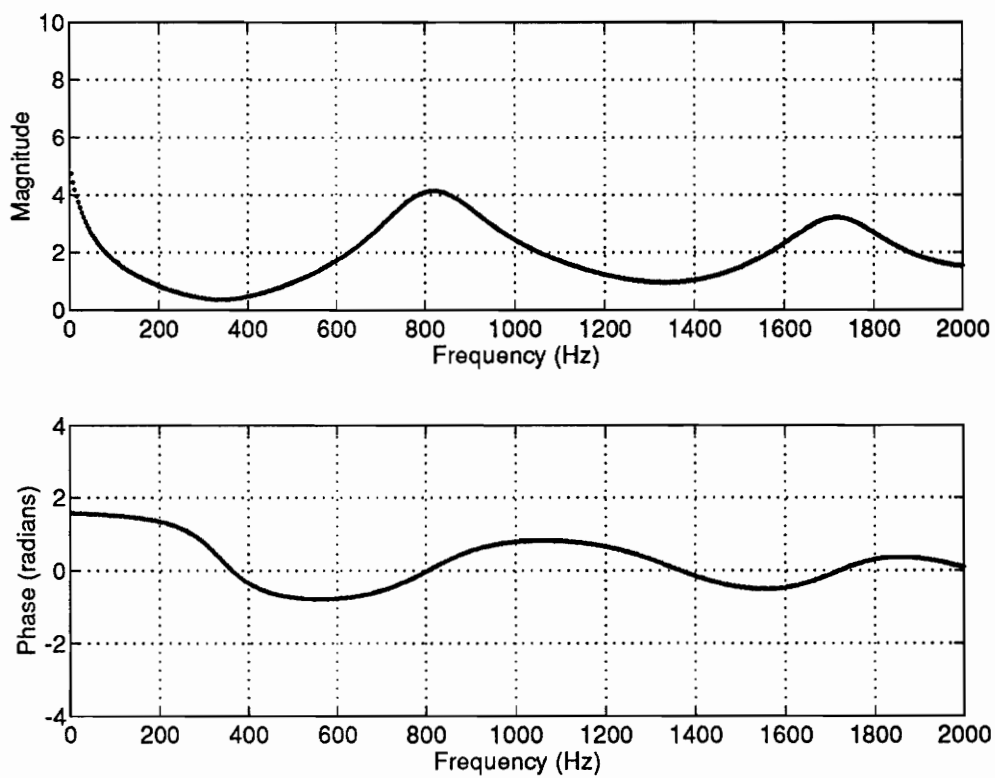


Fig. 3.4. Specific input impedance of passive system with 5.0cm foam layer and 10cm airspace.

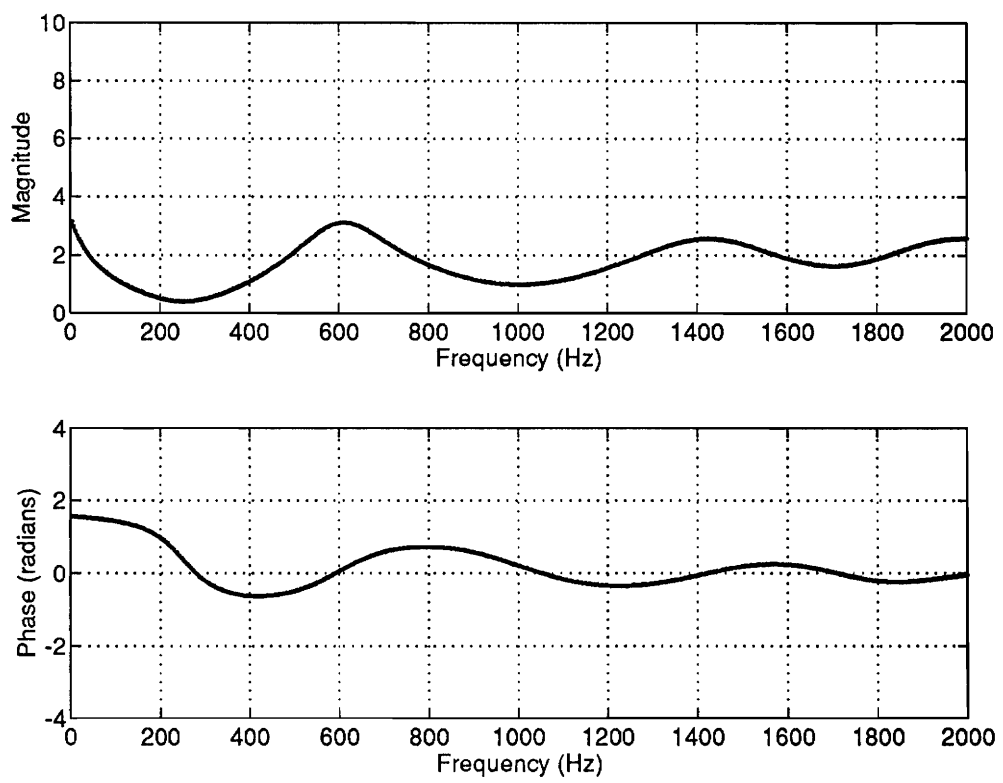


Fig 3.5 Specific input impedance of passive system with 7.5cm foam layer and 10cm airspace.

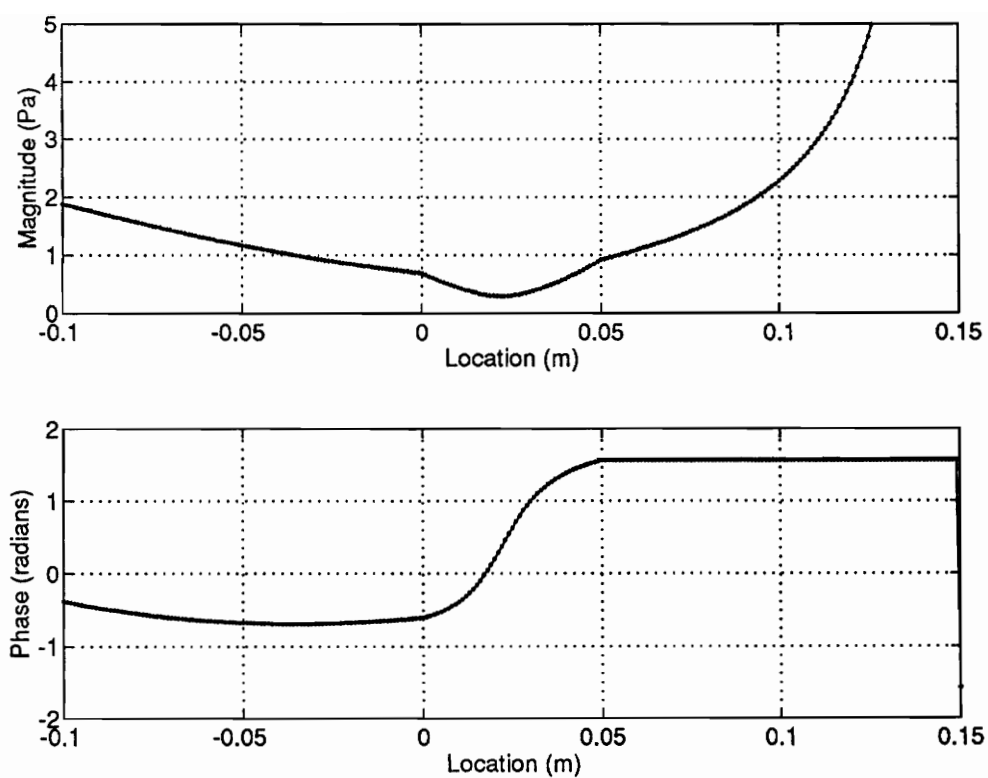


Fig. 3.6 Profile of specific impedance across two-layer passive system (frequency=450).  
0.0m-0.05m = absorbing layer, 0.05m - 0.15m = airspace



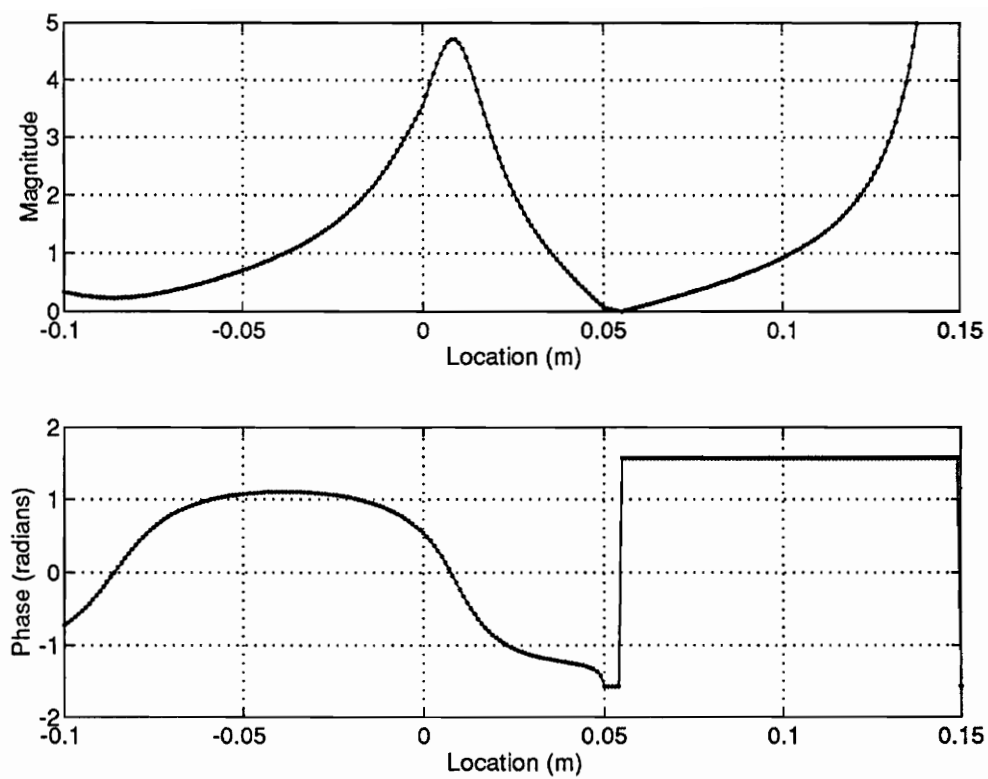


Fig. 3.7 Profile of specific impedance across two-layer passive system (frequency=900).

0.0m-0.05m = absorbing layer, 0.05m - 0.15m = airspace

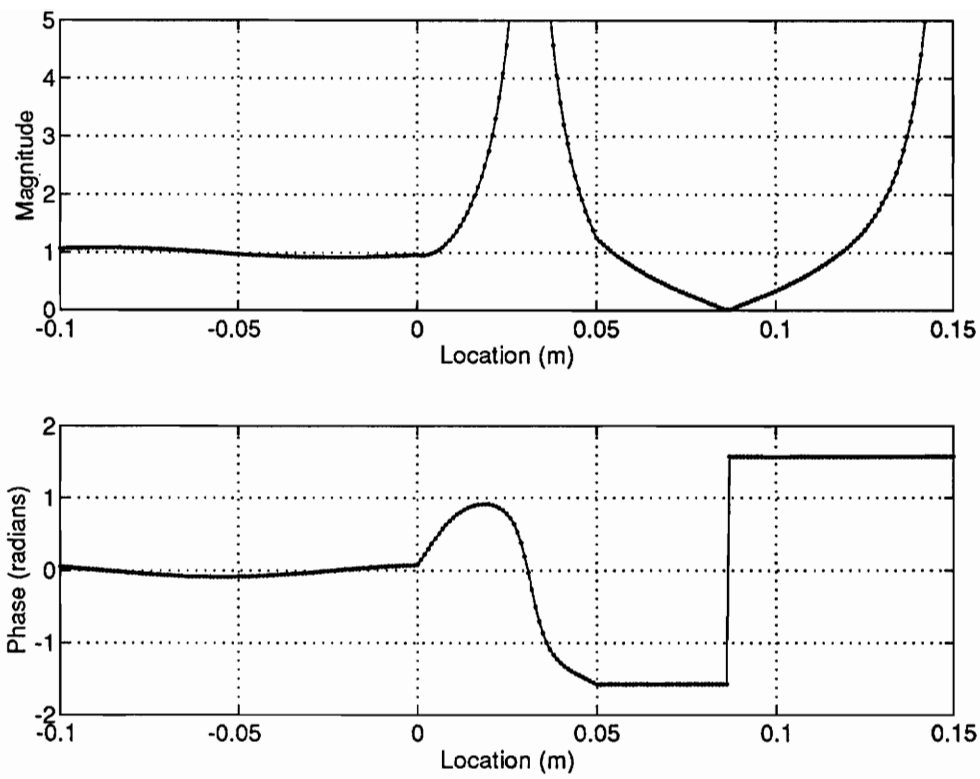


Fig. 3.8 Profile of specific impedance across two-layer passive system (frequency=1350).

0.0m-0.05m = absorbing layer, 0.05m - 0.15m = airspace

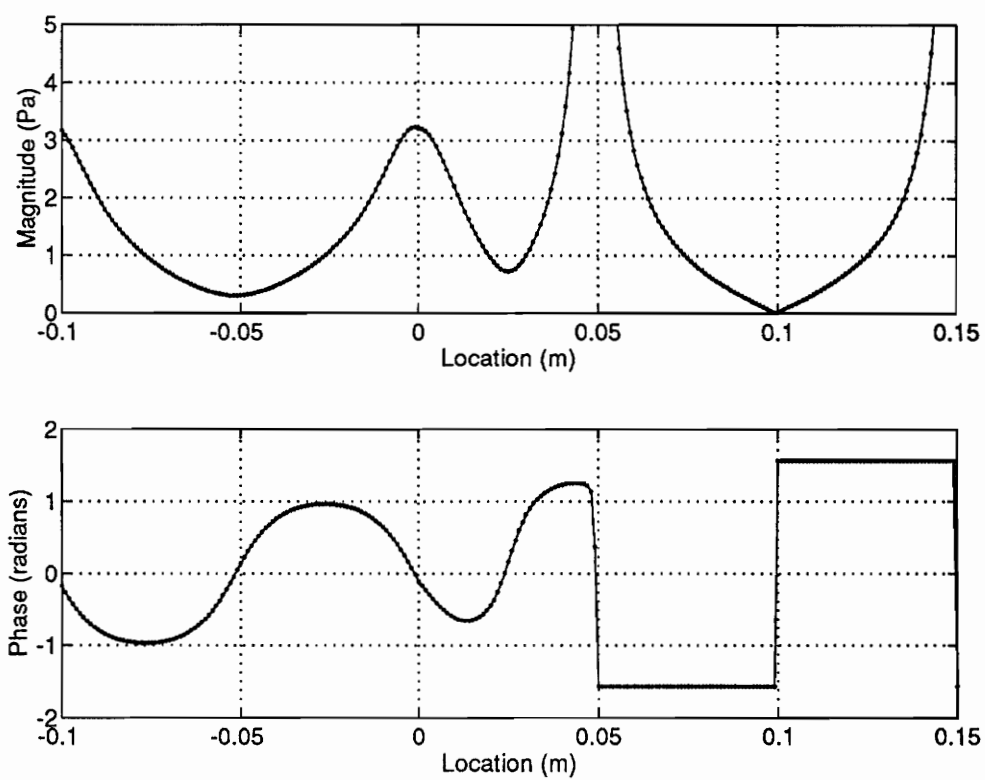


Fig. 3.9 Profile of specific impedance across two-layer passive system (frequency=1700).

0.0m-0.05m = absorbing layer, 0.05m - 0.15m = airspace

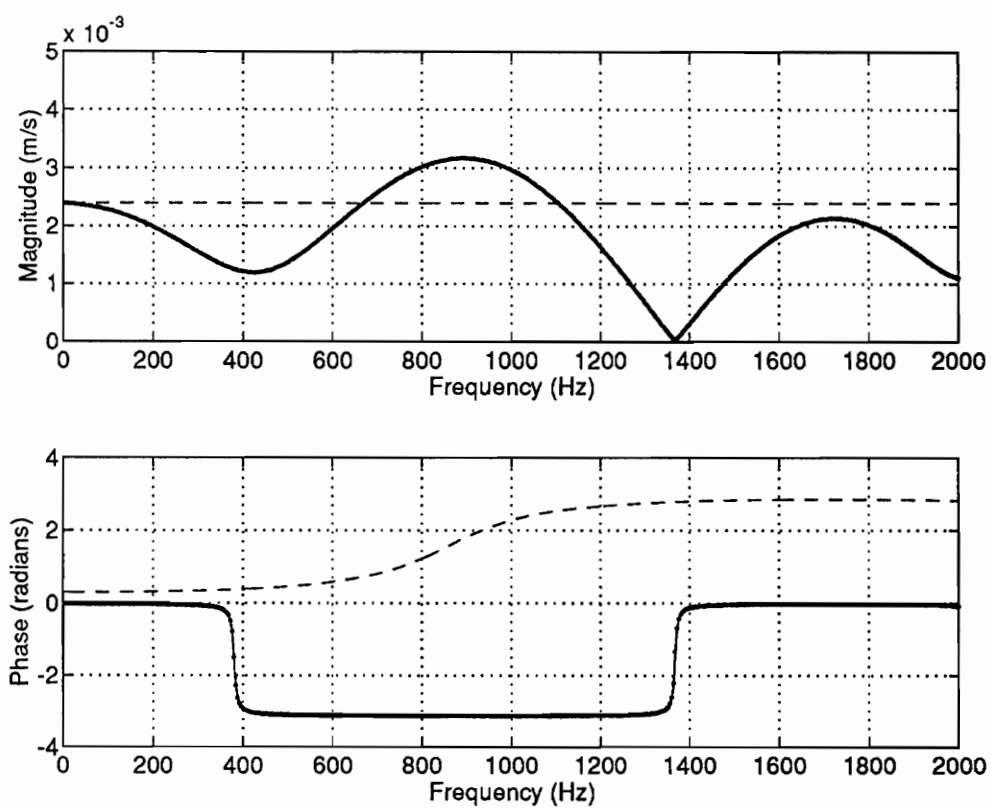


Fig. 3.10 Control wall velocity ( $v_{wall}$ ) required for direct minimization of reflected wave.

— Passive/Active system, --- Active system (without the passive absorber)

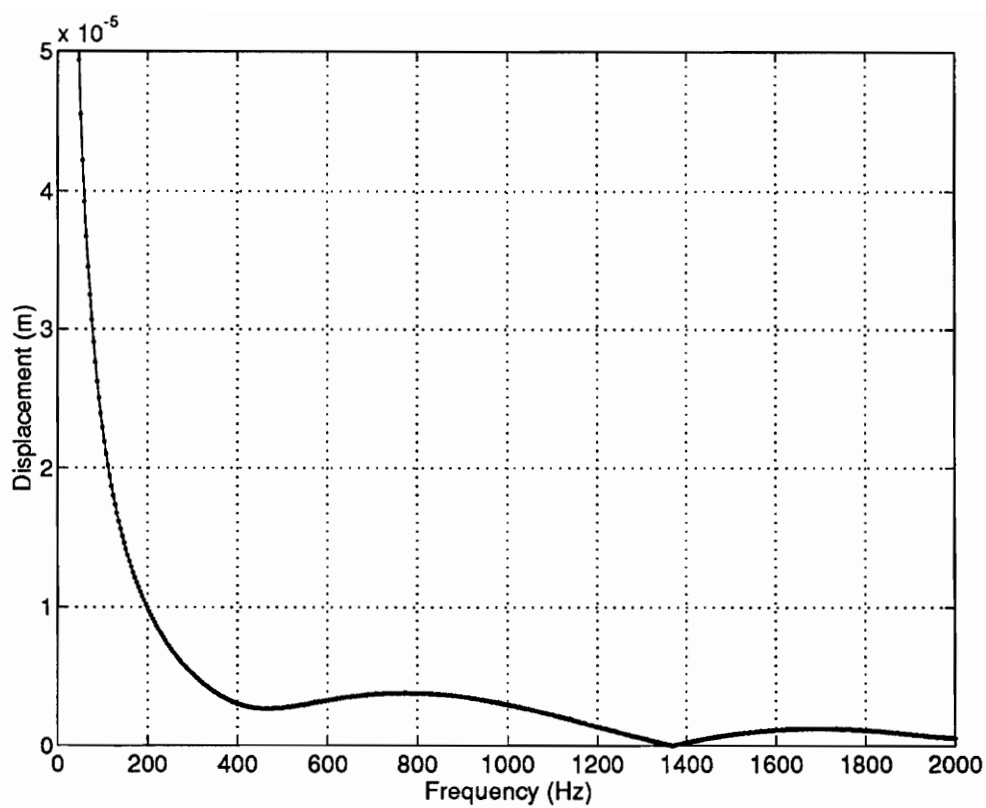


Fig. 3.11 Control wall displacement required for direct minimization of reflected wave.

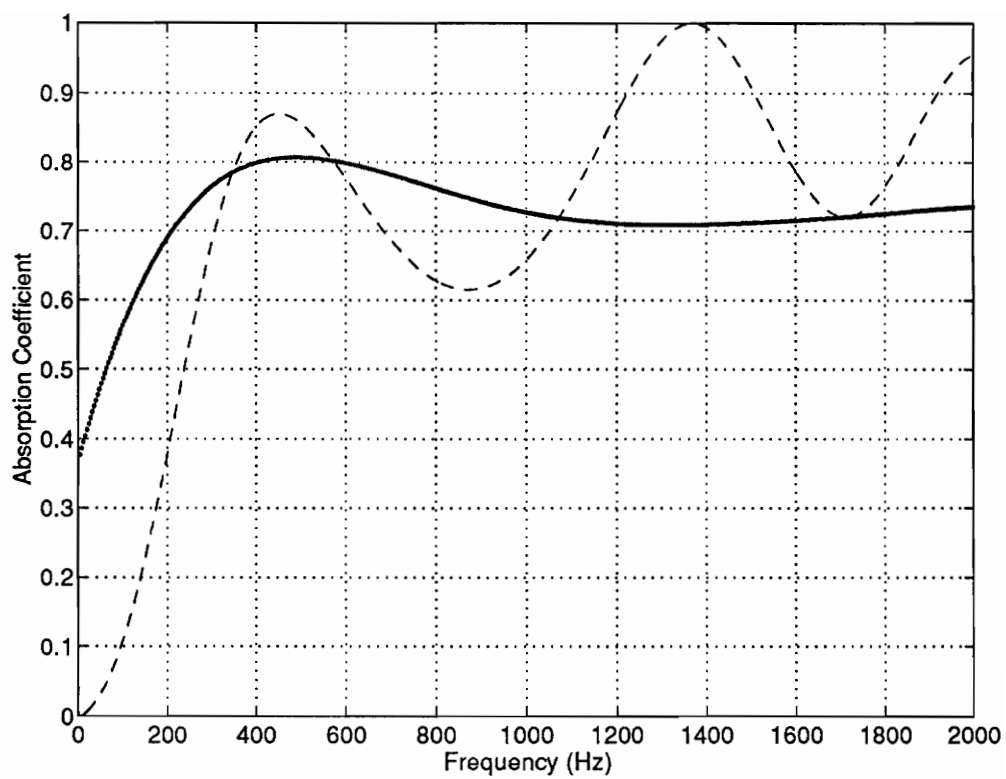


Fig. 3.12 Absorption coefficient due to pressure-release boundary simulation.

--- without control, \_\_\_ with control

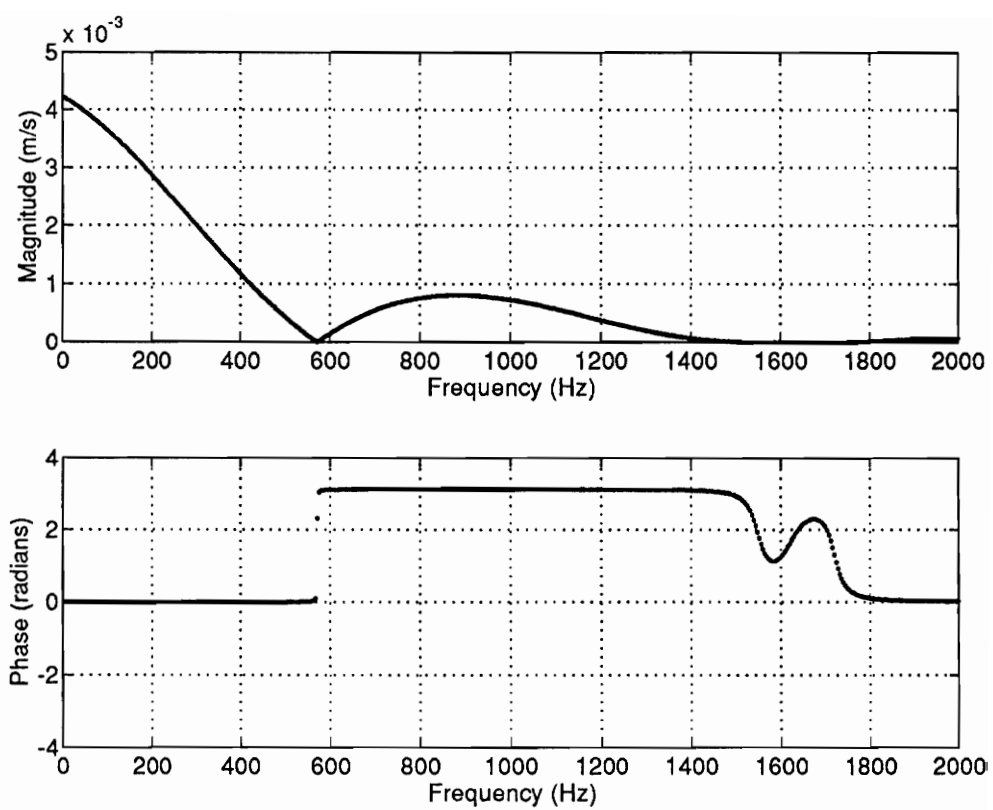


Fig. 3.13 Control wall velocity ( $v_{wall}$ ) required for pressure-release boundary condition.

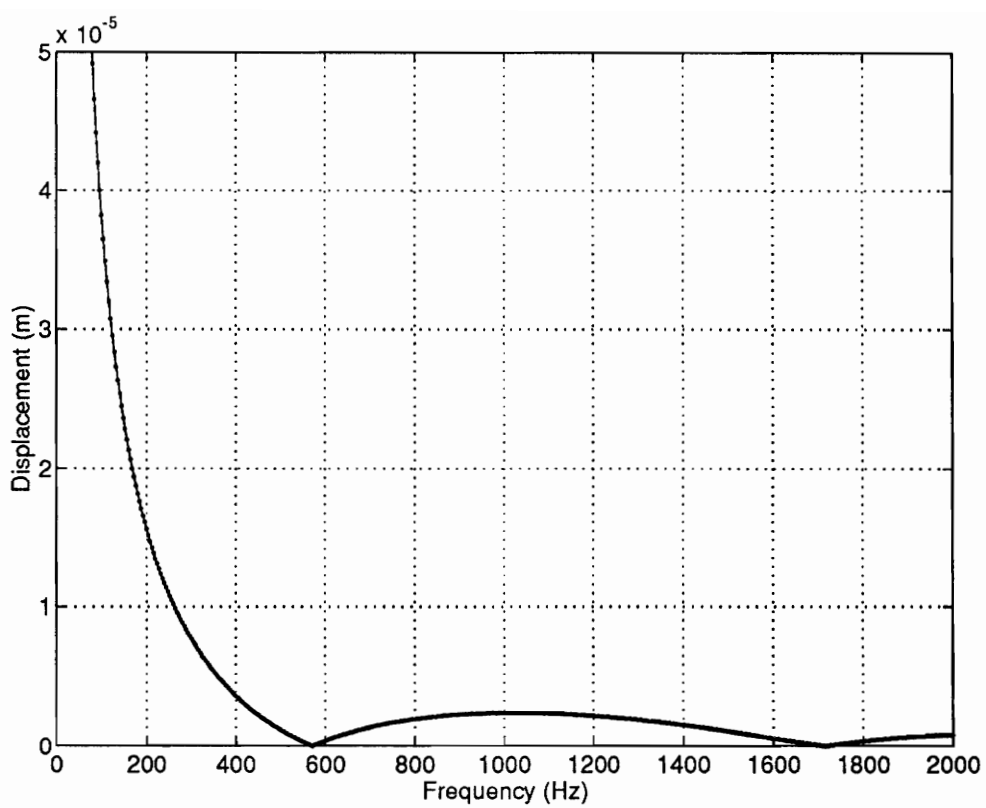


Fig. 3.14 Control wall displacement required for pressure-release boundary condition.



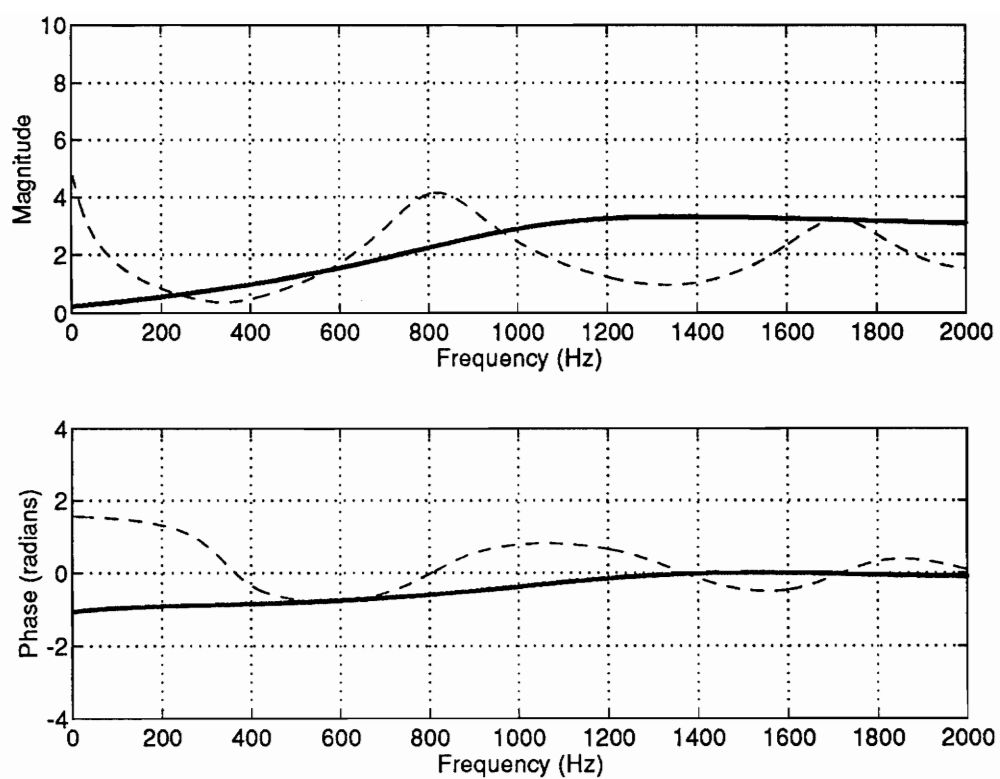


Fig. 3.15 Specific input impedance of system due to pressure-release boundary condition. --- before control, \_\_\_\_ after control

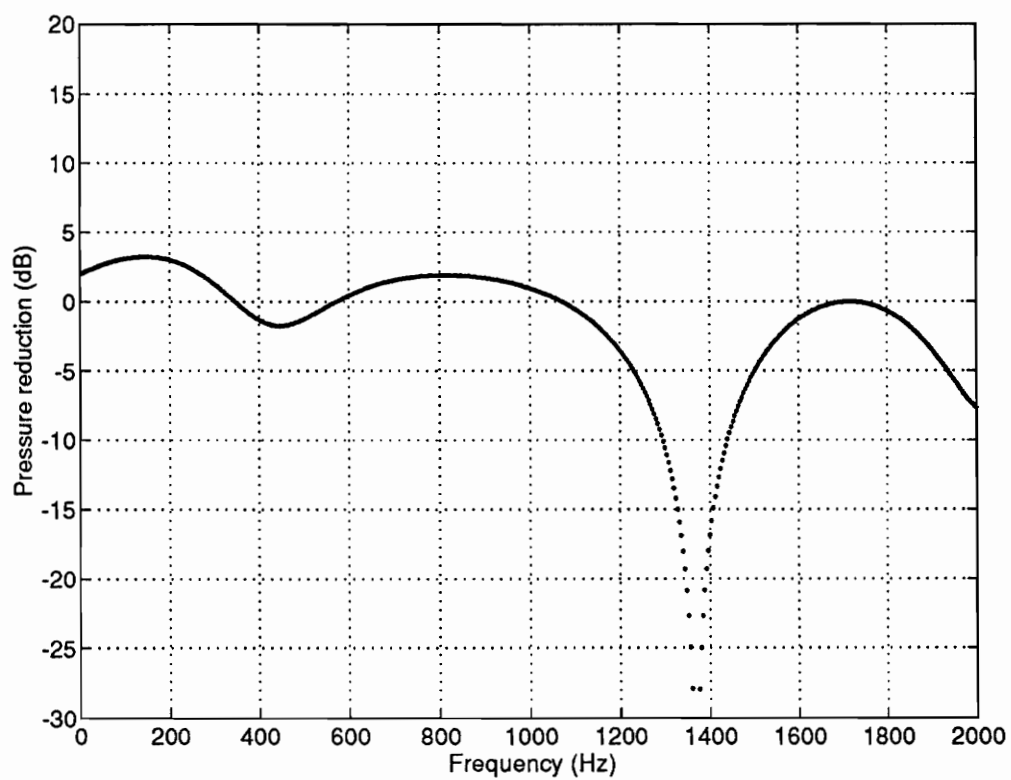


Fig. 3.16 Acoustic pressure reduction due to pressure-release boundary condition.

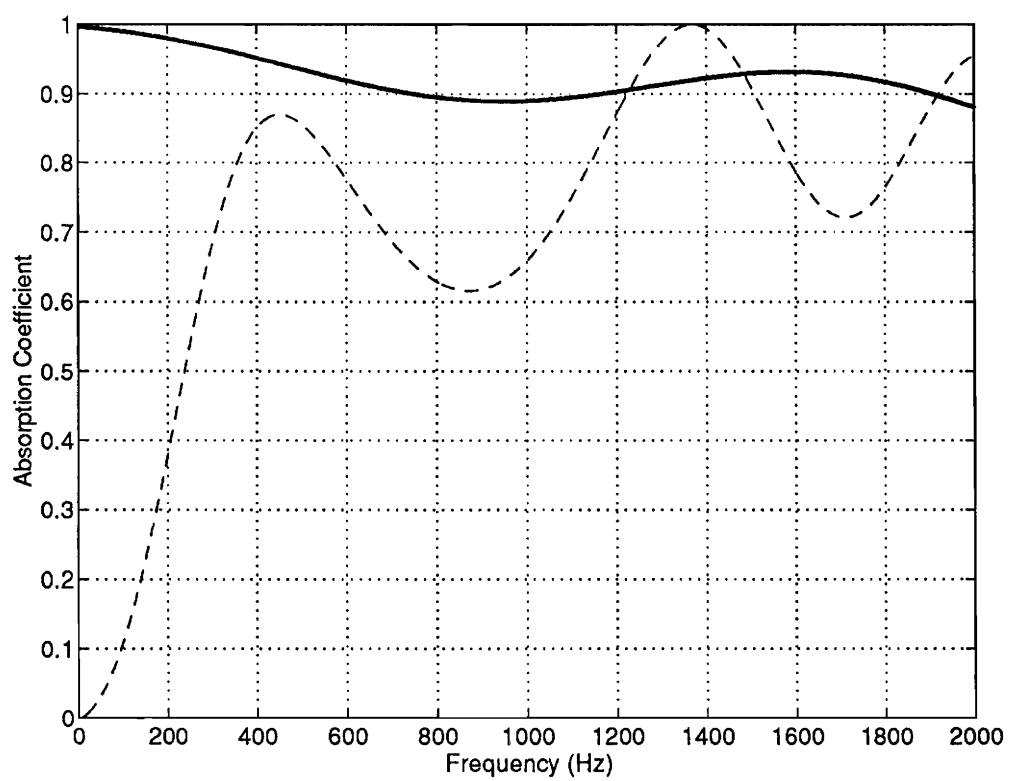


Fig. 3.17 Absorption coefficient of system due to impedance-matching condition.

--- without control, \_\_\_ with control

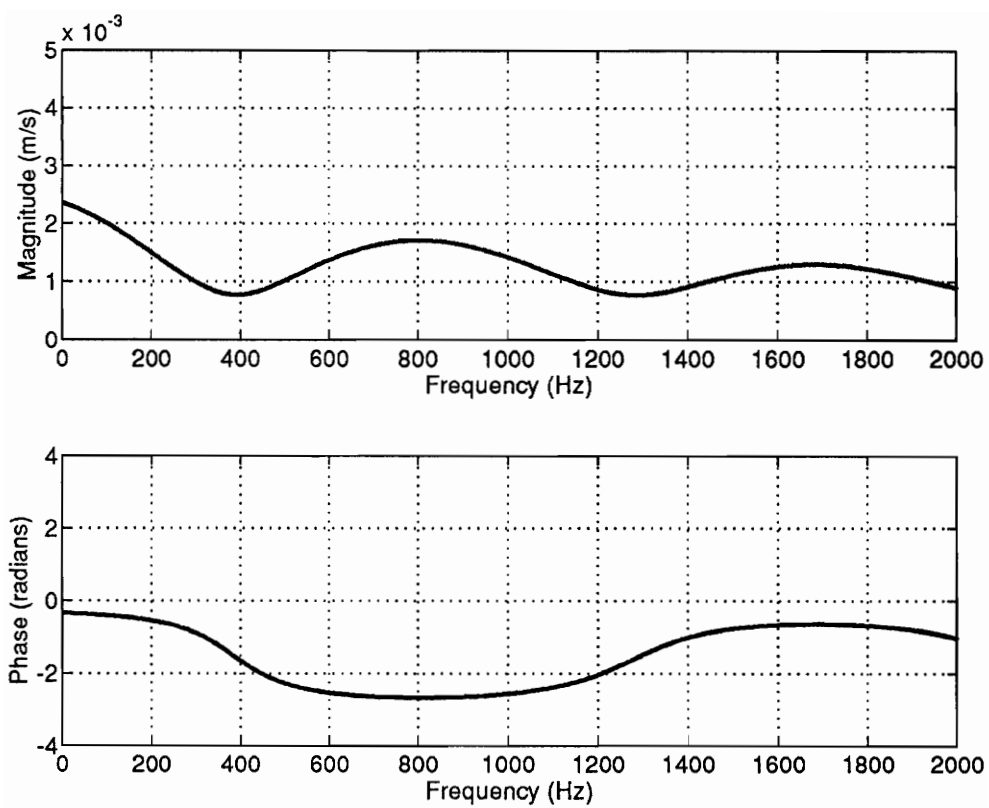


Fig. 3.18 Control wall velocity ( $v_{wall}$ ) required for impedance-matching.

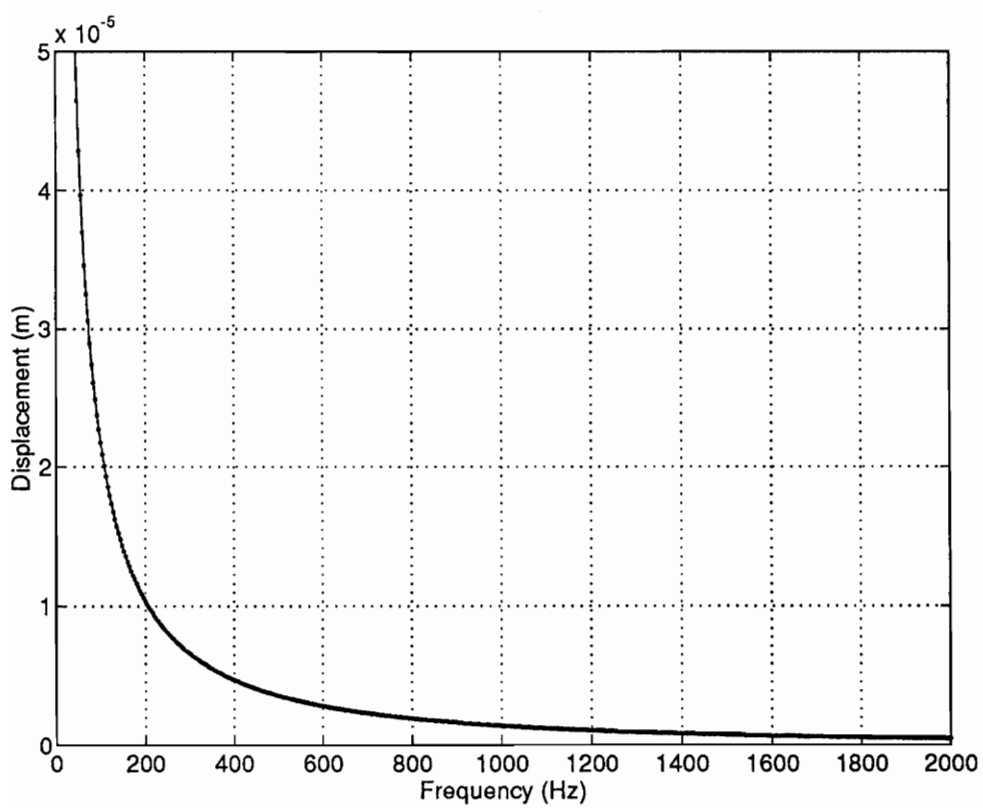


Fig. 3.19 Control wall displacement required for impedance-matching.

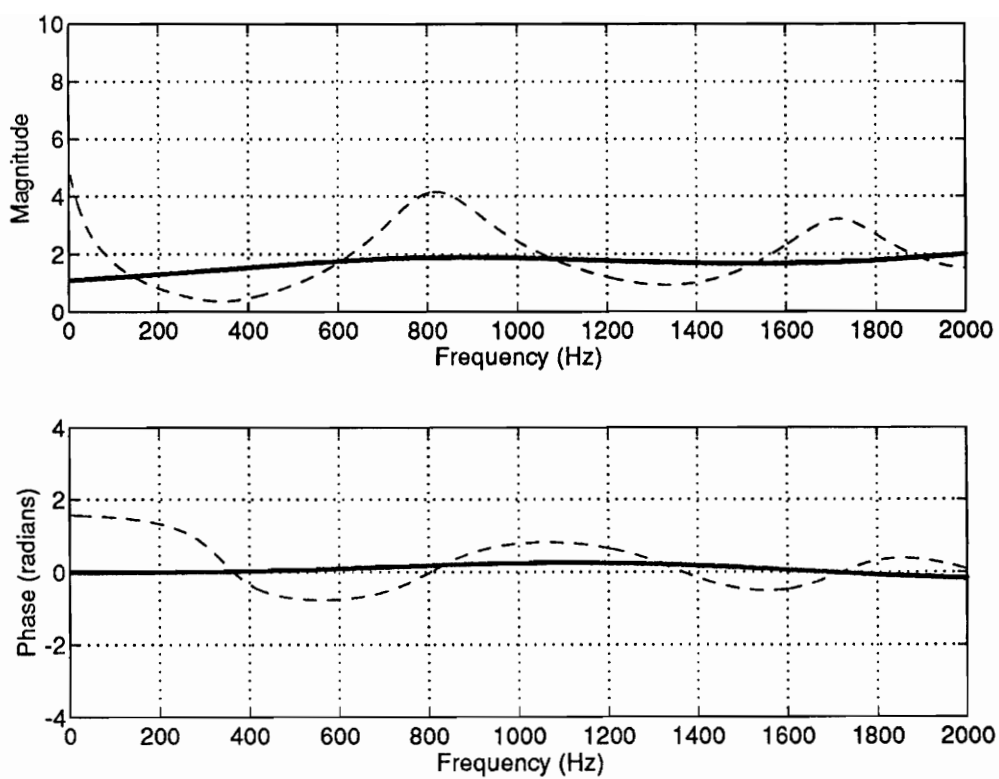


Fig. 3.20 Specific input impedance of system due to impedance-matching condition.

--- before control, — after control

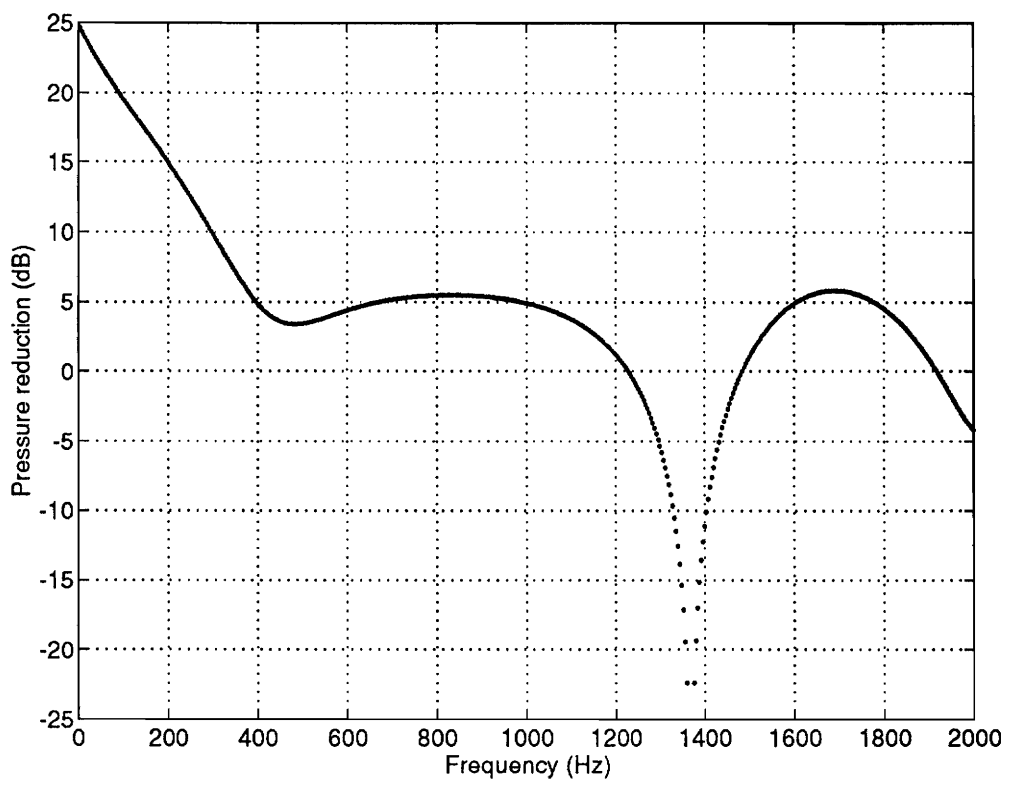


Fig. 3.21 Acoustic pressure reduction due to impedance-matching condition.

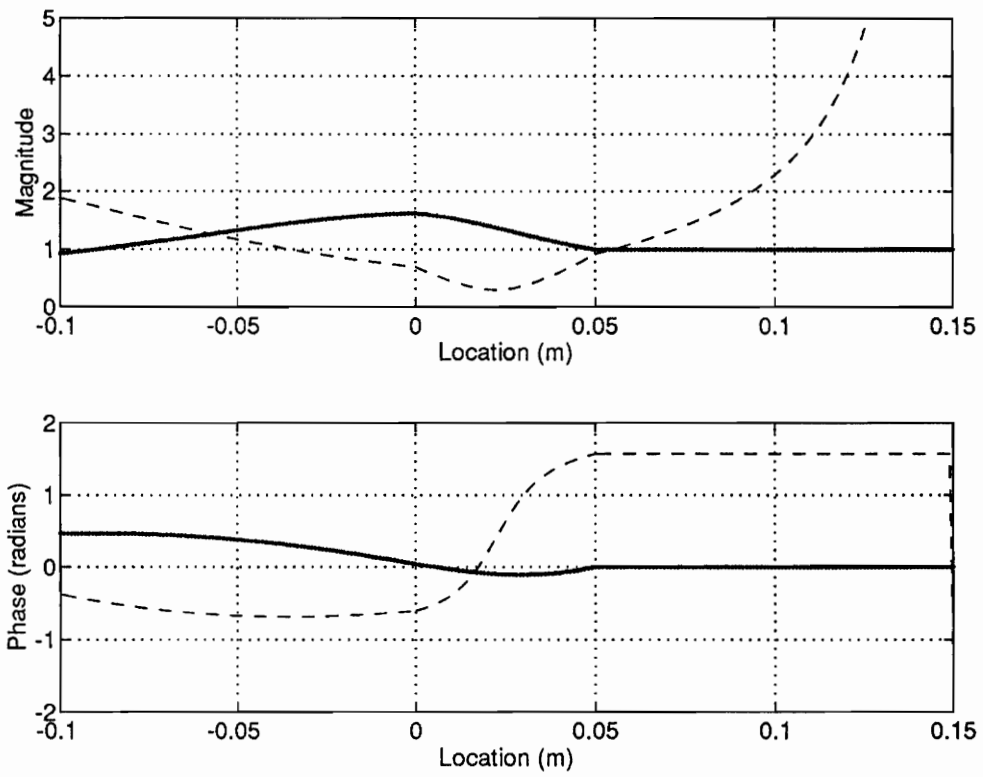


Fig.3.22 Profile of specific impedance across two-layer system for impedance-matching.

0.0m-0.05m = absorber layer, 0.05m-0.15m = airspace (frequency= 450Hz)

--- before control, \_\_\_\_ after control



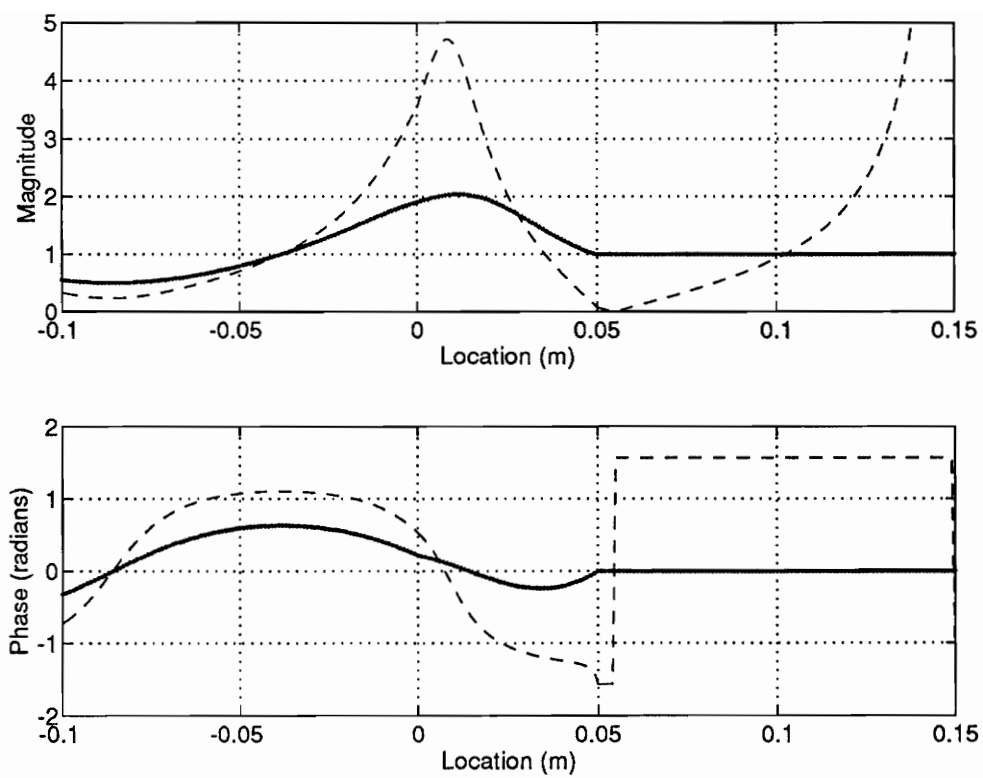


Fig. 3.23 Profile of specific impedance across two-layer system for impedance-matching.

0.0m-0.05m = absorber layer, 0.05m-0.15m = airspace (frequency = 900Hz)

--- before control, \_\_\_ after control

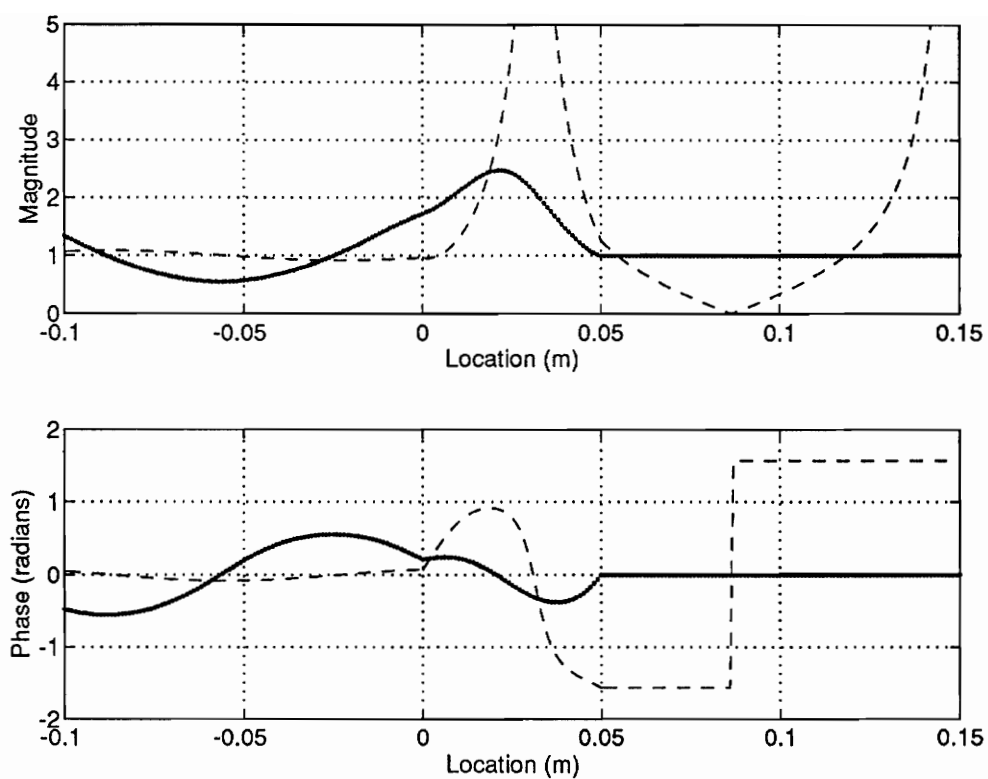


Fig. 3.24 Profile of specific impedance across two-layer system for impedance-matching.

0.0m-0.05m = absorber layer, 0.05m-0.15m = airspace (frequency = 1350Hz)

--- before control, \_\_\_ after control

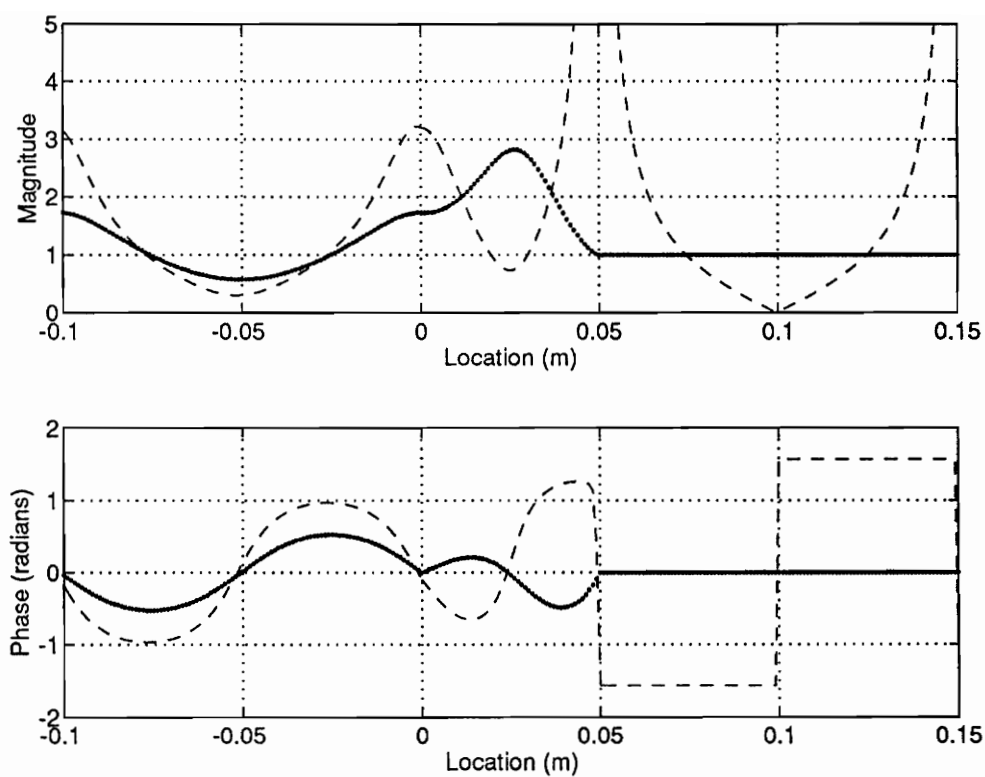


Fig. 3.25 Profile of specific impedance across two-layer system for impedance-matching.

0.0m-0.05m = absorber layer, 0.05m-0.15m = airspace (frequency = 1700Hz)

--- before control, \_\_\_\_ after control

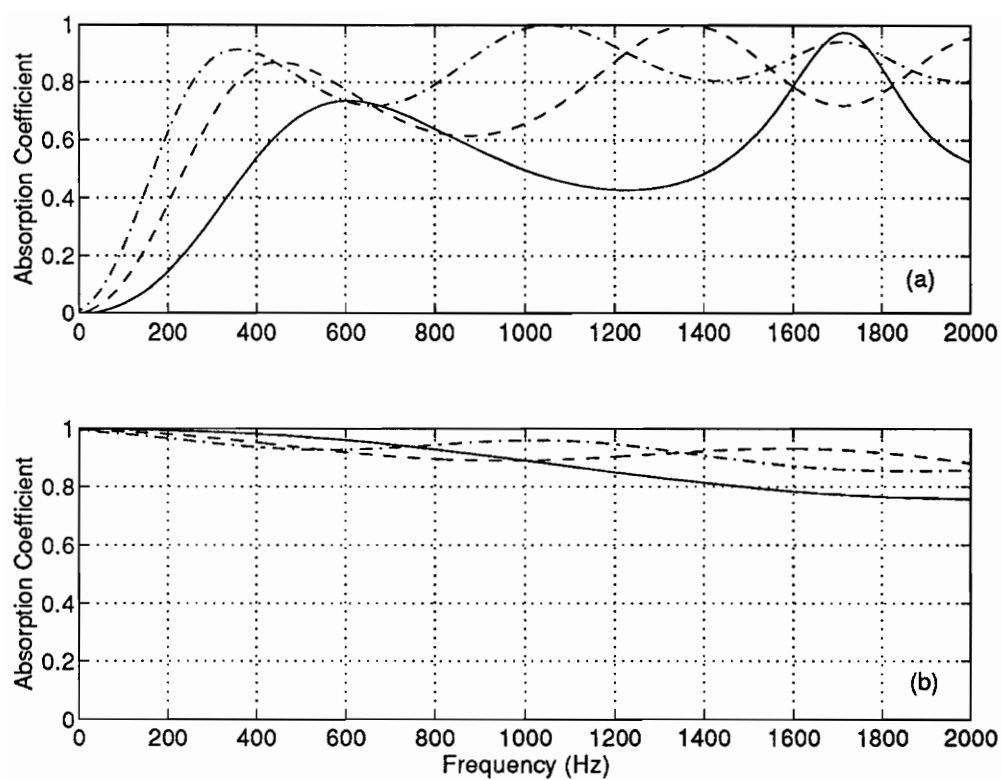


Fig. 3.26 Effect of change in foam sample thickness on absorption coefficient.

— 2.5cm, -.- 5.0cm, -.- 7.5cm (airspace depth = 10cm)

(a) before control (b) after control



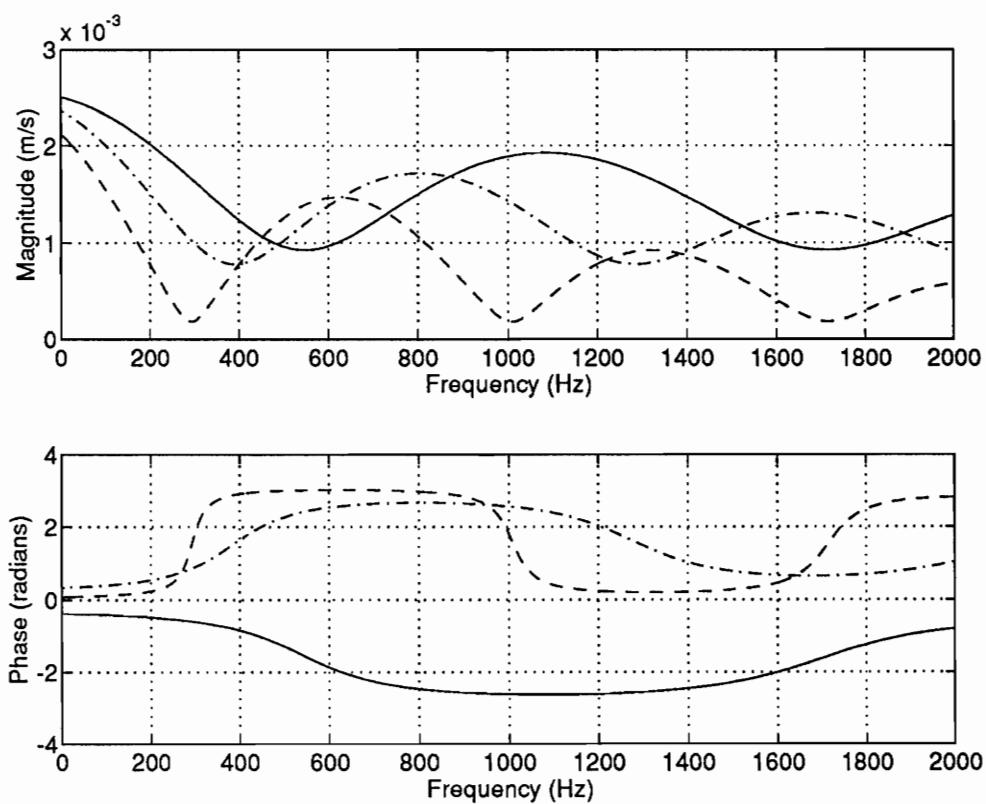


Fig. 3.27 Variation of control velocity requirement with foam sample thickness.

— 2.5cm, -.- 5.0cm, --- 7.5cm (airspace depth = 10cm)

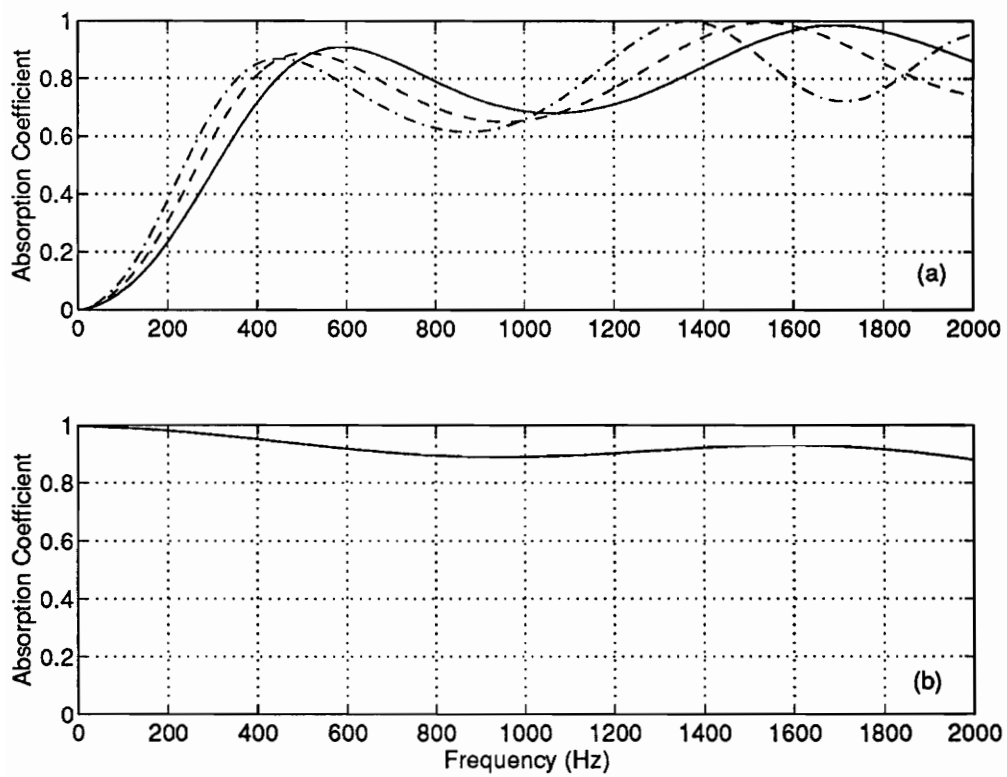


Fig. 3.28 Effect of change in airspace depth on absorption coefficient.

— 5.0cm, --- 7.5cm, -.- 10cm (foam thickness = 5cm)

(a) before control (b) after control

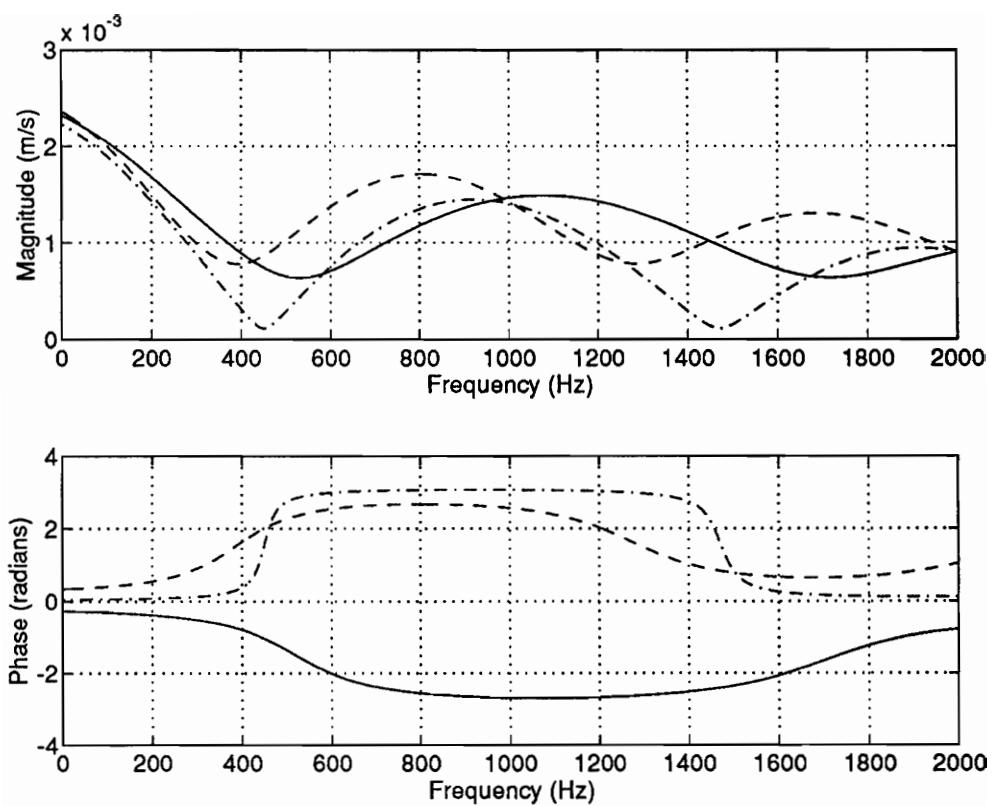


Fig. 3.29 Variation of control velocity requirement with airspace depth.

— 5.0cm, -.- 7.5cm, --- 10cm (foam thickness = 5cm)



## **CHAPTER 4**

### **EXPERIMENTAL RESULTS**

In this chapter, the experimental results obtained to validate the three control strategies for the Passive/Active systems will be presented. The experimental setup of the system will be described in section 4.1. The experimental results for the three control strategies will then be described in sections 4.2, 4.3 and 4.4, respectively. The experimental setup described in section 4.1 is for the direct minimization of the reflected wave control strategy. However, the experimental setups for the other two control strategies are very similar to what is described in section 4.1. The difference between the setups will be described for each control strategy in their respective sections. The effect of variation of sound absorbing thickness on the performance of the system was also investigated experimentally, and the result will be presented in section 4.5. To demonstrate the feasibility of using the Passive/Active system for different absorbing materials, the polyurethane foam layer was replaced with a porous metal sheet in an experimental investigation and the results for this case are found in section 4.6. Again, all of the experimental results presented in this chapter are for pure tone excitation.

#### **4.1 Experimental Setup**

Figure 4.1 shows the experimental setup for the Passive/Active system study. In Fig. 4.2 the laboratory arrangement for the experimental setup is shown. Due to the one-dimensional nature of the model, the experiments performed were carried out in a standard impedance tube. The particular tube used, a 10cm diameter Bruel & Kjaer Type 4002, has

a lower and upper frequency limits of 90Hz and 2000Hz, respectively. The disturbance source was located at one end of the impedance tube and the other end of the tube was terminated with a control speaker. The sound absorbing layer, a 5cm thick partially reticulated foam, was placed at 10cm from the control speaker creating an airspace between the foam and the control speaker. A Bruel & Kjaer Signal Analyzer Type 2032 provided the disturbance signal which was amplified by a PROTON model AA1150 stereo amplifier before it was sent to the disturbance speaker. The measurement of the absorption coefficient of the system was done using the standing wave technique (SWR) [22]. The SWR is the most widely used method of measuring acoustical properties of materials. Acoustic plane waves generated by the disturbance speaker at one end of the tube propagate along the tube towards the sample located at some location in the impedance tube. A traversing probe-tube microphone is then used to determine the magnitude and location of successive maxima and minima of the standing wave pattern along the tube. The signal detected by the probe microphone is then amplified and sent to the signal analyzer. The ratio of any maxima to the first minima gives the standing wave index 'n' from which the absolute value of the reflection coefficient  $|R|$  of the sample material could be calculated using the following equation [22]:

$$|R| = \frac{n - 1}{n + 1} \quad (4.1)$$

The absorption coefficient of the system was then determined from equation 2.16 as:

$$\alpha = 1 - |R|^2 \quad (4.2)$$

The absorption coefficient of the system was determined for the frequency range 100Hz - 2000Hz at an increment of 100Hz.

The particular experimental setup shown in Fig. 4.1 is for the 'ideal' case of directly minimizing the reflected wave in front of the sound absorbing layer. Since, the wave field in the tube includes both incident and reflected waves, the separation of these two waves was necessary before the reflected wave could be minimized. A wave deconvolution circuit first described by Fahy [21] was used to isolate the reflected wave. This circuit gives real time domain estimate of the incident and reflected components of a sound field from the outputs of two closely spaced identical microphones. A brief description of the formulation for this circuit could be found in Appendix C. The two microphones used in this experiment were 1.25cm diameter Bruel & Kjaer Type 4166. These microphones were fitted with extension probes. The probe tips of both microphones were located in front of the sound absorbing layer with a 5.0cm spacing between them. In general, the minimum spacing between the microphones should be  $\lambda/12$  [21]. The closest microphone to the sound absorbing layer was located at 5.0cm distance. The signals detected by these microphones were fed into the wave deconvolution circuit after passing through a low-pass filter and their respective pre-amplifiers and a dual channel microphone power supply, Bruel & Kjaer type 2807. The incident and reflected waves in front of the absorber were then separated by the deconvolution circuit and the reflected wave signal processed by a single channel Filtered x-LMS controller as an error signal. Since the excitation in this case is periodic, the disturbance signal was also fed into the Filtered x-LMS controller as a reference signal, avoiding the need for a detection sensor. The control algorithm was coded into assembly language and processed by a Spectrum TMS320C30 digital signal processing (DSP) board resident in a personal computer. The required control signal to minimize the reflected

wave was then generated by the controller and sent to the control speaker after passing a low pass filter. The sampling rate for each experiment was four times the operating frequency. A brief description of the feed-forward based Filtered x-LMS algorithm is presented in Appendix C.

## **4.2 Direct minimization of reflected wave - Experimental study**

The absorption coefficient of the Passive/Active system for the direct minimization of reflected wave control strategy is shown in Fig. 4.3 before and after control as a function of frequency. A high absorption coefficient of 0.85 - 1.0 is observed due to this control strategy over the frequency range 100Hz to 2000Hz. For convenience, the numerically simulated absorption coefficients of the system before and after control are also plotted along with the experimental results. The location of the maximum and minimum absorption bands of the experimental result coincide with the numerical prediction. The strong agreement between experimental and numerical results serve as further validation of the model developed. At lower frequencies, the experimental absorption coefficient after control was observed to be slightly lower than the numerical result. This discrepancy is due to the low frequency phase mismatch between the particular microphones used in the wave separation process. Elliot describing an absorption coefficient measurement method based on the wave deconvolution circuit had noted that a difference in the phase responses of the two microphones could lead to a systematic error [24].

### 4.3 Pressure-release boundary condition - Experimental study

The experimental setup for the pressure-release boundary condition is presented in Fig. 4.4. This experimental setup is similar to the experimental setup described for directly minimizing the reflected wave. In this experimental setup, instead of the dual microphones in front of the sound absorbing layer, a single error microphone was located on the back surface of the sound absorbing layer. The microphone used was a 1.25cm diameter Bruel and Kjaer type 4166 fitted with a probe. The microphone, itself located outside of the impedance tube, detects the acoustic pressure through the fitted probe which was located close to the surface of the absorber. The pressure-release boundary condition was maintained by minimizing the total pressure detected by the error microphone. This condition is simpler to implement than the previous case since there is no need for wave separation.

The absorption coefficient for this case is presented in Fig. 4.5. As the numerical model predicted, the experimental study did not indicate any improvement in the absorption coefficient of the system. At frequencies 400Hz and 1400Hz where absorption peaks were observed due to passive control, the absorption coefficient was reduced by almost 0.3. A discrepancy between the numerical and the experimental results was observed at the frequency range 500Hz - 800Hz. This discrepancy could be due to the fact that the error microphone probe was positioned near the surface while in the numerical model, the pressure release boundary condition was created exactly at the interface between the absorbing layer and the airspace. The positioning of the error microphone was deliberate in order to avoid any transmission of vibration from the absorbing layer to the microphone.

#### 4.4 Impedance-matching - Experimental study

The experimental setup for the impedance-matching study is presented in Fig. 4.6. Again, the experimental setup for this control strategy is similar to the setup described in section 4.1. The only difference between the two experimental setups is the location of the dual microphones required for wave separation. In this experimental setup, the same dual microphones used for the direct minimization of the reflected wave were employed but were located in the airspace rather than in front of the sound absorbing layer. Figure 4.7 shows the detail of the laboratory setup for the dual microphones. The signals detected at these microphones follow the same path as in the direct minimization of the reflected wave control strategy. The spacing between the microphones was again 5.0cm. The closest microphone to the sound absorbing layer was 1.25cm away from the surface and the second microphone was 3.75cm away from the control speaker diaphragm.

The absorption coefficient for this control strategy is shown in Fig. 4.8 before and after control as a function of frequency. As shown in the figure, this control strategy successfully resulted in absorption coefficient of 0.8 - 1.0 over the frequency range 100Hz - 2000 Hz. At the lower frequencies, the experimentally obtained absorption coefficient tends to be lower than the numerical result, and at the higher frequencies the opposite holds true. The maximum deviation between the experimental and numerical results is an absorption coefficient difference of 0.1, or an error of ten percent. This deviation occurs at the lower frequencies and was discovered to be due to a phase mis-match at these frequencies between the particular microphones used. Overall, a good agreement between the numerical and the experimental results was observed with deviation between the two results decreasing with increase in frequency.

#### **4.5 Effect of foam size on system performance - Experimental study**

In order to verify the numerical results of section 3.3.1, absorption coefficient of the Passive/Active system was experimentally determined for three different foam samples. The samples were 2.5cm, 5.0cm and 7.5cm thick. The depth of the airspace was kept at 10cm in all cases just as in the numerical study of section 3.3.1. The absorption plots for the three cases are presented in Figs. 4.9, 4.10, and 4.11, respectively. In Fig. 4.9, the experimentally determined absorption coefficient of the 2.5cm sample system shows the small declining pattern at higher frequencies already predicted by the numerical model. Figure 4.10 shows the experimentally obtained absorption coefficient of the system with 5.0cm absorbing layer. Note this result is already described in the above section 4.4. In Fig. 4.11, the absorption coefficient of the system with 7.5cm absorbing layer is shown. Curiously enough, the experimental absorption coefficient of this system at the lower frequencies is lower than both of the 2.5cm and 5.0cm layer sample cases. This goes contrary to intuition, as an increase in absorbing layer thickness leads to improvement in the absorption coefficient at the lower frequencies. However, overall high absorption coefficient of 0.79 to 1.0 was observed for all three cases. This experimental investigation confirms the analytical conclusion that the sensitivity of the Passive/Active system to changes in absorbing layer thickness is minimal.

#### **4.6 Feasibility of using other absorbing materials - Experimental Study**

A study to investigate the feasibility of using the developed system for other absorbing materials was carried out following the numerical and experimental conclusion that the Passive/Active is only marginally sensitive to parametric changes. This study was experimental and the intention is to prove that the developed system could be used for any

sound absorbing material without the need of developing numerical models. In this study, the polyurethane foam layer was replaced with a porous metal sheet and the absorption of the new system investigated. The commercial name of the absorber sheet is FELTMETAL. FELTMETAL is composed of porous metal sheets made by the sintering of metal fibers. Metal screens are then bonded to both sides of the fiber metal sheet to enhance its structural and acoustical properties. FELTMETAL is used as liners in noise absorption applications particularly where high temperature is involved. Due to FELTMETAL's structural strength, the need for perforated panels is avoided.

The experimental setup for this case was identical to the one shown in Fig. 4.1 with the foam layer replaced with a 2mm thick FELTMETAL. The FELTMETAL sample was cut for a snug fit in the impedance tube and was located at 7.5cm from the control speaker. The absorption coefficient for this system before and after active control is presented in Fig. 4.12. Before active control, a high absorption coefficient of 0.9 - 1.0 was achieved in the frequency range 600Hz - 1300Hz. However, at frequency ranges of 100Hz - 500Hz and also 1600Hz - 2000Hz, the absorption coefficient drops to almost 0.15. With the introduction of active control, the system resulted in a consistent high absorption coefficient of about 0.8 over the frequency range 100Hz - 2000Hz. The absorption peak observed due to passive absorption at the frequency range 500Hz - 1150Hz was slightly reduced. The experiment was repeated for an airspace depth of 10cm to investigate the effect of change in the airspace depth on the performance of the system. The absorption coefficient for this experiment before and after control is presented in Fig. 4.13. Before control, this experiment resulted in an absorption coefficient of 0.9 - 1.0 over the frequency range 500Hz - 1150Hz. At the lower frequency range of 100Hz - 350Hz and also the frequency range 1200Hz - 2000Hz, an absorption coefficient of less than 0.8 was observed. This fluctuation between high and low absorption coefficient is a



typical characteristic of resonators and liners and is a function of the wavelength of the operating frequency and the airspace dimension. After control, the system resulted in an absorption coefficient that is identical to the case with 7.5cm airspace. Again, the absorption peak noted before control due to the passive absorption of the material, in this case at the frequency range 500Hz - 1150Hz was slightly reduced. These reduction of absorption coefficient could be avoided by having the active control work only at the frequency ranges where good absorption was not achieved by the panel. By skipping over the band width of high passive absorption, the hybrid system would be optimized to give the best absorption possible over the whole frequency range.

The experiments with FELTMETAL proved once again the insensitivity of the Passive/Active system to parameter changes. In addition, these experiments proved that the Passive/Active system could be used with any sound absorbing material. This conclusion shows the robustness of the system and indicates it could be implemented in a diverse potential applications.

## 4.7 Summary

In this chapter, the numerical results of the three control strategies were validated experimentally. The main acoustic property that was studied experimentally was the absorption coefficient of the system. All experimental results were performed in an impedance tube using a standard measurement technique. In general, good agreement was observed between the experimental and numerical results for both, before and after control. A discrepancy was noted in the absorption plots of the direct minimization of the reflected wave at 100Hz - 400Hz and also for the pressure-release boundary condition in the frequency range 500Hz - 800Hz. The causes of these discrepancies were determined to be the low frequency phase mismatch between the dual microphones used in the wave

separation process, and the position of the error sensor used in the pressure-release boundary condition study. Overall, the direct minimization of the reflected wave and the impedance-matching control strategies showed impressive results. In particular, the impedance-matching control approach shows a potential for practical implementation. All sensors and actuators for this case are located in the airspace, and this system can be designed as a compact self contained unit. An array of these units could be used in series to cover walls in auditoriums and studios.

Experimental parametric studies performed with three different thickness foam samples agree with the numerical prediction that the system is marginally sensitive to change in absorbing layer thickness. In addition, in order to investigate the feasibility of using the developed model for different absorbing layers, an experiment was performed involving a porous metal sheet called FELTMETAL. The result of this experiment showed a consistent high absorption coefficient of 0.8 to 1.0 over the whole frequency range of interest. This result indicated the robustness of the Passive/Active system and showed that the system could simply be used for any absorbing material without the need of numerical study. The numerical analysis of the system presented in chapter 3 had shown that a reduction in the depth of the airspace has no effect on the performance of the system and requires a marginal increase in control effort. The only physical limitation on the reduction of the airspace depth from design point of view is the minimum required spacing between the two microphones used for signal separation. In general the minimum spacing between the microphones should be  $\lambda/12$  [21]. Therefore, reduction of the spacing compromises the accuracy of the wave separation at the lower frequencies.

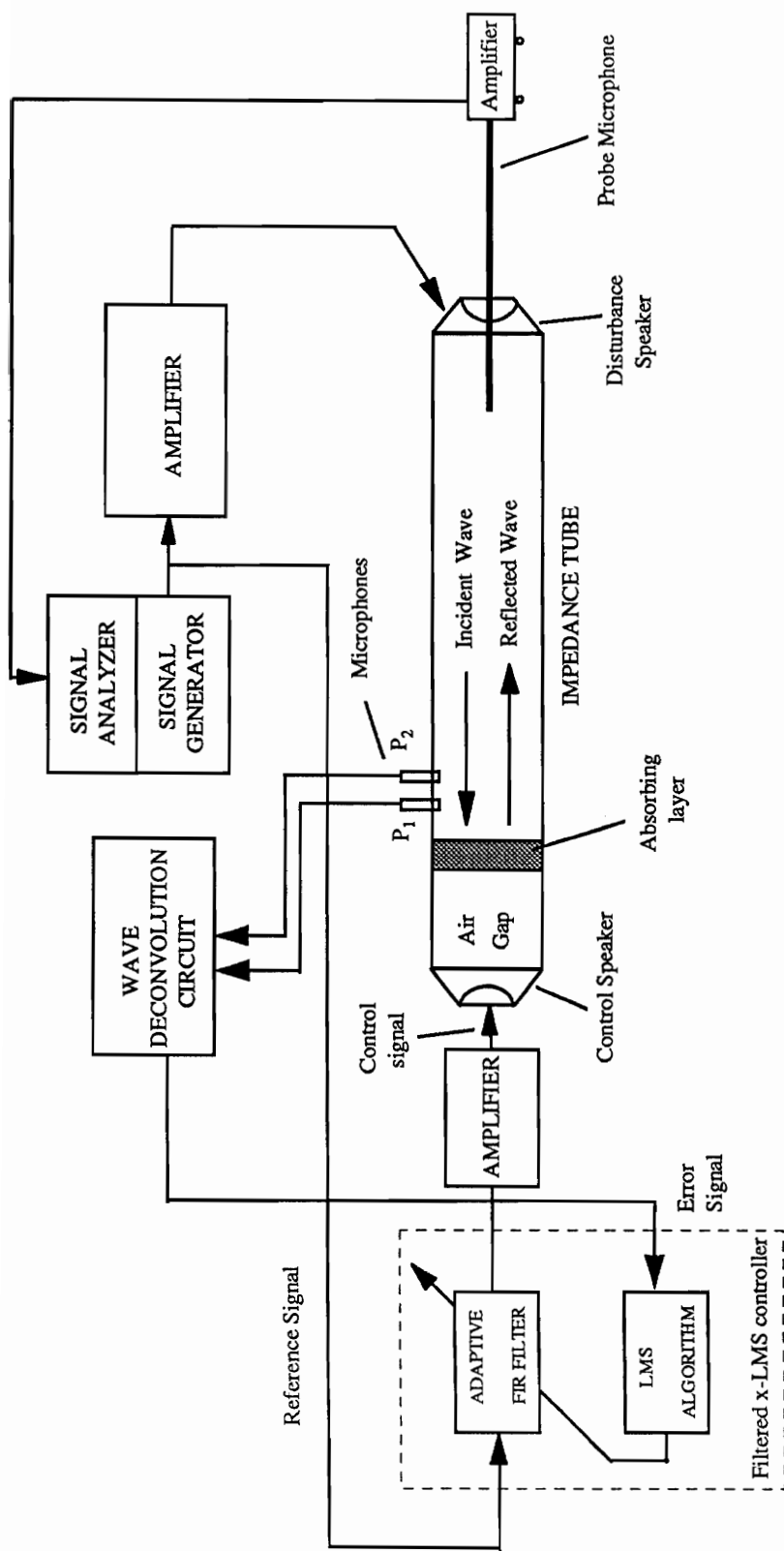


Fig. 4.1 Experimental setup for direct minimization of reflected wave

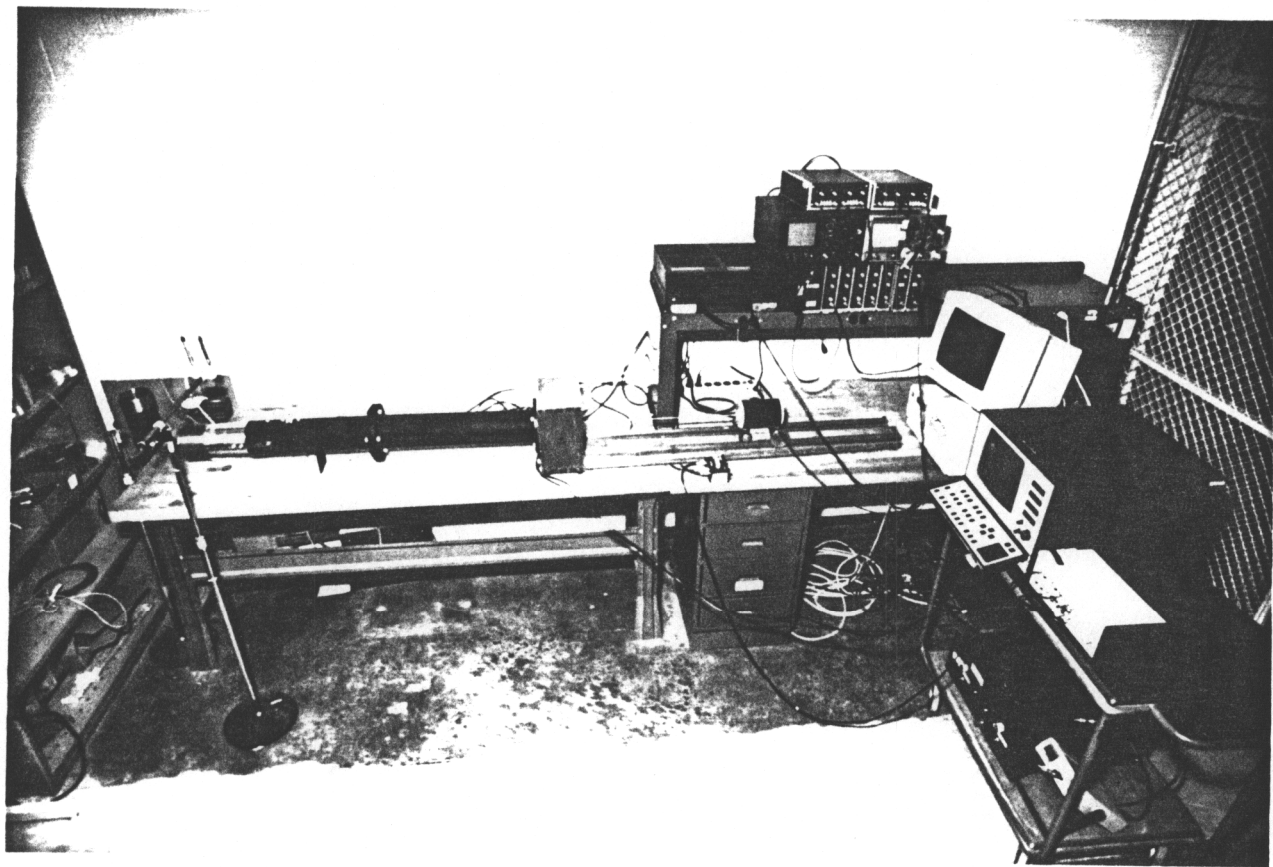


Fig. 4.2 Laboratory experimental setup.

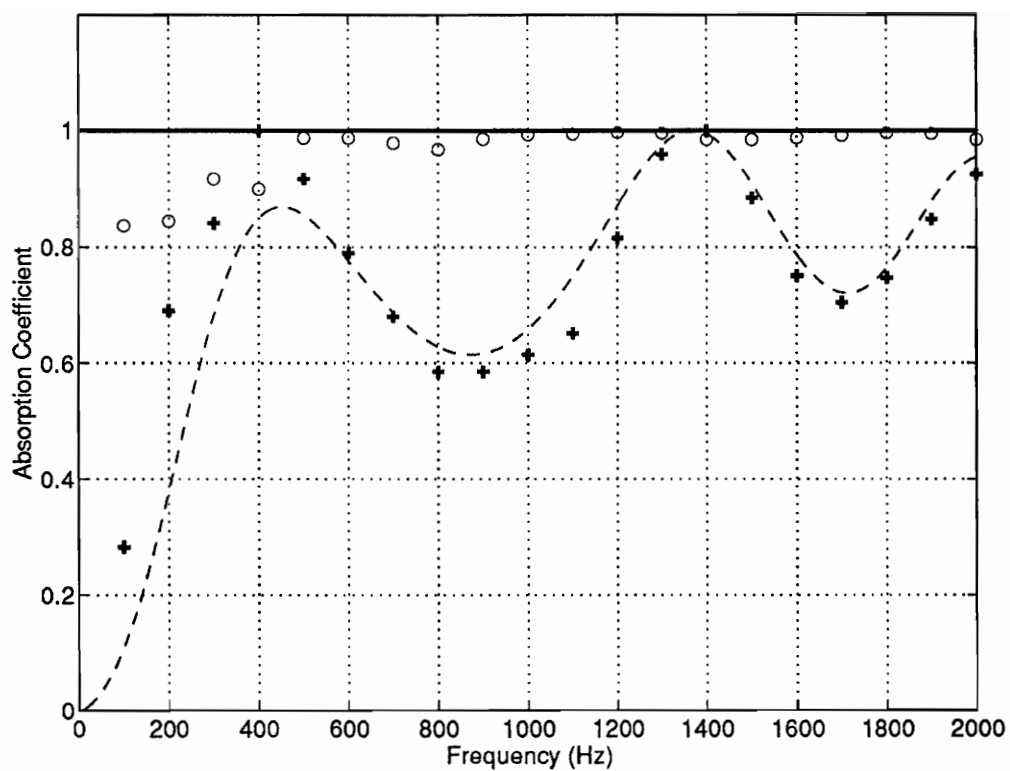


Fig. 4.3 Absorption coefficient of system when reflected wave is directly minimized.

---- analytical before control, — analytical after control

+++ experimental before control, ooo experimental after control

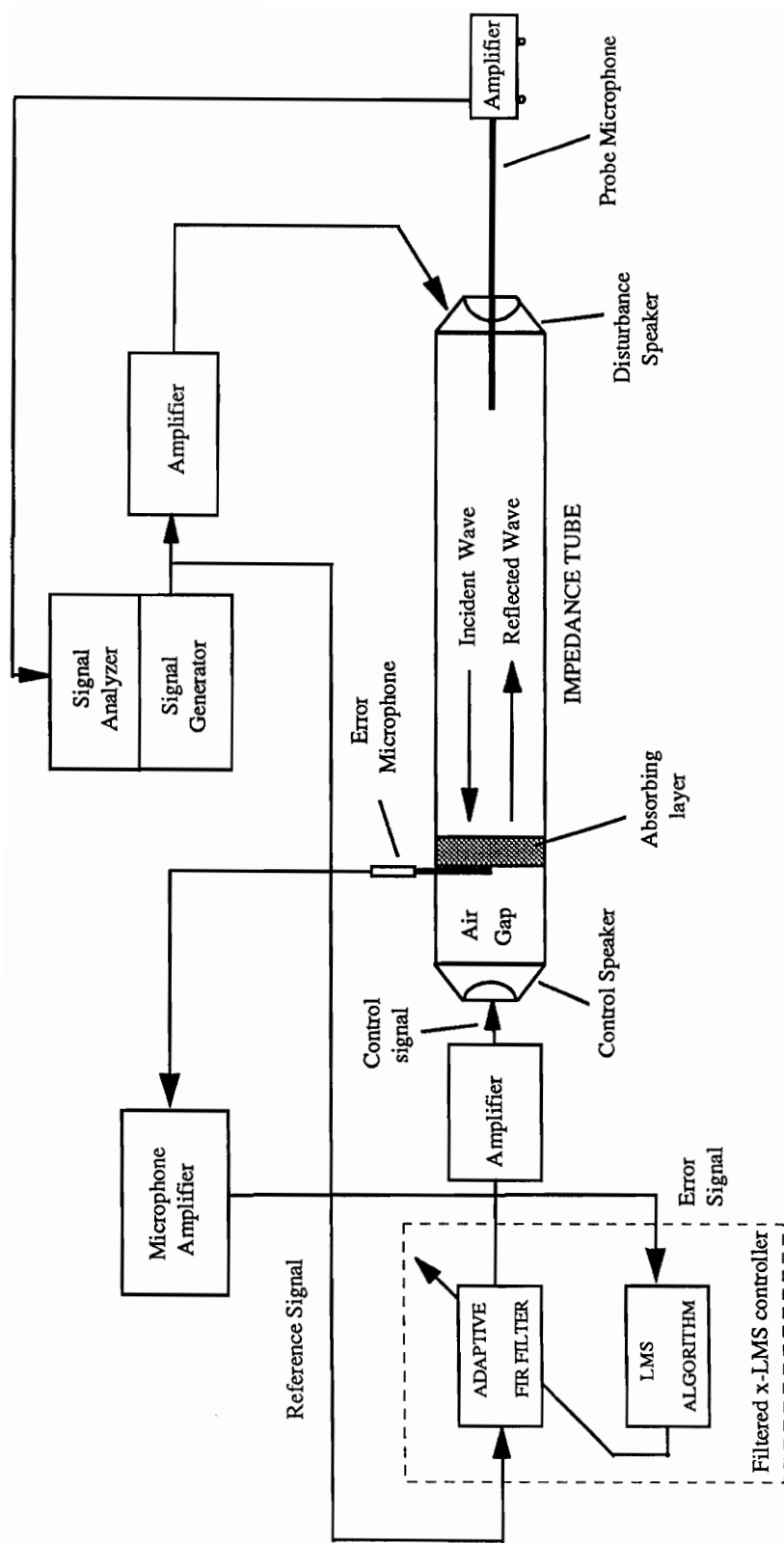


Fig. 4.4 Experimental setup for pressure-release boundary condition

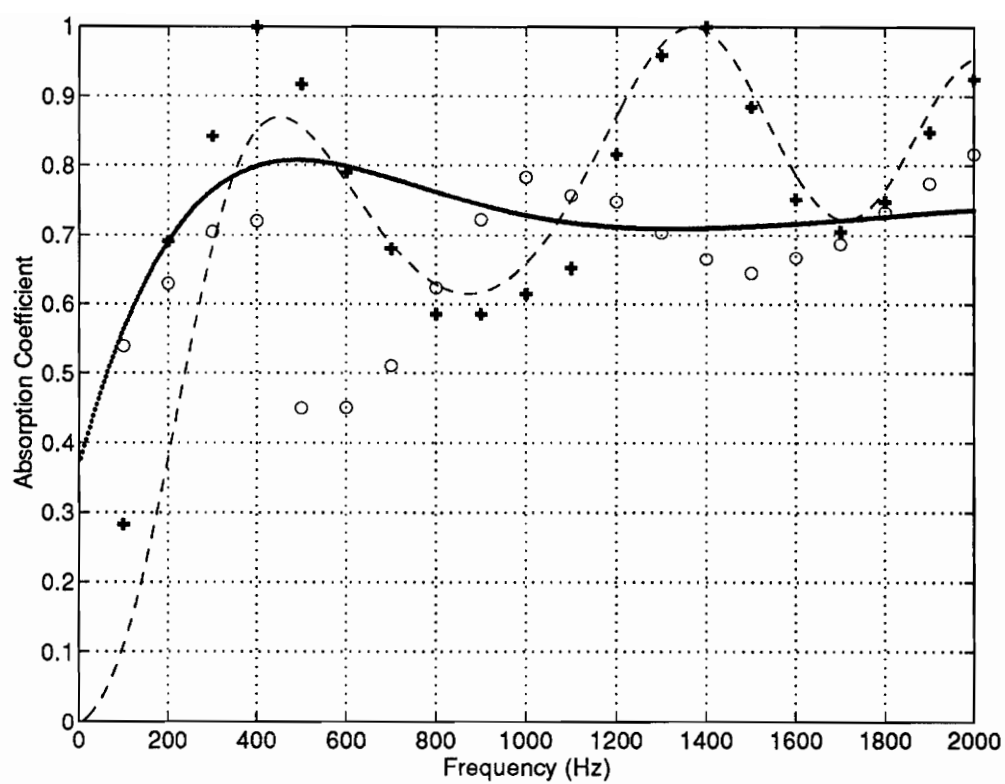


Fig. 4.5 Absorption coefficient due to pressure-release boundary condition.

---- analytical before control, \_\_\_\_ analytical after control

+++ experimental before control, ooo experimental after control

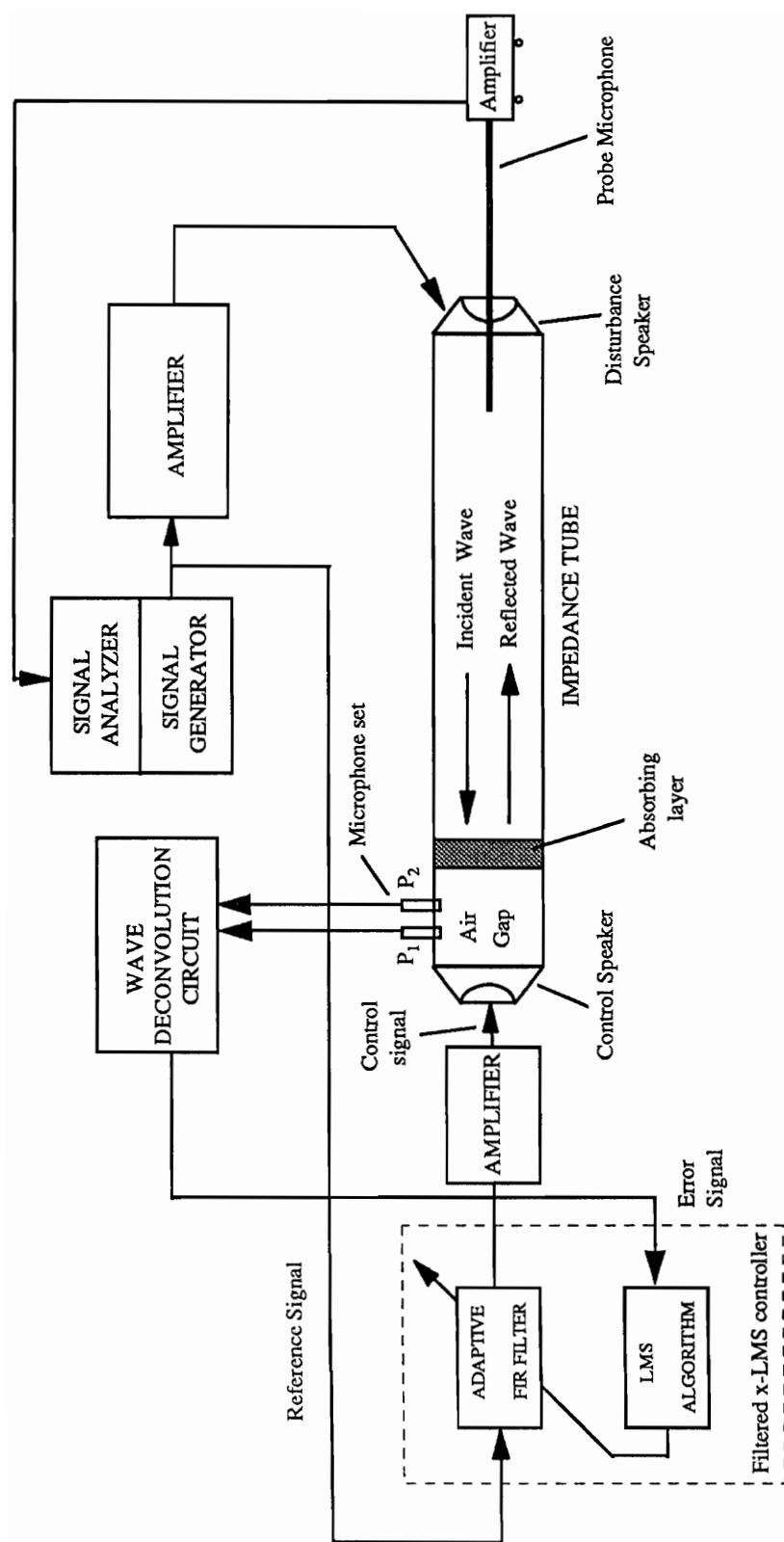


Fig. 4.6 Experimental setup for impedance-matching condition



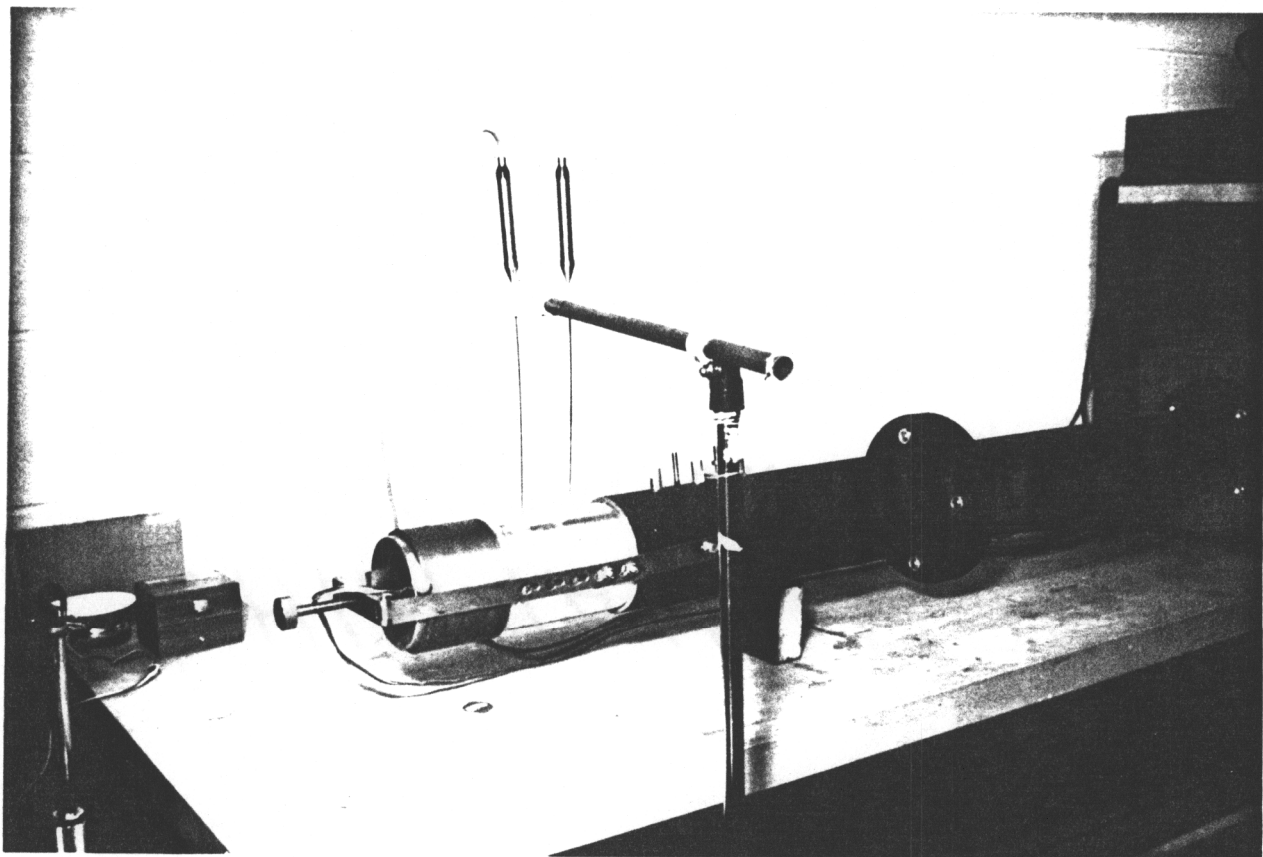


Fig. 4.7 Detail of dual-microphone setup for wave separation.

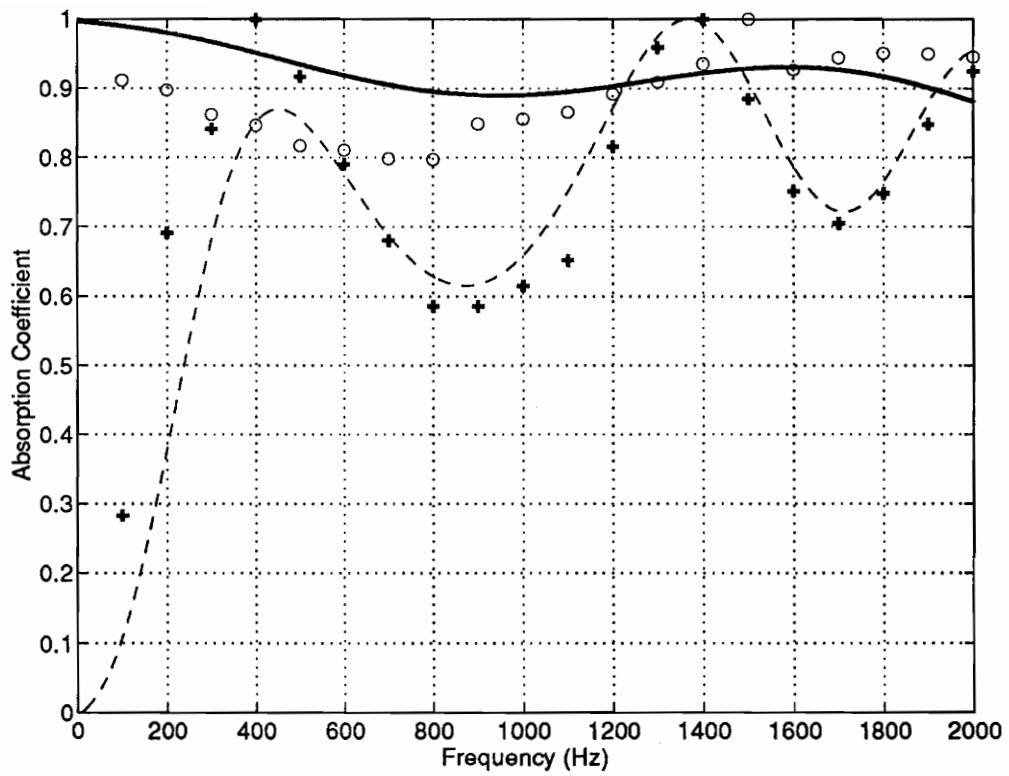


Fig. 4.8 Absorption coefficient of system due to impedance-matching condition.

---- analytical before control, \_\_\_\_ analytical after control

+++ experimental before control, ooo experimental after control

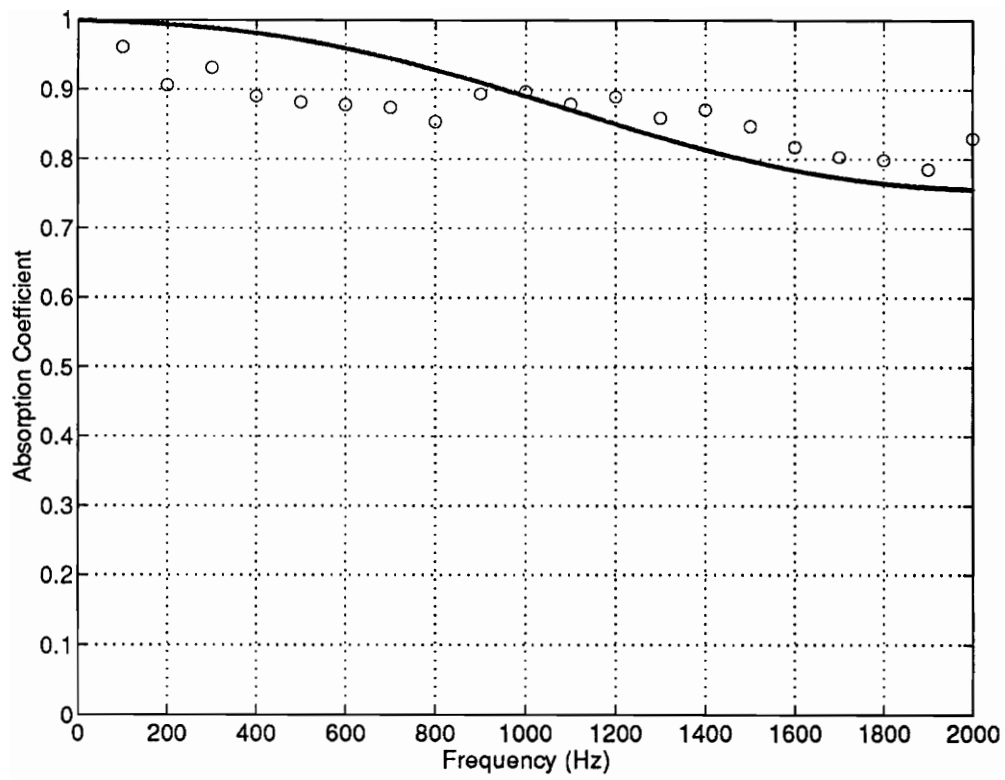


Fig. 4.9 Absorption coefficient of system with 2.5cm foam sample and air gap depth of 10cm.

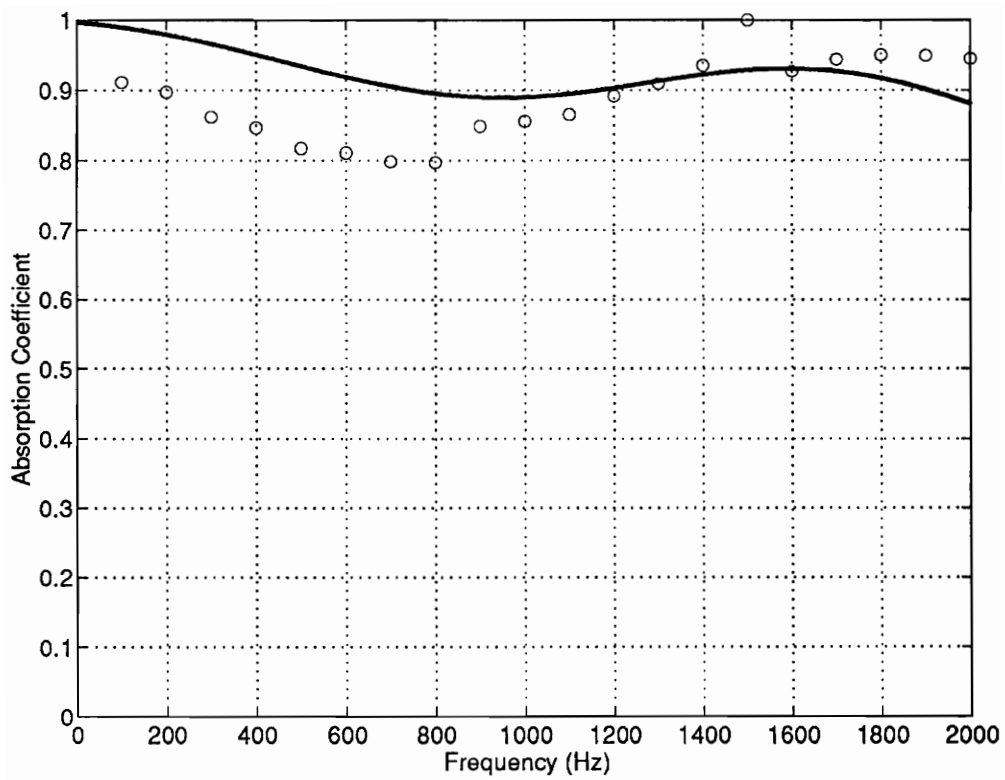


Fig. 4.10 Absorption coefficient of system with 5.0cm foam sample and  
air gap depth of 10cm

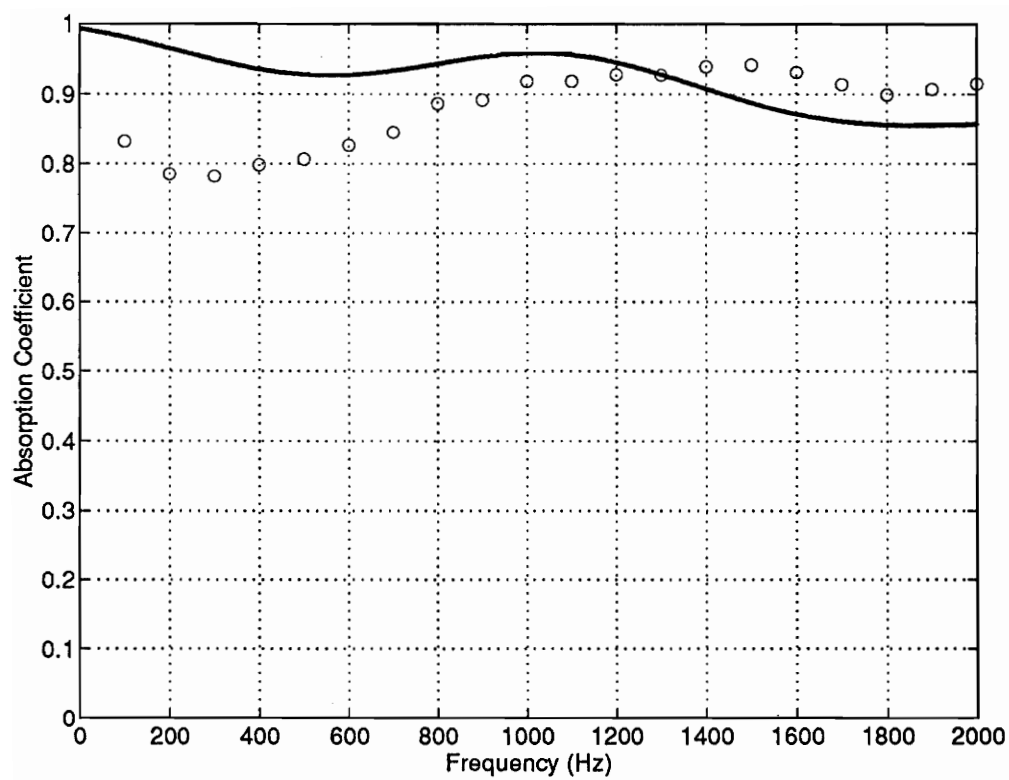


Fig. 4.11 Absorption coefficient of system with 7.5cm foam sample and air gap depth of 10cm

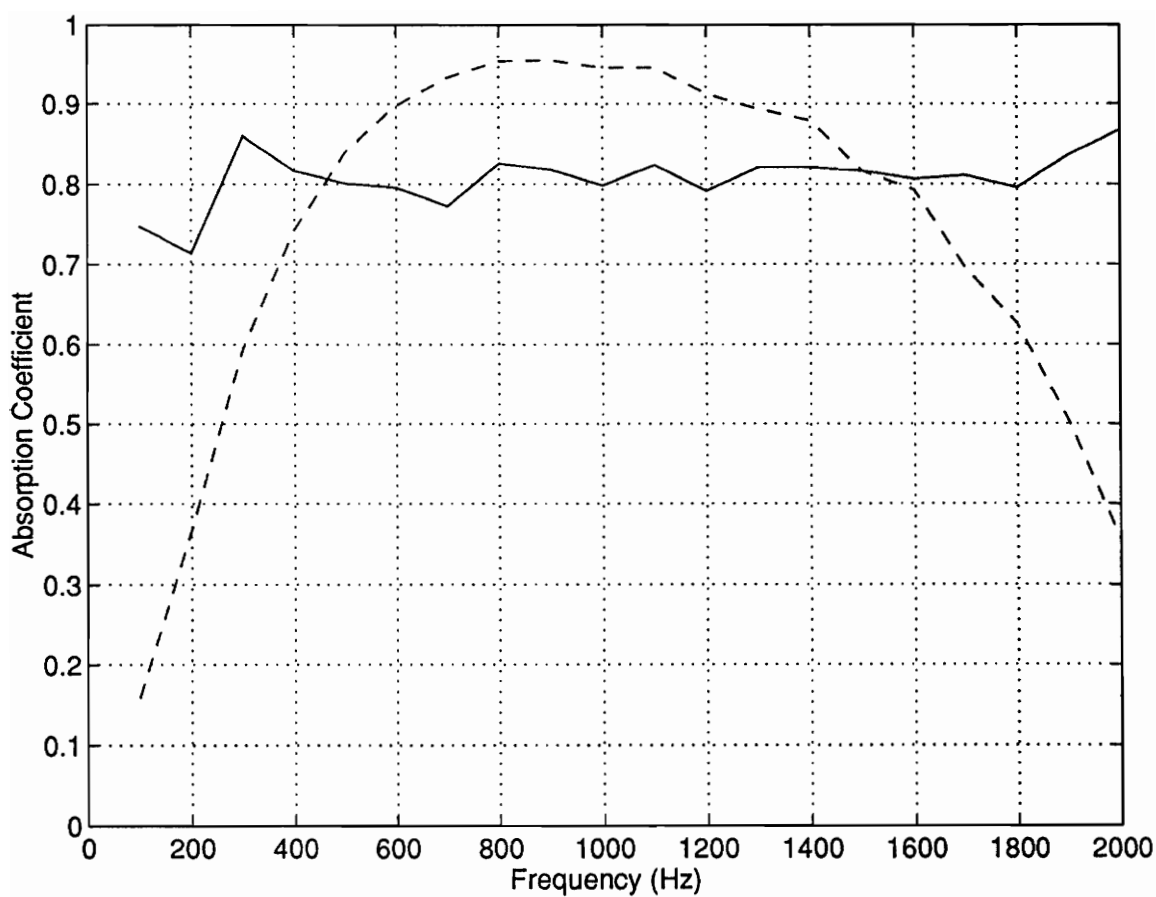


Fig. 4.12 Absorption coefficient of system using FELTMETAL® and 7.5cm airspace.

--- before control, — after control

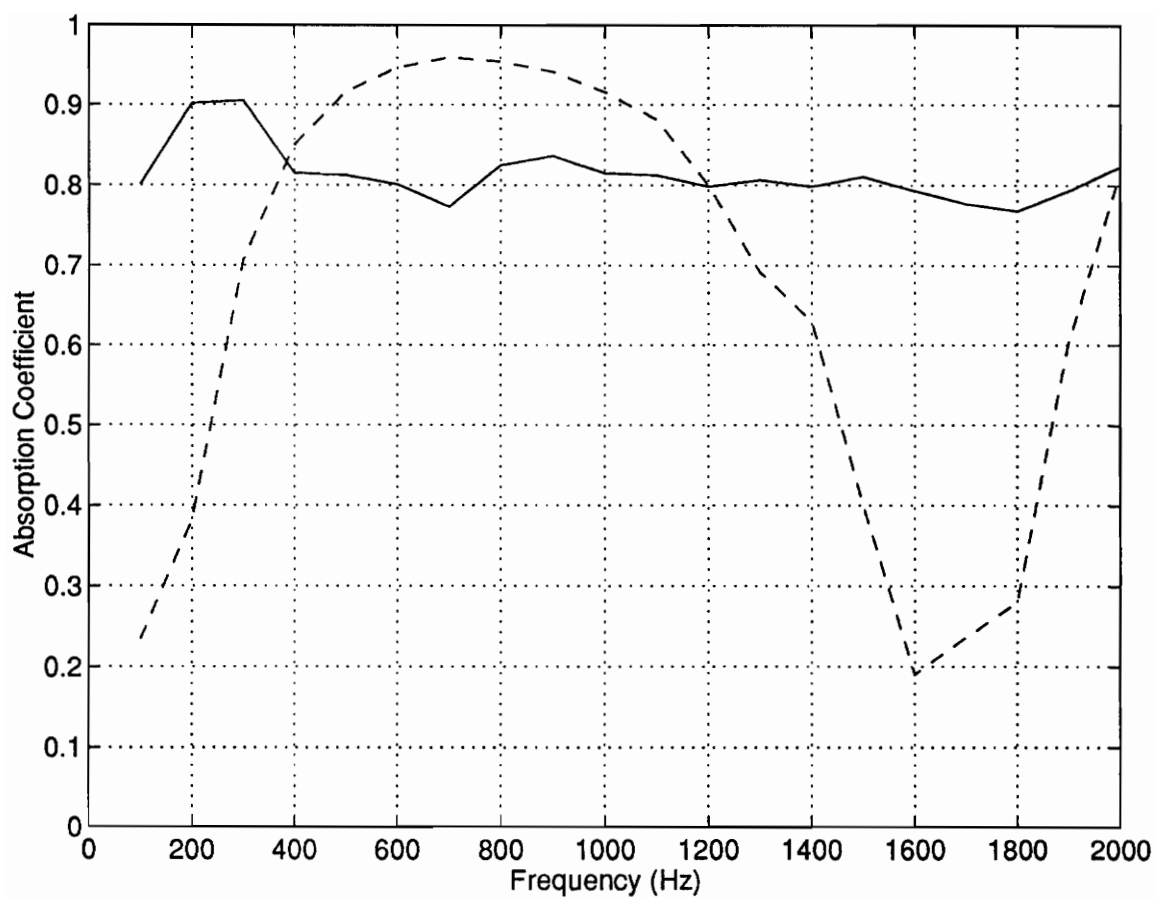


Fig. 4.13 Absorption coefficient of system using FELTMETAL® and 10cm airspace.

--- before control, — after control

## Chapter 5

### CONCLUSIONS AND RECOMMENDATIONS

#### CONCLUSIONS

The objective of the work described in this thesis was directed towards the development of a hybrid Passive/Active noise absorption system that would be effective over a broad frequency range. The Passive/Active system was based on an efficient integration of both passive and active noise control methods. Both theoretical and experimental investigations were carried out in this work.

The conceptual basis of the Passive/Active system comes from the simple arrangement of mounting sound absorbing layers at a distance from a rigid wall. In such passive systems, the presence of the airspace between the absorbing layer and the rigid wall results in high absorption peaks at frequencies where the depth of the airspace is one fourth of the wavelength of the operating frequency. However, these absorption peaks occur over a relatively narrow frequency bands and also low absorption bands are introduced along with the absorption peaks. In the Passive/Active system, the rigid wall was replaced with an active wall and the velocity of this wall controlled in such a way that the condition necessary for optimum absorption is maintained over a wide frequency range. A simple and useful model based on a two-layered media was developed to simulate this system. The sound absorbing layer used in the model was a partially reticulated polyurethane foam. This absorbing layer was characterized using its propagation constant  $\Gamma$  and its characteristic impedance  $Z_a$  which were determined using some empirical data.



Three different control strategies were studied for the Passive/Active system. The three control strategies investigated were: (i) the ideal case of minimizing the reflected wave directly, (ii) a pressure-release boundary condition on the back surface of the absorbing layer and (iii) a new approach that consists of minimization of the reflected wave in the airspace. This condition results in a match between the impedance in the airspace and the impedance of a plane wave in air,  $\rho c_0$ , and has been appropriately termed 'impedance-matching condition'. Among the three control approaches, only the direct minimization of the reflected wave and the impedance-matching condition met the objective of optimum absorption of sound over a wide frequency band. In the direct-minimization case, the error sensors were located in front of the sound absorbing layer where the response is desired. However, the location of error sensors at the desired "zone of quiet" are not usually at one's disposal. The impedance-matching control approach has the benefit of having all the necessary error sensors and actuator hidden in the airspace. In practical design, this advantage results in a compact and self-contained unit. In addition, the wall displacement required for optimum absorption was shown to be very small. Therefore, the control speaker could be replaced by a smaller and more efficient sound source. This should further reduce the size of the system.

Parametric analysis were performed on the system that utilizes the impedance-matching control approach in order to investigate the sensitivity of the Passive/Active system to variation in absorbing layer thickness and airspace depth. The performance of the system was determined to be independent of the airspace depth and marginally sensitive to absorbing layer thickness. In addition, in order to study the feasibility of using the developed model for other sound absorbing materials, an experimental investigation was performed with the polyurethane foam replaced by a porous metal sheet called FELTMETAL. The result of this investigation resulted in a consistent high absorption

coefficient of 0.8 to 1.0 over the frequency range 100Hz to 2000Hz. This result indicated the robustness of the Passive/Active system.

The numerical analysis of the system presented in chapter 3 had shown that a reduction in the depth of the airspace results in a marginal increase in the control effort and has no effect on the performance of the system. The only physical limitation on the reduction of the airspace depth from design point of view is the minimum required spacing between the two microphones used for signal separation. In general the minimum spacing between the microphones should be  $\lambda/12$  [21]. Therefore, reduction of the spacing compromises the accuracy of the wave separation at the lower frequencies.

In conclusion, the objective of the work reported here was the development of a hybrid noise absorption system that would be effective in absorbing sound over a wide frequency range. This objective has been met with the development of the Passive/Active system. The design of the Passive/Active system is based on an efficient integration of both passive and active noise control methods. Passive/Active system features a new control approach in which all of the necessary sensors and actuators are built into the system. This new control approach, referred here as impedance-matching condition, opens a wide potential of applications for the Passive/Active system. This system could be implemented in a number of applications such as reverberation control in architectural acoustics and absorption of low frequency noise in airplane fuselage design.

## RECOMMENDATIONS

Further work could concentrate in extending the one-dimensional Passive/Active model developed in this work to the more realistic three-dimensional model. The absorption property of the one-dimensional system developed here could first be analyzed

for an oblique incident plane wave. Perhaps the extreme case of a wave perpendicular to the surface of the sound absorbing layer could be considered since in a diffuse sound field, the waves impinging on the sound absorbing layer will have an angle of incident between  $90^\circ$  (normal incidence) and  $180^\circ$  (perpendicular incidence). This study should give some indication of the effectiveness of the system for a three-dimensional sound field.

In the development of the three-dimensional system, some applicable changes need to be considered. The wave deconvolution circuit described in this work for separating incident and reflected waves was designed for normally incident plane waves. Therefore, the arrangement of simply placing the dual-microphones in the airspace as in the one-dimensional system is not applicable in the three-dimensional system due to the presence of oblique waves in the airspace. However, this problem could be resolved by having a partitioned airspace. The partitioning of the airspace guarantees plane wave field in each partition, by prohibiting tangential wave transmission. Each partition would include its own individual control source and wave separation process. The three-dimensional system would then include an array of these partitions arranged serially. Once the three-dimensional system is developed and demonstrated for oblique incidence of plane waves, the study of broad-band noise control using such system could follow. In this study, the feasibility of using the incident wave within the airspace as the reference signal could be investigated in order to avoid the need for error detection microphones. The development of the three-dimensional system could open a number of potential applications.

## REFERENCES

- [1] "Noise Control", Charles E. Wilson, Harper & Row, Publishers, New York , 1989.
- [2] "Physical and Acoustical Properties of Urethane Foams", Edmund O'Keefe, *Sound and Vibration*, 16 - 21, July 1978.
- [3] "On the Invention of Active Noise Control by Paul Lueg", D. Guicking, *Journal of the Acoustical Society of America (Journal of the Acoustical Society of America)* **87** (5), 2251 - 2254, 1990
- [4] "The Active Control of Sound", S.J.Elliott and P.A. Nelson, *Electronics and Communication Engineering Journal*, 127-136, August 1990.
- [5] "Active Noise Control, applying Low-Frequency Techniques with DSP", J.Elliott and P.A.Nelson, *IEEE Signal Processing Magazine*, 12-35, Oct 1993.
- [6] "Process of Silencing Sound Oscillations", Paul Lueg, U.S. Patent No. 2,043,416, 1936.
- [7] "Electronic Sound Absorber", H. . Olson and E. G. May, *Journal of the Acoustical Society of America*, **25**, 1130-1136, 1953.
- [8] "Fighting Noise with Noise", W. B. Conover, *Noise Control Engineering*, **2**, 78 - 82, 1956.
- [9] "Active Attenuation of Noise - The State of the Art", Glenn E. Warnaka, *Noise Control Engineering*, **18** (3), 100-108, 1982.
- [10] "Active Impedance Control for One-dimensional Sound", D. Guicking and K. Karcher, *Journal of Vibration, Acoustics, Stress, and Reliability in Design*, **106**, 393 -396, 1984.
- [11] "An Active Sound Absorber with Porous Plate", D. Guicking and E. Lorenz, *Journal of Vibration, Acoustics, Stress and Reliability in Design*, **106**, 389-392, 1984.
- [12] "Piezocomposite Coating for Active Underwater Sound Reduction", Thomas R. Howarth, Vijay K. Varadan, Xiaoqi Bao, and Vasundara V. Varadan, *Journal of the Acoustical Society of America* **91** (2), 823-831, 1992.

- [13] "Acoustically Active Surfaces using Piezorubber", L. Dwyann Lafleur, F. Douglas Shields, and James E. Hendrix, *Journal of the Acoustical Society of America* **90** (3), 1230-1237, 1991.
- [14] "Smart Foams for Active Absorption of Sound", J. S. Bolton and E. R. Green, *Second Conference on Recent Advances in Active Control of Sound and Vibration*, Blacksburg, VA, 139-149, 1993, Technomic Press, Lancaster, PA.
- [15] "Active Enhancement of the Absorbent Properties of a Porous Material", Denis Thenail, Marie-Annick Galland and Michel Sunyach, and Michel Sunhack, *Smart Materials and Structures*, **3**, 18-25, 1994.
- [16] "Control of Sound Radiation/Reflection with Adaptive Foams", C. R. Fuller, M. J. Bronzel, C. H. Gentry, and D. E. Whittington, *Proceedings of Noise-Con 1994*, 429-436, May 1994.
- [17] "Sound Absorbing Materials", C. Zwicker and C. W. Kosten, Elsevier Publishing Co. Inc., London, 1949.
- [18] "The Acoustic Impedance of a Porous Layer at Oblique Incidence", J. S. Pyett, *Acustica*, **3** (6), 375-382, 1953.
- [19] "Noise and Vibration Control Engineering: Principles and Applications", Leo Beranek, John Wiley and Sons, Inc., 1992.
- [20] "Standard Test Method for Impedance and Absorption of Acoustical Materials using a tube, two microphones and a digital frequency analysis system", ASTM E1050, Philadelphia, USA, 1990.
- [21] "A Technique for Measuring Sound Intensity with a Sound Level Meter", F. J. Fahy, *Noise Control Engineering*, 155-162, November-December, 1977.
- [22] "Standard Test Method for Impedance and Absorption of Acoustical Materials by the Impedance Tube Method", ASTM C384, Philadelphia, USA, 1990.
- [23] "Sound Conditioning through DSP", Daniel Sweeney, *Audio*, 24 - 32, March, 1994.
- [24] "A Simple Two Microphone Method of Measuring Absorption Coefficient", S. J. Elliott, *Acoustical Letters*, **5** (2), 39 - 44, 1981.
- [25] "Adaptive Signal Processing", Bernard Widrow and Samuel D. Stearns, Prentice-Hall, Englewood Cliffs, New Jersey 07632, 1985.

**APPENDICES**

## Appendix A

### Determination of $\Gamma$ and $Z_a$

The Passive/Active model developed in chapter 2 was based on a two-layered media. The first layer of this model was a sound absorbing material while the second layer was an air cavity. The characterization of the sound absorbing material was based on its propagation parameters. These parameters were mainly the propagation constant  $\Gamma$  and the characteristic impedance  $Z_a$ .

The particular sound absorbing material investigated for the Passive/Active system was the partially reticulated polyurethane foam. This material is not well known however, and its propagation parameters were not available when this work started. Different methods of obtaining these parameters were investigated and a simple method that could be implemented in an impedance tube using standard measuring techniques was selected. This method was first described by Pyett [18]. The following is the formulation for this method.

The input impedance of a layer of absorptive material placed against a hard wall can be expressed as:

$$Z = Z_a \coth(\Gamma d) \quad (A1)$$

Using the input impedance ratio of two samples of the same material with thickness of  $d_1$  and  $d_2$ ,

$$\begin{aligned} \frac{Z_1}{Z_2} &= \frac{Z_a \coth(\Gamma d_1)}{Z_a \coth(\Gamma d_2)} \\ \frac{Z_1}{Z_2} &= \frac{\coth(\Gamma d_1)}{\coth(\Gamma d_2)} \end{aligned} \quad (A2)$$

The only unknown variable in equation (A2) is  $\Gamma$ . Pyett have shown the choice of the thickness ratio of the two samples should be 1:2 for simplification ( $d_2=2d_1$ ). Then,

$$\frac{Z_1}{Z_2} = \frac{Z_a \coth(\Gamma d_1)}{Z_a \coth(\Gamma d_2)} = \frac{\frac{\cosh(\Gamma d_1)}{\sinh(\Gamma d_1)}}{\frac{\cosh(2\Gamma d_1)}{\sinh(2\Gamma d_1)}} \quad (\text{A3})$$

Using the following hyperbolic identities::

$$\sinh(2\Gamma d) = 2\sinh(\Gamma d)\cosh(\Gamma d) \quad (\text{A4})$$

$$\cosh(2\Gamma d) = 2\cosh^2(\Gamma d) - 1 \quad (\text{A5})$$

Equation (A3) reduces as follows:

$$\frac{Z_1}{Z_2} = \frac{\coth(\Gamma d_1)}{\coth(2\Gamma d_1)} = \frac{\frac{\cosh(\Gamma d_1)}{\sinh(\Gamma d_1)}}{\frac{\cosh(2\Gamma d_1)}{2\sinh(\Gamma d_1)\cosh(\Gamma d_1)}} \quad (\text{A6})$$

$$= \frac{\coth(\Gamma d_1)}{\frac{\cosh(2\Gamma d_1)}{2\cosh(\Gamma d_1)}} = \frac{2\cosh^2(\Gamma d_1)}{\cosh(2\Gamma d_1)} \quad (\text{A7})$$

$$\frac{Z_1}{Z_2} = \frac{R_1 + iI_1}{R_2 + iI_2} = \frac{1 + \cosh(2\Gamma d)}{\cosh(2\Gamma d)} \quad (\text{A8})$$

$$\text{Let } \cosh(\Gamma d) = U + iV \quad (\text{A9})$$

$$\frac{Z_1}{Z_2} = \frac{R_1 + iI_1}{R_2 + iI_2} = \frac{1 + U + iV}{U + iV} \quad (\text{A10})$$



$$(R_2 + iI_2)(1 + U + iV) = (R_1 + iI_1)(U + iV) \quad (A11)$$

Collecting real and imaginary terms from each side,

$$VR_1 + UI_1 = R_2V + I_2 + I_2U \quad (\text{real}) \quad (A12)$$

$$R_1U - I_1V = R_2 + R_2U - I_2V \quad (\text{imaginary}) \quad (A13)$$

and eliminating U from both equations,

$$\frac{R_2 + V(I_1 + I_2)}{(R_1 - R_2)} = \frac{I_2 + V(R_2 - R_1)}{(I_1 - I_2)} \quad (A14)$$

$$V = \frac{I_2(R_1 - R_2) - R_2(I_1 - I_2)}{(I_1 - I_2)^2 + (R_1 - R_2)^2} \quad (A15)$$

Substituting (15) in either (A12) or (A13),

$$U = \frac{R_2(R_1 - R_2) + I_2(I_1 - I_2)}{(I_1 - I_2)^2 + (R_1 - R_2)^2} \quad (A16)$$

Substituting (A15) and (A16) in (A9),  $\Gamma$  can be easily solved.  $Z_a$  is then determined from equation A1 as,

$$Z_a = Z_1 \tanh(\Gamma d_1) \quad \text{or} \quad (A17)$$

$$Z_a = Z_2 \tanh(\Gamma d_2) \quad (A18)$$

## Appendix B

### Separation of Incident and Reflected Waves

The deconvolution circuit employed in this work was first described by Fahy [21]. Fuller, *et al.*, used the same circuit for their “Adaptive Foam” study [16]. This circuit gives real time domain estimate of the incident and reflected components of a sound field from the outputs of two closely spaced identical microphones. Using the voltage output of the microphones, Fahy has shown that the pressure gradient at a point mid-way between them could be estimated. This pressure gradient can be related to the particle velocity at the same location. The estimated values of the pressure and velocity can then be used to compute different acoustic parameters. The circuit was used in this work to give a voltage proportional of the incident and reflected components of the standing-wave field in the impedance tube. A block diagram of the wave deconvolution circuit is given below.

$P_1$  and  $P_2$  are the instantaneous acoustic pressures detected by the microphones at their respective locations. The pressure between the two microphone locations could then be estimated as:

$$P \approx \frac{(P_1 + P_2)}{2} \quad (B1)$$

and the particle velocity  $U$  is related to the pressure by Euler’s equation as:

$$\frac{\partial P}{\partial x} = -\rho \frac{\partial U}{\partial t} \quad (B2)$$

The difference of the instantaneous pressures divided by the separation distance of the microphones  $\Delta x$  is an approximation to the term  $\partial P / \partial x$ . Therefore, the particle velocity is expressed as:

$$U = \frac{1}{\rho} \int \frac{(P_1 - P_2)}{\Delta x} dt = \frac{(P_1 - P_2)}{j\omega\rho\Delta x} \quad (B3)$$

A voltage proportional of the pressure ( $V_p$ ) can be obtained by adding the outputs of the two microphone signals as:

$$V_p = S(P_1 + P_2) \approx 2SP \quad (B4)$$

where  $S$  is the sensitivity of the microphones. A voltage proportional of the velocity ( $V_u$ ) can also be determined by integrating the difference of the two microphone signals with an integrator of transfer function  $T = \omega \circ j\omega$  as follows:

$$V_u = S(P_1 - P_2) \omega \circ j\omega \quad (B5)$$

Substituting equation B1 in the above equation,  $V_u$  reduces as:

$$V_u \approx S\omega \circ \rho\Delta x U \quad (B6)_$$

For plane wave excitation,  $V_p = V_u$ , and this is achieved by setting the gain of the integrator to be  $\omega \circ = 2c / \Delta x$ .

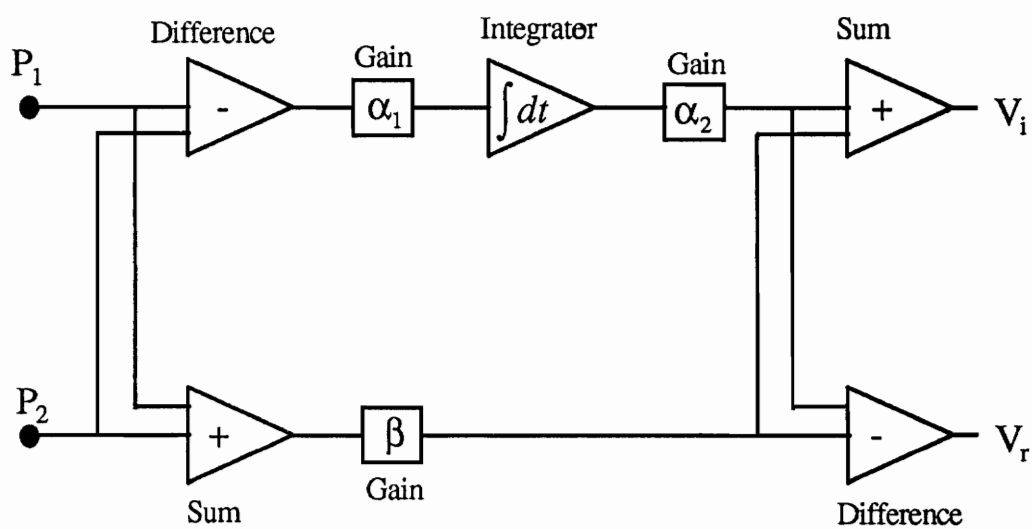
$$V_u \approx 2Sp\omega U \quad (B7)$$

The total pressure  $P$  is composed of its incident component  $P_i$  and the reflected component  $P_r$ . Therefore,  $P = P_i + P_r$  and since impedance of air is  $\rho c$ , using the equation  $Z=p/v$ ,

The total pressure  $P$  is composed of its incident component  $P_i$  and the reflected component  $P_r$ . Therefore,  $P = P_i + P_r$  and since impedance of air is  $\rho c$ , using the equation  $Z=p/v$ ,  $U = (P_i - P_r)/\rho c$ . The voltage proportional of the incident and reflected waves are then expressed as,

$$V_i = V_p + V_u \approx 4SP_i \quad \text{and} \quad (B8)$$

$$V_r = V_p - V_u \approx 4SP_r \quad (B9)$$

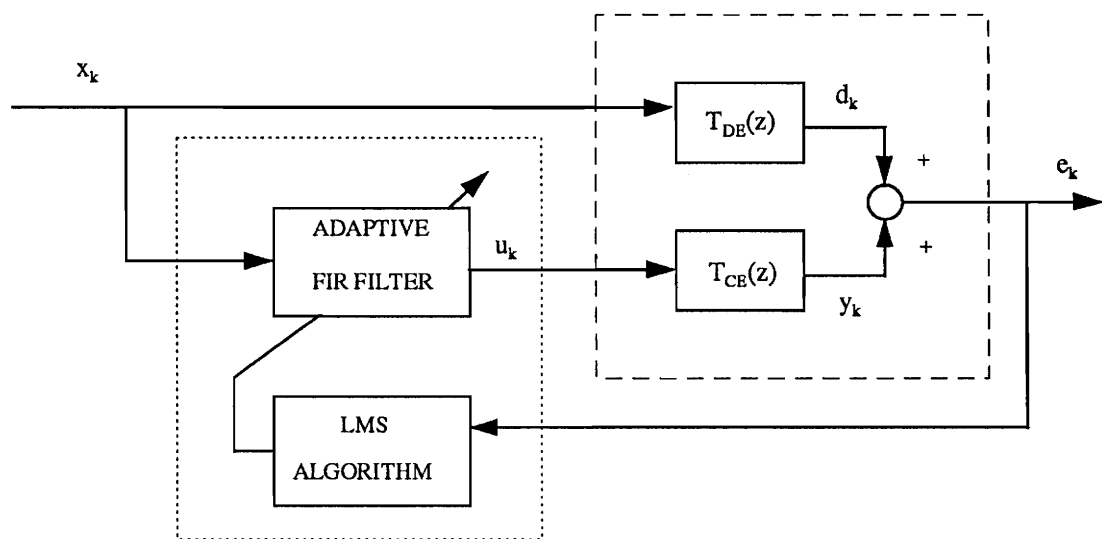


Block diagram of wave deconvolution circuit

# Appendix C

## Adaptive controller

The adaptive control algorithm used in the experimental study was the feed-forward based Filtered x-LMS controller. The following is a block diagram of a single-input-single-output (SISO) Filtered x-LMS control algorithm [25].



Block diagram of SISO Filtered x-LMS control algorithm

$e_k$  = error signal

$x_k$  = disturbance signal

$u_k$  = control signal

$y_k$  = output signal

$T_{de}$  = disturbance path transfer function

$T_{ce}$  = control path transfer function

The control signal  $u_k$  is obtained by filtering the reference signal that is coherent to the disturbance signal  $x_k$  through an adaptive FIR filter  $W(z)$ . In practice,  $u_k$  is generally computed in a system identification sequence prior to control and can be expressed as:

$$u_k = \sum_{j=0}^L W_{j,k} x_{k-j} \quad (C1)$$

where  $W_{j,k}$  is the adaptive FIR weight (adaptive filter coefficient) at the  $k^{\text{th}}$  time step,  $L$  is the order of the FIR filter and the subscript  $k$  indicates a signal sample at time  $t_k$ . The filter output can also be expressed in convolution form as

$$u_k = W(z) * x_k \quad (C2)$$

where  $*$  denotes a convolution.  $T_{de}(z)$  and  $T_{ce}(z)$  are the disturbance and control path transfer functions respectively.

The error signal  $e_k$  is given as:

$$e_k = d_k + y_k \quad (C3)$$

where  $d_k$  is the response due to the disturbance signal  $x_k$ . The error signal  $e_k$  can also be expressed in terms of the convolution of the control input  $u_k$  and the control path transfer function  $T_{ce}(z)$  as:

$$e_k = d_k + T_{ce}(z) * u_k \quad (C4)$$

where  $u_k = W(z) * x_k$ .

The task of the adaptive control algorithm is the formation of a performance or cost function and the control input parameters that minimize the cost function. The cost function is a representative of the system response to be minimized and is defined as the mean square value of the error signal. The cost function is expressed below as function of the FIR filter weights:

$$C(W_j) = E[e_k^2] \quad (C5)$$

The cost function is clearly a quadratic function of each of the weights  $W_j(j=0,1,...,L)$  of the adaptive FIR filter  $W(z)$ . Generating the control input involves finding the optimal values for the FIR coefficients  $W_j$ . The LMS algorithm adapts the FIR coefficients  $W_j$  in order to minimize the cost function, thus the error signal. This is done using the steepest decent method, a technique for computing the gradient of a quadratic performance surface by searching along the negative direction towards the minima.

Substituting the expression of the error signal by equation C4, equation C5 yields,

$$C(W_{j,k}) = E[(d_k + T_{ce}(z) * W_{j,k} * x_{k-j})^2] \quad (C6)$$

Differentiating the cost function with respect to the filter weights gives,

$$\frac{\partial C}{\partial W_{j,k}} = 2E\left[e_k \frac{\partial e_k}{\partial W_{j,k}}\right] = 2E[e_k (T_{ce}(z) * x_{k,j})] \quad (C7)$$



Letting the convolution of the disturbance signal through the control path transfer function be termed as the filtered-x signal  $\hat{x}_k$ , i.e.,

$$\hat{x}_k = T_{ce}(z) * x_k \quad (C8)$$

yields the cost function gradient as,

$$\frac{\partial C}{\partial W_{j,k}} = 2[e_k \hat{x}_{k-j}] \approx 2e_k \hat{x}_{k-j} \quad (C9)$$

Substituting this expression for the cost function gradient into the filter update equation C4 yields the final filter weight update equation,

$$W_{j,k+1} = W_{j,k} - 2\mu e_k \hat{x}_{k-j}; \quad j = 0, \dots, L \quad (C10)$$

where  $\mu$  is a parameter that controls the rate and stability of the convergence process.

In the experimental setup for the Passive/Active system,  $e_k$  would correspond to the reflected wave processed by the wave deconvolution circuit,  $x_k$  to the disturbance and  $u_k$  to the acoustical pressure generated by the control speaker. The Filtered x-LMS algorithm used in this work employed a FIR filter with two variable coefficients.

## **Vita**

Samson Beyene was born on December 17, 1969 in Asmara, Eritrea, a small country located along the Red Sea coast in east Africa. In 1987, he immigrated to the United States with his family due to a political climate that existed in his homeland at that time. After a year and half of high school education in Alexandria, Virginia, he entered the College of Engineering at Virginia Tech in 1989. He graduated from the Department of Mechanical Engineering with a B.S. degree in 1993 and immediately began his post graduate studies in the same department. He completed his M.S. degree in May, 1995 and accepted a job offer from LORD Corp. in Erie, Pennsylvania.